DEVELOPMENT, CHARACTERIZATION AND IMAGING OF BONE METASTASIS MOUSE MODELS - THE EFFECT OF SAGOPILONE ON TUMOR GROWTH AND BONE RESORPTION -

Dissertation zur Erlangung des akademischen Grades des

Doktors der Naturwissenschaften (Dr. rer. nat.)

eingereicht im Fachbereich Biologie, Chemie, Pharmazie

der Freien Universität Berlin

vorgelegt von

Anne-Kathrin Strube

aus Hildesheim

Juni 2009

Die Arbeit wurde im Zeitraum von September 2006 bis Juni 2009 unter der Leitung von Dr. Sanna-Maria Käkönen in der TRG Oncology, Bayer Schering Pharma AG, Berlin, angefertigt.

1. Gutachter	**Sanna-Maria Käkönen, Adjunct Professor**
	Therapeutic Research Group Oncology
	Bayer Schering Pharma AG, Berlin
	Institute of Biomedicine
	University of Turku, Turku, Finland
2. Gutachter	**Petra Knaus, Professor**
	Institute of Biochemistry
	Free University of Berlin

Disputation am 28.09.2009

Weine nicht, weil es vorbei ist.

Lache, weil es überhaupt passiert ist.

(Gabriel García Márques)

ABSTRACT

Bone metastasis is an incurable disease considerably decreasing quality of life of patients with metastatic tumors of particularly breast, prostate, lung and kidney. The vicious cycle of bone metastasis is a multi step process in which tumor cells, osteoclasts, osteoblasts, the organic bone matrix and other factors are involved. Combination therapies that target different steps of the cycle could be especially effective in inhibiting growth of osteolytic bone metastases. However, current therapies are palliative and mostly target either tumor cells or osteoclasts. Thus, to develop therapy options and better understand the biology of breast and renal cell cancer (RCC) bone metastasis, it is crucial to develop new animal models.

In this thesis, we have established a new experimental model of RCC bone metastasis by intracardiac (i.c.) inoculation of human 786-O/luciferase cells in athymic nude mice. The animals developed extensive osteolytic bone destruction as monitored by radiography and micro-CT scans within 10 weeks. The bone destruction observed was comparable to clinical settings and mainly occurred in hind limbs, forelimbs and the spine. To increase the bone-metastatic potential of the 786-O cell line and make the model suitable for evaluating compounds, an *in vivo* selection was done yielding a subclone causing osteolytic lesions in 7 weeks. To conclude, this model provides a reliable reproduction of the clinical situation and allows for designing effective treatments by better understanding the molecular mechanisms of RCC bone metastasis.

In addition, the effect of sagopilone on tumor-induced osteolysis and tumor burden in athymic nude mice inoculated i.c. with MDA-MB-231(SA)/luciferase human breast cancer cells was examined. Imaging modalities (bioluminescent imaging, micro-CT, radiography) were evaluated for their use to monitor therapeutic effects in preclinical models of bone metastasis. Sagopilone, a novel, fully synthetic epothilone, inhibits the growth of breast cancer cells *in vitro* and *in vivo.* In this thesis its potency was determined in treatment models simulating the adjuvant (preventive) and metastatic (therapeutic) settings in the clinic. The study demonstrated that sagopilone significantly inhibited tumor

burden and bone destruction compared with vehicle group and reduced tumor-induced cachexia and paraplegia. In the therapeutic model, sagopilone treatment significantly lowered the number of activated osteoclasts, and significantly reduced osteolytic lesion area, bone volume loss and bone resorption compared with vehicle treatment, while simultaneously inhibiting tumor burden. In this setting, sagopilone showed superior efficacy compared to paclitaxel. *In vitro* assays confirmed that sagopilone inhibited osteoclast differentiation and activation without cytotoxic effects and more efficiently than paclitaxel. Finally, the effect of sagopilone on osteoclasts was confirmed *in vivo* using a mouse model of ovariectomy (OVX)-induced osteoporosis. OVX mice treated with sagopilone showed higher trabecular bone density compared to OVX mice without treatment. Consequently, sagopilone appears to inhibit the vicious cycle of bone metastasis at both the tumor growth and bone resorption stages, suggesting the possibility for substantial benefit in the treatment of patients with breast cancer at risk from bone metastases or with bone lesions already present as well as possibly in other diseases with increased bone resorption.

ZUSAMMENFASSUNG

Knochenmetastasen (KM) setzen die Lebensqualität von Patienten mit metastasierendem Brust-, Prostata, Lungen- und Nierenkrebs erheblich herab. Tumormetastasen im Knochen benötigen für ihr Wachstum Unterstützung von Osteoklasten, Osteoblasten und der Knochenmatrix. Kombinationstherapien sollten besonders effektiv sein, die Entstehung von osteolytischen KM zu hemmen. Derzeit zur Verfügung stehende Therapien sind palliativ und greifen entweder Tumorzellen oder Osteoklasten an. Tiermodelle, die diese Interaktionen *in vivo* modellieren, sind eine wichtige Voraussetzung, um die Entstehung von KM besser zu verstehen und neue Therapieansätze zu entwickeln.

In der vorliegenden Arbeit wurde ein neues experimentelles Nierenkrebs-KM-Modell durch Inokulation von humanen 786-O/luciferase Zellen in den linken Herzventrikel von athymischen Mäusen etabliert. Diese Tiere entwickeln innerhalb von 10 Wochen ausgeprägte osteolytische KM, wie mit Röntgen- und mikro-CT-Aufnahmen gezeigt wurde. Art und Ort der Osteolysen waren vergleichbar mit klinischen Befunden. Um die knochenmetastasierende Fähigkeit der 786-O Zellen zu erhöhen und das Modell zur Evaluation von Substanzen verwenden zu können, wurde eine *in vivo* Selektion durchgeführt, die in einer 7-wöchigen Ausbildung von KM resultierte. Dieses Modell kommt der klinischen Situation sehr nahe und erlaubt die Suche nach und Validierung von Behandlungen gegen durch Nierenkrebs verursachte KM.

Um verschiedene Imagingtechniken (Biolumineszenz-Imaging, Mikro-CT, Röntgenaufnahmen) zum Nachweis von Therapieeffekten in präklinischen Modellen zu validieren, wurde der Effekt von Sagopilone auf tumorinduzierte Osteolyse und Tumorwachstum in athymischen Mäusen untersucht, die mit humanen Brustkrebszellen, MDA-MB-231(SA)/luciferase, intrakardial inokuliert wurden. Sagopilone, ein vollständig synthetisches Epothilon, inhibiert das Wachstum von Brustkrebszellen *in vitro* und *in vivo*. In den durchgeführten präklinischen Versuchen wurde die Wirksamkeit von Sagopilone in adjuvanten und therapeutischen Ansätzen entsprechenden Studien geprüft. Die Ergebnisse belegen, dass Sagopilone im präventiven Ansatz signifikant Tumorwachstum und Osteolyse im Vergleich zur Vehikelgruppe hemmt und tumorinduzierten

Körpergewichtsverlust und Lähmungen reduziert. Im therapeutischen Modell senkte Sagopilone signifikant die Zahl an aktivierten Osteoklasten, reduzierte signifikant die osteolytische Läsionengröße, den Verlust an Knochenvolumen und -resorption als auch das Tumorvolumen im Vergleich zur Vehikel- und Paclitaxelbehandlung. *In vitro* assays bestätigten die stärkere Hemmung der Osteoklastenaktivierung und -differenzierung durch Sagopilone im Vergleich zu Paclitaxel, ohne zytotoxische Effekte auszuüben. Der Effekt von Sagopilone auf Osteoklasten wurde *in vivo* anhand eines Mausmodells für durch Ovarektomie (OVX)-induzierte Osteoporose bestätigt. OVX Mäuse, die mit Sagopilone behandelt wurden, zeigten höhere Knochendichten im Vergleich zu OVX Mäusen ohne Behandlung. Die Ergebnisse lassen die Schlussfolgerung zu, dass Sagopilone die Entstehung von KM über eine Wirkung sowohl auf Tumorzellen als auch auf Osteoklasten verhindert. Besonders Patienten mit Brustkrebs, die ein Risiko haben, KM zu bekommen als auch diejenigen, die schon an KM leiden, sowie möglicherweise auch Patienten mit erhöhter Knochenresorption könnten von einer Therapie mit Sagopilone profitieren.

TABLE OF CONTENTS

ABBREVIATIONS

ANOVA	analysis of variance
ANT	adenine nucleotide (ADP/ATP) translocase
bFGF	basic fibroblast growth factor
BLI	bioluminescence imaging
BMD	bone mineral density
BMP	bone morphogenetic proteins
BP	bisphosphonate
BSP	bone sialoprotein
CTX	C-terminal telopeptide of type I collagen
EGF	epidermal growth factor
EGF-R	epidermal growth factor receptor
ELISA	enzyme-linked immunosorbent assay
ET-1	endothelin 1
FDG	fluorodeoxyglucose
HCC	hepatocellular carcinoma
H&E	hematoxylin and eosin
i.c.	intracardial
IGF	insulin-like growth factor
IL	interleukin
i.p.	intraperitoneal
i.v.	intravenous
luc	luciferase
M-CSF	macrophage colony-stimulating factor
micro-CT	micro-computed tomography
MMP	matrix metalloproteinase
MRI	magnetic resonance imaging
OPG	osteoprotegerin
OPN	osteopontin
OVX	ovariectomy
P	P-value
PDGF	platelet-derived growth factor
PET	positron emission tomography
P-gp	P-glycoprotein
PINP	procollagen type I N-terminal propeptide
PTHrP	parathyroid hormone related protein
pQCT	peripheral quantitative computed tomography
RANK	receptor activator of nuclear factor κB
RANKL	receptor activator of nuclear factor κB ligand
RCC	renal cell cancer
SDS-PAGE	sodium dodecyl sulfate polyacrylamide gel electrophoresis
SPECT	single photon emission computed tomography
TGF-β	transforming growth factor β
TGF-βR	transforming growth factor β receptor
TRACP	tartrate-resistant acid phosphatase
VEGF	vascular endothelial growth factor
VHL	von Hippel-Lindau
ZOL	zoledronic acid

1 INTRODUCTION

1.1 Bone biology and remodeling process

The functions of the skeleton are manifold. First, the bones provide structural support and stabilization for the body. Second, the elasticity and flexibility of the skeleton permits movement and locomotion. Third, it provides protection for the internal organs, maintenance of the mineral homeostasis, the environment for hematopoiesis within the marrow space and serves as a reservoir for cytokines and growth factors (Clarke, 2008; Taichman, 2005).

1.1.1 Bone composition

The bones of the adult skeleton consist of either cortical (or compact) bone that comprises 85% of the total bone in the body and provides the mechanical and protective functions, or cancellous (or trabecular) bone that comprises only 15% of the skeleton and provides the metabolic functions. Whereas cortical bone is dense and solid and sourrounds the marrow space, trabecular bone is composed of a sponge-like trabecular network (Mundy, 1999). The bone mineral content accounts for 50-70% of adult mammalian bone, the organic matrix for 20-40%, water for 5-10% and lipids for <3%. The bone mineral is mostly composed of hydroxyapatite [$Ca_{10}(PO_4)_6(OH)_2$] which contains vacancies (missing OH^-) and numerous impurities (carbonate, magnesium, acid phosphatase) enabling bone to act as a reservoir for calcium, phosphate and magnesium ions. The basic component, approximately 95% of the organic bone matrix, is type I collagen. The remaining 5% is composed of proteoglycans and numerous noncollagenous proteins (serum albumin, α_2-HS-glycoprotein, alkaline phosphatase, osteonectin, osteocalcin) (Robey et al., 2006).

1.1.2 Bone cells

Bone is composed of four different cell types: osteoblasts, osteoclasts, bone lining cells and osteocytes. Except from the osteocytes which are located throughout the mineralized bone matrix, the other bone cells are present on

bone surfaces. Whereas osteoblasts, osteocytes and bone lining cells originate from mesenchymal stem cells, osteoclasts derive from hematopoietic stem cells of the bone marrow (Clarke, 2008).

Osteoblasts are responsible for the production of the bone matrix by secreting type I collagen and the noncollagenous proteins of the bone matrix, regulate the mineralization and produce different growth factors. They are characterized by a large nucleus, enlarged golgi and extensive endoplasmic reticulum. An early marker of osteoblast phenotype is alkaline phosphatase; osteocalcin, osteopontin and bone sialoprotein are markers of the mature osteoblast (Aubin et al., 2006).

Osteocytes are terminally differentiated osteoblasts within the bone matrix which support bone structure and metabolic functions. On the one hand, osteocytes have the capacity to synthesize bone and regulate the deposition of mineral, on the other hand they also function in osteolysis and resorb bone matrix to a limited extent. They are characterized by filopodial processes which allow them to communicate with adjacent cells such as other osteocytes, surface osteoblasts or lining cells to regulate bone formation and resorption and respond to physiological signals (Bonewald, 2007).

Bone lining cells are inactive cells that cover bone surfaces and exert a protective function. They are neither undergoing bone formation nor resorption and very little is known regarding function and origin of these cells (Aubin et al., 2006).

Osteoclasts are large, multinucleated cells which are the exclusive bone resorbing cells. The two cytokines, RANKL and M-CSF, are essential and sufficient for basal osteoclastogenesis (Väänänen and Laitala-Leinonen, 2008). During bone resorption, the osteoclast adheres to bone through the integrin αvβ3 and generates two polarized structures which mediates the resorptive process: the sealing zone and the ruffled border. The sealing zone surrounds the ruffled border and serves as the point of attachment of the osteoclast to the underlying bone matrix. Exocytosis of intracellular vesicles inserts a vacuolar H^+-ATPase into the bone-opposed ruffled border membrane for proton extrusion and leads to the secretion of proteases (cathepsin K, MMP9, MMP13) responsible for the degradation of bone organic matrix (Ross, 2006).

1.1.3 Bone remodeling

The term bone remodeling describes a process whereby the human skeleton is constantly renewed by the coupling of bone formation and bone resorption. This process maintains the mineral homeostasis of the bones, regulates the gain and loss of bone mineral density in the adult skeleton and preserves bone strength by replacing old bone by new, mechanically strong bone. The bone mass changes with age due to different bone turnover rates which is very high during growth (Mundy, 1999). Consequently, bone mass reaches a peak in young adult life until 30 years and then steadily declines in both men and women (age-related bone loss and osteoporosis) (chapter 1.3). The remodeling cycle consists of four different phases: activation, resorption, reversal and formation (Fig. 1) and occurs at the so-called “basic multicellular units” (BMU), a group of cells that collaboratively accomplish the remodeling (osteoclasts, osteoblasts) (Mundy, 1999). Remodeling activation describes the conversion of a previously quiescent region of bone surface to a remodeling one, a process requiring recruitment of new osteoclasts. Consequently, bone remodeling is initiated by an increase in osteoclast activity by recruitment of mononucleated osteoclast precursor cells from the monocyte-macrophage lineage in the circulation and subsequent fusion of the mononuclear cells to form multinucleated preosteoclasts. Osteoclast formation, activation and resorption is regulated by the ratio of RANKL to OPG, IL-1, IL-6, colony-stimulating factor (CSF), parathyroid hormone (PTH), 1,25-dihydroxyvitamin D and calcitonin (Blair and Athanasou, 2004; Boyle et al., 2003). During the resorption phase, the mineral and organic phases of the matrix are digested by several lysosomal enzymes such as TRACP and cathepsin K as well as matrix metalloproteinases (MMP-9) which are all active at low pH (Delaisse et al., 2003). Due to acidification of the resorbing compartment by proton pumps in the osteoclast membrane, the pH in the resorption lacunae is around 4.5 (Silver et al., 1988) which helps mobilize bone mineral. The resorption process ends with osteoclast apoptosis and is followed by a reversal phase in which osteoblasts are recruited into the resorption cavities so that bone resorption can transition to bone formation. Formation is characterized by increased attraction and proliferation of osteoblast precursors followed by the

differentiation into mature osteoblasts which synthesize organic matrix, replace the bone that has been removed and regulate its mineralization. When matrix-formation is completed most of the osteoblasts die by apoptosis, the remainder are incorporated into the matrix as osteocytes or on the surface as bone-lining cells (Sims and Gooi, 2008).

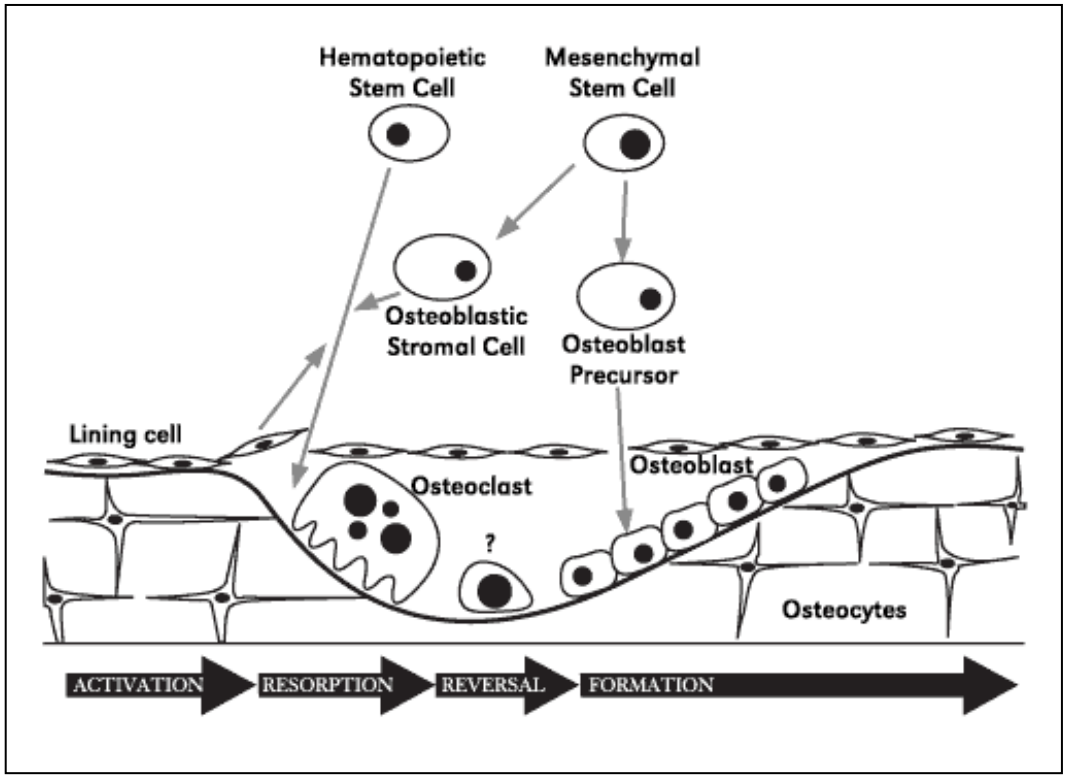

Figure 1. Bone remodeling process. The sequence of activation, resorption, reversal and formation is illustrated. Bone remodeling is initiated by differentiation of osteoclast precursors into mature multinucleated osteoclasts which are activated for bone resorption. This phase is followed by a reversal phase characterized by increased attraction and proliferation of osteoblast precursors which differentiate into mature osteoblasts to repair the resorption defects caused by osteoclasts. After bone formation some of the osteoblasts are incorporated into the bone matrix as bone-lining cells or osteocytes.
(from: http://www.surgeongeneral.gov/library/bonehealth/chapter_2.html)

1.1.4 Biochemical markers of bone turnover

Biochemical markers of bone turnover are released into the circulation during the process of bone formation and resorption and thus can be divided in two classes: bone resorption and bone formation markers. They are used to assess changes in bone turnover for example in patients with known or suspected osteoporosis or bone metastases and also to monitor therapy (Camacho and Kleerekoper, 2006).

A useful marker of bone resorption and osteoclast number is the tartrate-resistant acid phosphatase 5b (TRACP 5b) (Halleen et al., 2000). TRACP circulates in two different forms in human blood. TRACP 5a is expressed in macrophages and dendritic cells, whereas TRACP 5b is derived from osteoclasts (Halleen et al., 2006). At acidic pH, TRACP 5b functions as a phosphatase and destroys matrix degradation products in transcytotic vesicles of the osteoclast (Halleen et al., 1999). At low pH, TRACP 5b is reported to generate reactive oxygen species (ROS) to finalize the degradation of organic bone matrix components (Vääräniemi et al., 2004).

Another bone resorption marker which can be measured in both serum and urine is the carboxyterminal cross-linked telopeptide of type I collagen (CTX-I). CTX-I is a degradation product of type I collagen and can be measured by specific immunoassays (Herrmann and Seibel, 2008).

Widely used bone formation markers are for example osteocalcin (OC) and procollagen type I propetide (PINP) which can be measured in serum or plasma. OC is a non-collagenous protein secreted by osteoblasts and its levels correlate with bone formation rates (Camacho and Kleerekoper, 2006). PINP derives from type I collagen and is released from the amino- and carboxyterminal parts of the procollagen molecule during collagen synthesis (Delmas et al., 2000).

1.2 Bone metastasis

1.2.1 Background and significance

Metastatic dissemination is the major cause of mortality in all cancer patients. After lung and liver, bone is one of the three most common sites of cancer metastasis. Bone metastasis occurs frequently with nearly all cancers but some cancers, especially breast and prostate, have a special predilection for the skeleton (Kingsley et al., 2007). Metastasis to bone is clinically and biologically a critically important step in tumor progression. First, breast cancer is typically incurable after it has metastasized to bone. Second, bone metastases can increase the rate of metastatic progression and generate novel metastases, also in soft tissues. Third, patients with metastatic cancer suffer from bone destruction and the associated pain, hypercalcemia, fracture and nerve compression syndromes (Kozlow and Guise, 2005; Mundy, 2002). It is therefore crucial to understand the molecular mechanisms of bone metastasis, as well as develop intervention strategies that would enable a more aggressive approach to prevent the development of bone metastases as well as to treat established metastatic lesions.

1.2.2 Breast cancer bone metastasis

Bone is the most common site for a distant metastasis in women with breast cancer (Hortobagyi, 2002), with a reported incidence of up to 75% (Brown and Coleman, 2002; Coleman, 2001) and an average survival time of approximately 2 years after diagnosis (Coleman, 2001). Symptoms of bone metastases include skeletal complications, pathologic fractures, hypercalcemia and bone pain, which affects up to 80% of patients and greatly impacts on their quality of life (Cameron et al., 2006). In 1889, Stephen Paget proposed the “seed and soil” theory reflecting the high affinity of breast cancer cells to bone: “When a plant goes to seed, its seeds are carried in all directions; but they can only grow if they fall on congenial soil” (Paget, 1989). The seed is the cancer cell which can only grow on a congenial soil meaning particularly compatible areas of the body like the bone which is a storehouse of a variety of cytokines and

growth factors and thus provides an extremely fertile environment for the cells to grow. Furthermore, the SDF-1/CXCR4 axis is involved in cancer cell chemoattraction. The chemokine receptor CXCR4 is highly expressed in human breast cancer cells, malignant breast tumors and metastases whereas its ligand, SDF-1, is expressed in organs to which tumor cells preferentially metastasize, such as lymph nodes, lung, liver and bone marrow thus leading to a directional migration of cancer cells along a gradient of chemokines (Dewan et al., 2006; Müller et al., 2001).

Primary breast tumors express osteolytic and osteoblastic factors, stimulating different types of bone metastases, with osteolytic lesions occurring more commonly (Guise et al., 2005; Käkönen and Mundy, 2003). In the normal adult skeleton the processes of bone resorption and bone formation are approximately balanced and there is no major net gain or net loss of bone. The adult skeleton is rather in a dynamic state, being continually broken down and reformed by the coordinated actions of osteoclasts and osteoblasts as explained in chapter 1.1.3. The development of osteolytic bone metastases has been described as a vicious cycle (Fig. 2), with increased osteoclast activity implicated as the predominant mechanism of bone destruction (Käkönen and Mundy, 2003). The metastasis of tumor cells is not a random event that is solely determined by blood flow. It is rather a directed and multi step process that is dependent on factors in the bone microenvironment that favor metastasis. Tumor cells in bone produce factors, such as parathyroid hormone-related protein (PTHrP), which are responsible for an increase of osteoclast activity, and consequent bone resorption (Guise, 1997; Guise et al., 1996). PTHrP then increases the expression of the receptor-activated NF-κB ligand (RANKL) in osteoblasts. Simultaneously, the production of osteoprotegerin (OPG), a soluble decoy receptor for RANKL, is down-regulated. RANKL in turn binds to its receptor RANK in osteoclasts and enhances osteoclast activity. During osteoclastic bone resorption, bone-derived growth factors, such as TGF-β (transforming growth factor-β), are released and increase tumor production of osteolytic factors such as PTHrP. These factors again increase osteolysis by stimulating osteoclast function, thus perpetuating the vicious cycle. In summary, the predominant mechanism of bone resorption is an

increase in osteoclast activity. However, the presence of PTHrP is not sufficient for cancer cells to metastasize to bone. There are many other mediators of the vicious cycle that tumor cells produce and that act on bone cells and other cells in the bone microenvironment, such as interleukins (IL-11, IL-8, IL-6) which have been found to increase osteoclast activation (Bendre et al., 2003; Girasole et al., 1994; Manolagas, 1995) or vascular endothelial growth factor (VEGF) which plays an important role in angiogenesis (Dvorak, 2002). In addition to TGF-β, other bone-derived growth factors are probably involved in this process, namely bone morphogenetic proteins (BMPs), platelet-derived growth factors (PDGFs), and insulin-like growth factors I (IGF-1) and II (IGF-2) (Yin et al., 2005). All in all, the crosstalk between tumor cells and the bone microenvironment occurs via multiple factors and signaling pathways. However, the factors most important for promoting the vicious cycle differ between tumor types and even within one tumor histiotype. Whereas PTHrP, as mentioned, plays a central role in osteolytic breast cancer bone metastasis, endothelin-1 (ET-1) has been shown to promote osteoblastic breast cancer bone metastasis (Kingsley et al., 2007). On the other hand, the Wnt signaling pathway is dominant in prostate cancer bone metastasis and the EGF-R and TGF-βR pathways have a major role in RCC bone metastasis (Weber et al., 2007; Dai et al., 2008) (chapter 1.2.3). Despite a profound knowledge of the mechanisms of bone metastasis, not all signaling pathways and growth factors have been discovered yet.

The increase in osteoclast activity and osteolysis is associated with an increase in bone resorption markers, such as TRACP 5b (tartrate resistant acid phosphatase 5b). TRACP 5b is expressed in and secreted by bone-resorbing osteoclasts and serum TRACP 5b is therefore considered to be a useful marker of bone resorption rate (Halleen et al., 2000) as well as a diagnostic marker to monitor bone metastasis (Chao et al., 2005).

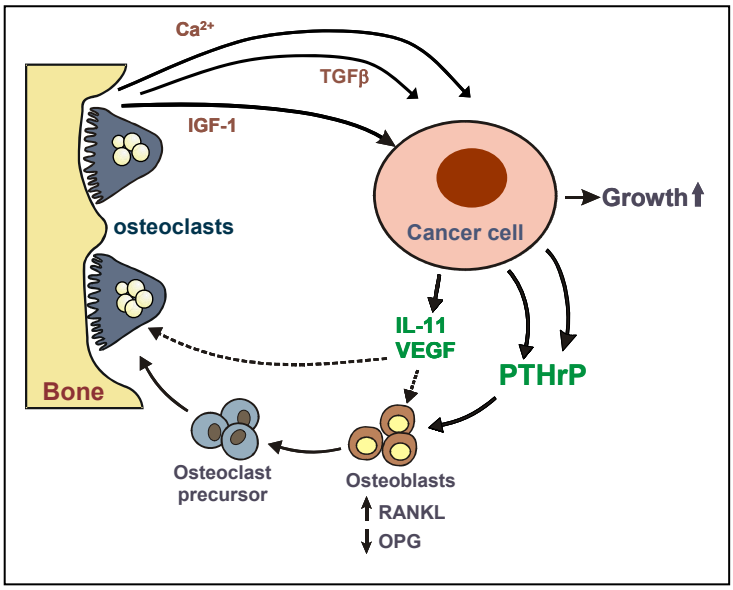

Figure 2. Vicious cycle of breast cancer bone metastasis. Tumor-produced factors such as PTHrP, IL-11 or VEGF stimulate osteoclast differentiation via RANKL and consequently induce osteoclastic bone resorption. During bone resorption, bone-stored growth factors are released, such as TGF-β and IGF-1. TGF-β induces the production of IL-11, VEGF and PTHrP of tumor cells. IGF-1 stimulates breast cancer cell growth (Käkönen and Mundy, 2003).

1.2.3 Renal cell cancer bone metastasis

About one third of patients with renal cell carcinoma (RCC) develop metastatic disease (Figlin, 1999). RCCs most commonly metastasize to lung, bone, liver and brain (Zekri et al., 2001). Approximately 35% of patients with metastases have skeletal complications causing pathologic fractures, nerve compression syndromes, severe pain and hypercalcemia (Galasko, 1981; Zekri et al., 2001). Bone metastasis in renal cell cancer is becoming more prevalent because survival times among patients with disseminated cancers are increasing due to advances in targeted therapy of RCC. In a phase III trial, the tyrosine kinase inhibitor sunitinib demonstrated statistically significant improvement in progression-free survival compared to interferon-α (IFN-α), a previous standard therapy for patients with metastatic RCC (Pickering et al., 2009). RCC tumors are highly vascular (Durr et al., 1999; Iwai et al., 2004; Takahashi et al., 1994) and mainly cause destructive, osteolytic lesions in bone. As they are relatively radio- and chemoresistant (Motzer and Russo, 2000), it is important to identify targets to prevent tumor cell growth and simultaneously the activation of osteoclasts by tumor cells.

However, so far very little is known about the molecular mechanism of skeletal metastases of RCC. The molecular pathways involved in RCC bone metastasis are presumably not the same as those identified in breast and prostate cancer bone metastasis (Weber et al., 2007). Epidermal growth factor receptor (EGF-

R) and transforming growth factor receptor-β (TGF-βR) pathways are suggested to be most important for RCC stimulated osteoclast-mediated bone destruction (Kominsky et al., 2007; Mydlo et al., 1989; Weber et al., 2002). In addition, there is evidence that TGF-α and EGF stimulate bone resorption by increasing the proliferation of osteoclast precursors which in turn increases the number of osteoclasts (Takahashi et al., 1986). Because of the hypervascularity noted clinically, it is reasonable to assume that pro-angiogenic factors are present in these tumors such as VEGF, basic FGF or IL-8 (Durr et al., 1999). Another factor known to be a predictor of the metastatic potential of RCC is CXCR4 which expression on human RCC correlated with the metastatic ability in both heterotopic and orthotopic SCID mouse models (Pan et al., 2006).

1.2.4 Animal models of bone metastasis

To better understand the process of bone metastasis, to identify targets for potential treatments to inhibit bone metastasis and to test the efficacy of the developed drug compounds many animal models have been developed. Since spontaneous bone metastasis in animals is uncommon, most animal models of bone metastasis must be experimentally derived (Rosol et al., 2003). Besides chemical induction of cancers in selected strains of rats and mice, commonly used models of bone metastasis are xenografts of tumors or cell lines derived from human cancers into immunodeficient mice. These are either injected subcutaneously, into the left cardiac ventricle or directly into bones such as tibia or femur. The inoculation of human cancer cell lines into the left cardiac ventricle of immunodeficient mice has been a routinely used technique to induce bone metastasis *in vivo* (Guise, 2000; Rosol, 2000; Yoneda et al., 2000). A widely used experimental mouse model of bone metastasis to study the molecular mechanisms of breast cancer bone metastasis and reveal new targets for therapy uses human MDA-MB-231 breast cancer cells which are inoculated into the left cardiac ventricle of female athymic nude mice (Yin et al., 1999). These mice develop osteolytic bone metastasis similar to that observed in humans with breast carcinoma occurring frequently in the spine, ribs, pelvis, proximal tibia and humerus and distal femur. Furthermore, several orthotopic

models are available in which tumor cells are implanted for example into the mammary fat pad, lungs or prostate gland (Iwasaki et al., 2002; Yang et al., 1999; Yoneda et al., 2000). The site and occurrence of metastasis and the nature of the lesions vary depending on the biological properties of the cancer cell line. The disadvantage of the intracardiac injection model is the uncertain pathogenesis of bone metastasis after left ventricular injection of tumor cells. Many metastases occur in the metaphyses of the long bones which are sites of active bone modeling and remodeling in young mice. Metabolically active areas of the bone, especially metaphyseal bone, are well-vascularized due to their proximity to the blood supply and allow various cells to easily enter and exit (Mundy and Guise, 2000). Thus, they are attractive sites for metastatic cancer cells.

In contrast to human xenografts which can only be used in nude animals, some syngeneic models of bone metastasis are available. These models consist in injecting tumor cells in a host animal of the same species as the tumor cells (allografts). The main disadvantage is that tumor cells are rodent and express the mouse / rat homologues of the desired targets which can be a limiting factor especially for instance in antibody-targeted therapy; the advantage is the use of immunocompetent animals (Teicher, 2006). However, most of the syngeneic models of breast and prostate cancer in rats and mice do not metastasize to bone unless a more metastatic subline is generated by *in vivo* selection (Rosol et al., 2003). Suitable syngeneic models are for example the 4T1 orthotopic mammary fat pad model (Lelekakis et al., 1999) or the i.c. inoculation of the MATLyLu androgen-independent subline of the Dunning (R-3327) rat prostate adenocarcinoma in Copenhagen rats resulting in the development of osteolytic bone metastases (Blomme et al., 1999).

1.2.5 Small animal imaging of bone metastasis

Small animal imaging in cancer is a useful tool to monitor tumor progression and metastasis. Various small animal whole-body imaging technologies have been developed to follow tumor development and treatment response such as computed tomography (CT), positron emission tomography (PET), single photon emission computed tomography (SPECT), magnetic resonance imaging

(MRI), ultrasound imaging and optical imaging methods such as bioluminescence imaging (BLI) and fluorescence imaging. Depending on the specific application, certain imaging methods are more suitable than others. Whereas CT and MRI provide high resolution images of anatomical structures, PET and BLI are more valuable to localize tumor burden and metastasis. Compared to PET, SPECT and MRI, optical imaging technologies are relatively inexpensive and fast, thereby allowing moderate throughput analysis of a large number of animals. However, resolution and depth sensitivity are limiting factors of optical imaging (Kaijzel et al., 2007; Weissleder and Pittet, 2008).

Considering animal welfare, imaging tools are favourable and contribute to the 3R concept. The 3R concept was proposed by Russell and Burch in 1959 and represents a concept to refine, reduce and replace animals in experiments (Balls and Straughan, 1996). Replacement includes the use of non-animal methods such as cell cultures, human volunteers or computer modeling to achieve the defined scientific goal. Refinement includes the use of methods that alleviate or minimize pain, suffering or distress, to avoid fear and generally to improve animal welfare for those animals that cannot be replaced. Reduction means obtaining the best quality and most precise information with the smallest possible number of animals (Hagelschuer et al., submitted). Experiments that are well-designed and well-conducted deliver reliable results, and eliminate the need for endless repetition of the same tests. This includes the use of methods that enable researchers to obtain more information from the same number of animals.

1.2.5.1 Bioluminescence imaging (BLI)

Whole-body non-invasive BLI is applied for the detection of tumor growth and metastasis in small animals. The luciferase (*luc)* gene from the North-American firefly *Photinus pyralis* is the most widely used bioluminescence reporter in life science research which can be inserted into tumor cells making them applicable for BLI. The basic principle for creating luminescent light is that luciferase, which acts as a catalyst in the presence of oxygen and ATP, converts chemical luciferin into oxyluciferin releasing light in this process (Fig.

3). The substrate D-luciferin is either injected i.v. or i.p., distributes rapidly throughout the body of the animal and is quickly taken up by the cells. The emitted light is detected by a cooled charged coupled device camera (CCD) and has a wavelength from 500 to 620 nm which is sufficient to penetrate small animal tissue (Helms et al., 2006; Sato et al., 2004).

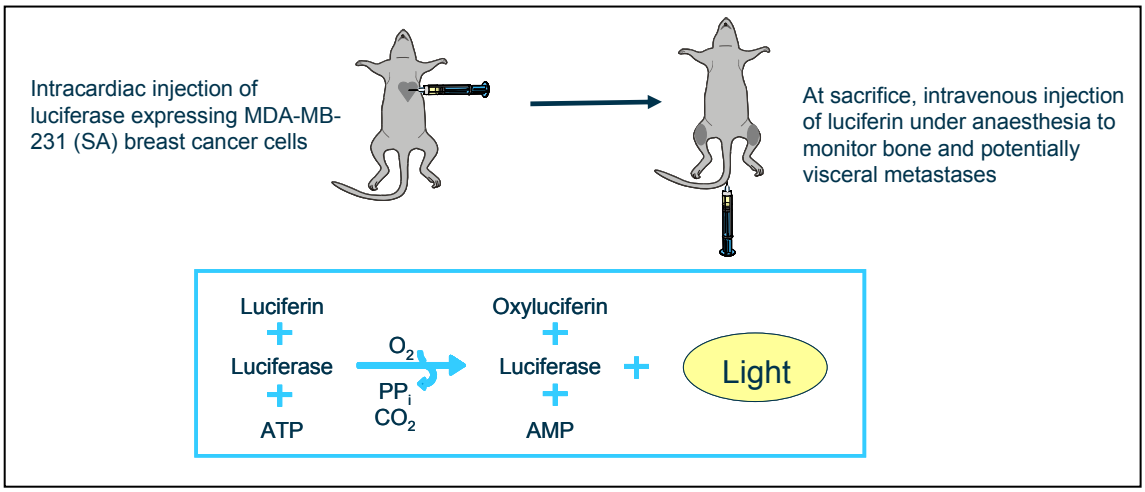

Figure 3. Bioluminescence imaging. After i.c. injection of luciferase expressing MDA-MB-231 (SA) breast cancer cells, metastases grow in bone and can be detected by BLI following i.v. injection of luciferin. The enzyme luciferase catalyzes the conversion of its substrate luciferin into oxyluciferin in the presence of oxygen and ATP. During this process light is emitted that can be detected by a cooled charged coupled device camera.

1.2.5.2 Computed tomography (CT) and radiography

Both plain radiography and CT are X-ray based methods and provide information about bone structure in a two- and three-dimensional manner respectively. However, micro-CT more accurately reflects the morphological changes in bone as its resolution is about ten times greater than radiography and additionally offers the ability to obtain axial images. Thus, micro-CT allows an easier characterization of lesions as osteolytic, osteoblastic or mixed. However, quantitation of bone volume from micro-CT data is very time-consuming whereas the determination of lesion area from radiography scans is a reliable method allowing for the measurement of a large number of animals in a moderate time (Paulus et al., 2000; Ritman, 2004).

1.2.5.3 Positron emission tomography (PET)

PET is a nuclear medicine imaging modality making it possible to visualize the uptake and accumulation of positron-emitting radiopharmaceuticals by tissues. A widely used PET-tracer is ^{18}F-fluorodeoxyglucose (^{18}F-FDG) which is taken up by the cells like glucose but is then metabolically trapped in the cell after phosphorylation by hexokinase and accumulates due to an enhanced glucose metabolism in tumor cells. Thus, PET imaging is especially useful to detect metastases in soft tissues or bone. However, the disadvantages of PET are high costs and long scanning times (Mittra and Quon, 2009).

For skeletal metastases, ^{18}F-fluoride, a bone-imaging agent, can be employed which uptake is not specific for tumoral bone involvement but deposits at sites of high bone turnover and remodeling. The ^{18}F-fluoride ion is exchanged by an hydroxyl group in the hydroxyapatite crystal, thereby forming fluoroapatite. It is reported that ^{18}F-fluoride has a high lesion-to-normal bone ratio and especially accumulates in lytic and sclerotic lesions (Cook and Fogelman, 2001; Petren-Mallmin et al., 1998).

There are also integrated systems available allowing the fusion of PET and CT images, thus providing improved diagnostic accuracy in detecting tumors and metastases simultaneously (Mittra and Quon, 2009).

1.2.5.4 Single-photon emission computed tomography (SPECT)

SPECT is a nuclear medicine modality used in many areas of radionuclide imaging because of its ability to image in 3 dimensions. High energy emitting molecules are administered to the patient which differentially accumulate in tissue based on its cellular physiology. The distribution of radiotracers in humans can be quantified by SPECT (Frangioni, 2008). In contrast to the radioisotopes used in PET imaging which emit a positron which results in the generation of two 511 keV photons (γ-rays) after an annihilation reaction with an electron, SPECT utilizes isotopes that are direct gamma emitters in one direction such as 99m-technetium (^{99m}Tc) or 123-iodine (^{123}I). Moreover, SPECT imaging is less sensitive than PET (Helms et al., 2006). With respect to the detection of bone metastases, it could be shown that a ^{18}F-fluoride bone scan

by PET is more sensitive than SPECT (Even-Sapir et al., 2006). The fusion of SPECT/CT improves the assessment of possible bone metastasis (Utsunomiya et al., 2006).

1.2.6 Therapeutic interventions against osteolytic bone metastases

The quality of life of breast cancer patients could be considerably increased by a potent inhibitor of bone metastasis (Lipton, 2006), and a drug that could simultaneously and effectively inhibit both tumor cell growth and osteoclast activity would have great potential in the treatment of these patients, especially because currently all therapies are only palliative for advanced metastatic breast cancer patients. Due to the multifactorial process of bone metastasis various targets for therapeutic intervention are possible. Currently approved drugs for the treatment of bone metastasis include the bisphosphonates clodronate (Bonefos®, Bayer Schering Pharma AG, approved in 2004 by the United States Food and Drug Administration), zoledronate (Zometa®, Novartis, approved in 2002 by the United States Food and Drug Administration) and pamidronate (Aredia®, Novartis, approved in 1995 by the United States Food and Drug Administration).

1.2.6.1 Bisphosphonates (BPs)

BPs are recommended as the gold standard therapy for breast cancer with bone metastases. They are potent inhibitors of osteoclast-mediated bone resorption and are effective in reducing skeletal complications such as bone pain, hypercalcemia or pathologic fractures. Not only patients with bone metastasis but also with other osteoclast-activating diseases benefit from the anti-resorptive action of BPs such as Paget´s disease, osteoporosis, myeloma or hypercalcemia of malignancy (Coleman, 2008). BPs adsorb strongly to hydroxyapatite crystals, are internalized by osteoclasts and interfere with specific biochemical processes in osteoclasts. Their strong affinity for bone mineral is due to their molecular structure. BPs are analogs of pyrophosphate that contain a carbon instead of an oxygen atom (Fig. 4). BPs can chelate calcium ions by bidentate coordination through the oxygen atoms of the

phosphonate group and can be divided in two classes with different mode of action: nitrogen-containing BPs (for example zoledronic acid (ZOL), alendronate, risedronate) and non-nitrogen-containing BPs (for example clodronate, etidronate).

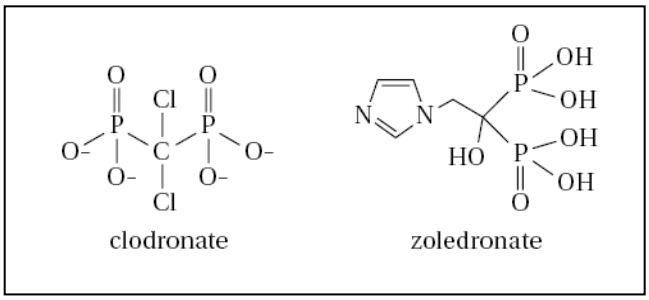

Figure 4. Structure of the bisphosphonates clodronate and zoledronate (ZOL). Clodronate belongs to the so-called first-generation BPs whereas ZOL is a highly potent third-generation BP (structures from Rogers et al., 1997).

Non-nitrogen-containing BPs can be incorporated into toxic, non-hydrolyzable ATP analogues which accumulate within osteoclasts, inhibit their function and induce apoptosis by inhibiting the mitochondrial adenine nucleotide translocase (ANT) (Lehenkari et al., 2002). In contrast, the more potent N-containing BPs interfere with the mevalonate pathway by inhibiting the farnesyl diphosphate synthase, thereby preventing the prenylation (lipid modification) of small GTPases (such as Rho, Ras, Rac and Rab) which are signaling proteins essential for the adequate function and survival of osteoclasts (Rogers et al., 1997). However, it was reported that N-containing BPs induce the formation of a novel pro-apoptotic ATP analogue, ApppI (1-adenosin-5´-yl-ester 3-(3-methylbut-3-enyl) ester triphosphoric acid) (Mönkkönen et al., 2006). ApppI has been shown to inhibit the ANT, comparable to the metabolites of the non-N-containing BPs, thus causing apoptosis in osteoclasts. The formation of ApppI by ZOL was recently confirmed in osteoclasts *in vivo* suggesting that ApppI is a biologically important molecule in the action of N-BPs (Räikkönen et al., 2009). At present, BPs are mainly used as palliative treatment for improving the quality of life of patients with bone metastases. ZOL is the most potent BP currently available in inhibiting osteoclast-mediated bone resorption in both *in vitro* and *in vivo* preclinical models (Green, 2005). In clinical trials, zoledronate also showed superior efficacy compared to pamidronate in the treatment of hypercalcemia of malignancy, a serious complication of cancer that affects patients with and without bone metastases (Major et al., 2001). Clodronate

(Bonefos®, Bayer Schering Pharma AG), the leading oral bisphosphonate globally in the malignant indication, was also shown to significantly reduce the risk of bone metastases by 45% after 2 years of treatment (Powles et al., 2004). However, the effect of BPs on tumor cell growth inhibition are still controversial (Coleman, 2007). A frequently occurring side effect after prolonged treatment with BPs is osteonecrosis of the jaw (ONJ) which is defined as “exposed bone in the mandible, maxilla or both that persists for at least 8 weeks, in the absence of previous radiation and of metastases in the jaws” (Rizzoli et al., 2008). The incidence of ONJ is unknown. A proposed mechanism suggests that BPs induce low bone turnover by inhibition of osteoclasts leading to decreased blood flow, bone cell necrosis and apoptosis. In conjunction with infection, this can cause the development of exposed bone in the mouth (Rizzoli et al., 2008).

1.2.6.2 Microtubule stabilizers

Among the most commonly prescribed anticancer drugs are compounds that target microtubules. Microtubules are found in all eukaryotic cells and are components of the cytoskeleton with various functions including the organization of the intracellular structure, cell division and intracellular transport. They are dynamic polymers that consist of two closely related globular proteins, α- and β-tubulins, which form heterodimers. Microtubule assembly is accompanied by hydrolysis of GTP associated with β-tubulin. A dynamic equilibrium exists between the intracellular pool of α,β-tubulin heterodimers and the microtubule polymer (Morris and Fornier, 2008). This equilibrium is the target for microtubule-disrupting agents, such as the taxanes and epothilones. Both compound classes bind to the β-tubulin subunit in the interior of the microtubule (Nogales et al., 1995) and are more susceptible to rapidly dividing cells like tumor cells than slowly dividing cells. An essential part of normal microtubule function at mitosis is the formation of the mitotic spindle, which allows for cell division and replication (Mitchison, 1988). Binding of microtubule stabilizing agents results in a disturbance of the dynamic equilibrium of the microtubules and spindle dysfunction leading to a mitotic block and inhibition of the proliferation of tumor cells. More precisely, the

dynamics of the mitotic spindle are disrupted resulting in an arrest of tumor cells in mitosis such that the cells cannot proceed from metaphase to anaphase (G2/M-arrest of the cell cycle) and die via apoptosis.

1.2.6.2.1 Paclitaxel

A commonly used drug in the treatment of metastatic breast cancer is the taxane paclitaxel (Fig. 5), which, like other microtubule-stabilizing agents, inhibits tumor cell division by inducing a mitotic block at the metaphase-anaphase transition, thereby leading to apoptosis (Horwitz, 1992).

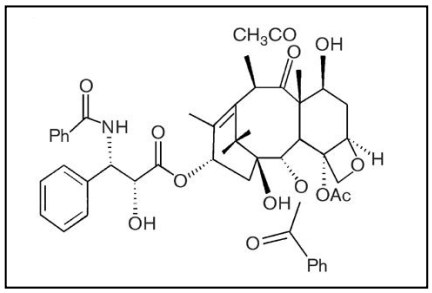

Figure 5. Chemical structure of paclitaxel. Paclitaxel can be synthesized from the needles of the European yew tree *Taxus baccata* (structure from (Mani et al., 2004).

However, the usefulness of especially the taxanes is limited by the development of drug resistance (Horwitz et al., 1993), and response rates of bone metastases in breast cancer patients to single-agent paclitaxel range from 0 to 30% (Abrams et al., 1995; Kim et al., 2003), although there are few detailed reports in the literature. Drug resistance is primarily due to over-expression or activation by the drug efflux pump, P-glycoprotein (P-gp), encoded by the *mdr1* gene (Dumontet and Sikic, 1999; Melton, 2001). Secondly, point mutations in β-tubulin can cause drug resistance by altering drug binding and the equilibrium of the tubulin dimer and microtubulin polymer (Giannakakou et al., 1997; Hari et al., 2006).

1.2.6.2.2 Sagopilone (ZK-EPO)

The epothilones isolated from myxobacteria comprise a novel class of microtubule stabilizers that are structurally distinct from the taxanes, yet have similar mechanisms of action, leading to cell cycle arrest and apoptosis. Certain epothilones, however, are less susceptible to P-glycoprotein-mediated efflux mechanisms than the taxanes. However, natural epothilones are not optimal

candidates for anticancer therapy due to limitations in therapeutic index and poor tolerability (Chou et al., 2001; Kamath et al., 2005; Lichtner et al., 2001). Sagopilone (ZK-EPO), the first fully synthetic epothilone in clinical development (Fig. 6), was rationally designed to overcome limitations of other microtubule stabilizers (Klar et al., 2006): Sagopilone is not a substrate of P-gp efflux pumps leading to more efficient retention in tumor cells and increased antiproliferative effects, it is water-soluble favouring formulation, it is able to cross the blood-brain barrier in humans and it is active in taxane-resistant models *in vitro* and *in vivo* (Alexander, 2008). In addition to its rapid cellular uptake, it could be shown that sagopilone almost fully localized to the nuclear/cytoskeletal fraction whereas paclitaxel appears to preferentially accumulate in the cytosolic fraction in all cell types examined in one study (Klar et al., 2008). However, the clinical relevance of this observation is unknown.

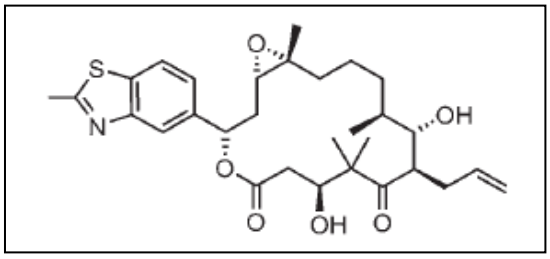

Figure 6. Chemical structure of sagopilone. Sagopilone is a fully synthetic analogue of epothilone B designed to combine high activity of natural epothilones with a low side effect profile (structure from Klar et al., 2008).

Like other microtubule stabilizers it binds to the β-tubulin subunits of the cellular microtubule network (Klar et al., 2006), thereby stabilizing microtubules and inhibiting the dynamic instability of the microtubule spindle, crucial for chromosome segregation during mitosis, leading to cell cycle arrest followed by the activation of the mitochondrial apoptotic pathway (Hoffmann et al., 2008). Proteins of the Bcl-2 family have been identified as major regulators of sagopilone induced cell death (Hoffmann et al., 2008). Sagopilone has shown *in vitro* and *in vivo* activity at sub-nanomolar concentrations (IC_{50} < 1 nM) with balanced tolerability against a broad range of tumor models, including superior activity compared with paclitaxel in many breast cancer cell lines (Hoffmann et al., 2008; Klar et al., 2006), suggesting that sagopilone may have potential in the treatment of breast cancer. The activity of sagopilone is currently examined in phase II of clinical trial program throughout North America and Europe in patients with various solid tumors, including metastatic breast cancer, lung

cancer and ovarian cancer. The ability of sagopilone to cross the blood brain barrier and leading to highly effective, well-tolerated levels of the drug in the brain tissue as shown in preclinical studies (Hoffmann et al., 2009) has led to phase II studies in patients with recurrent glioblastoma and brain metastases. In terms of safety and tolerability, observations suggest that sagopilone has manageable toxicities, neuropathy in particular (Schmid et al., 2005).

1.2.6.3 RANK ligand inhibition

RANKL is a mediator in the vicious cycle of bone metastasis as well as a mediator for osteoclast differentiation, survival and function in general exerting its effects by binding to its receptor RANK on the surface of osteoclasts and osteoclast precursors. OPG, a soluble decoy receptor of RANKL, blocks the RANK/RANKL interaction, thereby inhibiting and modulating bone resorption (Dougall and Chaisson, 2006). Denosumab (Amgen Inc, Thousand Oaks, CA, USA), a fully human monoclonal antibody with high affinity and specifity for RANKL, was developed to treat patients with bone loss caused by bone metastases, multiple myeloma or osteoporosis. Preclinical studies showed that denosumab mimics the effect of OPG on bone density and turnover. Denosumab is currently in phase III of clinical trial program for the treatment of bone loss in postmenopausal women as well as in patients with bone metastases (Lipton et al., 2007; Bone et al., 2008).

1.2.6.4 Cathepsin K inhibitor

Cathepsin K is a lysosomal cysteine protease which is expressed in osteoclasts and degrades type I bone collagen. Thus, cathepsin K is a novel therapeutic target which inhibition leads to antiresorptive effects as shown in preclinical models of osteoporosis (Le Gall et al., 2008). Odanacatib, a selective cathepsin K inhibitor (Merck & Co. Inc, Whitehouse Station, NJ, USA) given orally, showed reduced measures of bone turnover in a phase II trial of patients with bone metastases (Gauthier et al., 2008). A phase III trial to determine efficacy of odanacatib in patients with osteoporosis in postmenopausal women is underway.

1.3 Osteoporosis

1.3.1 Pathogenesis of osteoporosis

Osteoporosis is a metabolic bone disease characterized by low bone mass, deterioration in bone microarchitecture and increased fracture risk making this disease to a major public health problem. Fractures predominantly occur in the vertebral bodies, in the hip and in the femoral neck which is the most serious and life-threatening complication. In addition to fractures, the most common clinical problem is severe pain, particularly in the vertebrae. A decrease in bone mineral density (BMD) occurs in all individuals after middle life (Cooper, 2003; Raisz, 2005). The major reasons for this age-related bone loss are sex hormone deficiency, disuse, calcium and vitamin D deficiency. All these factors contribute to changes in bone cell activity during bone remodeling finally inducing the decrease in BMD. Especially sex hormone deficiency makes the disease more prone to females than to males due to abrupt cessation of ovarian function in the menopause (Eastell, 2003). Not only elderly people suffer from osteoporosis (senile or postmenopausal osteoporosis), aggressive and with high bone-turnover associated osteoporosis can also occur in male or female during adolescence or in the 20s (juvenile osteoporosis) (Norman, 2003). The most widely used methods for evaluating bone mass is dual energy X-ray absorptiometry (DEXA) measuring volumetric bone density but also peripheral quantitative computed tomography (pQCT) which can distinguish between trabecular and cancellous bone (Kanis, 2003).

1.3.2 Mechanism and treatment of osteoporosis

The mechanism of osteoporosis is based on an increase in the rate of remodeling as well as an imbalance between osteoblast and osteoclast activity and finally results in irreversible bone loss. The factors for age-related bone loss are manifold. Both men and women, especially housebound elderly, show vitamin D deficiency which reduces intestinal calcium absorption (Eastell, 2003). This in turn results in an increased PTH secretion causing increased bone turnover und subsequent bone loss. Moreover, decreased physical activity and decreased secretion of growth hormones cause impaired

osteoblast function and thereby bone loss. The pathogenesis of menopausal bone loss is associated with an increased secretion of the cytokines IL-1, IL-6, TNF and macrophage colony stimulating factor (M-CSF) by monocytes and marrow stromal cells which additionally secrete RANK ligand (Pacifici, 1996). The increased cytokine activity results in increased bone resorption by recruitment and activation of osteoclasts. These effects can be compensated by estrogen replacement therapy which is reported to increase BMD and decrease skeletal fragility (Delmas, 1997). An alternative to hormone replacement therapy are SERMs (selective estrogen receptor modulators) such as raloxifene which is the first SERM available worldwide for the treatment of osteoporosis (Delmas, 2003). These compounds bind to the estrogen (ER) receptor exerting estrogen agonistic or antagonistic activity depending on the type of estrogen-responsive tissue. In bone, they exert estrogenic action preventing postmenopausal bone loss and reducing fracture risk. However, the compounds of choice for most patients with osteoporosis are bisphosphonates such as alendronate which was the first BP approved for use in osteoporosis in 1995 (Watts, 2003). As described in chapter 1.2.6.1, BPs reduce osteoclastic bone resorption. Their benefit for patients suffering from osteoporosis is that they increase BMD, reduce the risk of vertebral fractures even in patients with established osteoporosis and are the only compounds shown to reduce hip fractures (Black et al., 1996; Tonino et al., 2000).

1.3.3 Animal models of osteoporosis

The rat is the most frequently used animal model of osteoporosis compared to monkeys, dogs and mice (Turner et al., 2001). It has been shown that ovariectomy (OVX) induces rapid bone loss in the proximal tibial metaphysis of rats and is consequently a good model for postmenopausal osteoporosis (Wronski et al., 1985). Similar but reversible bone loss can be induced by estrogen receptor antagonists (Gallagher et al., 1993). In mice, OVX also causes bone loss. Several studies report that mice lose a significant amount of bone mineral density 4 weeks after OVX (Alexander et al., 2001; Bouxsein et al., 2005). It was shown that a major cause for bone loss in mice after OVX is the enhanced T-cell production of TNF-α followed by induction of M-CSF- and

RANKL-mediated osteoclastogenesis (Cenci et al., 2000).

1.4 Aims of this work

Bone metastasis is an incurable disease considerably decreasing quality of life of patients with metastatic cancers of particularly breast, prostate, lung and renal cancer. In breast cancer, most current therapeutic approaches aim to interrupt the vicious cycle to inhibit growth of osteolytic bone metastases. As this cycle is a multi step process in which tumor cells, osteoclasts, osteoblasts and the organic bone matrix are involved, combination therapies that target different steps could be especially effective. However, current therapies are only palliative, not curative and mostly target either tumor cells or osteoclasts. Consequently, in addition to new treatment approaches, the need for animal models that are the basis for testing new developed drugs is high to better understand the molecular mechanisms of bone metastasis.

The focus of my work was to establish and characterize mouse models representative for breast and renal cell cancer bone metastasis. Especially for renal cell cancer metastasis there are only few models described in the literature. As a consequence, further understanding of the interactions between tumor and bone in RCC bone metastasis may help to identify targeted therapeutic interventions to halt tumor growth and bone metastasis. The same is true for breast cancer bone metastasis, although, in contrast, the mechanisms of osteolytic breast cancer bone metastasis have been extensively studied for example in a pre-clinical model by Yin et al., 1999, where human MDA-MB-231 breast cancer cells form bone metastases from the bloodstream when inoculated into the left cardiac ventricle of immunodeficient mice. Instead of the parental MDA-MB-231 cell line, a highly metastatic subline, MDA-MB-231 (SA), was used for intracardiac inoculations which was stably transfected with a firefly luciferase cDNA. The RCC model developed during this PhD thesis work also uses a luciferase labeled cell line (786-O/luc) making it possible in both models to longitudinally monitor tumor burden by bioluminescent imaging *in vivo*. In addition to BLI, other imaging modalities such as micro-CT, radiography or PET-imaging were applied for the characterization of both tumor burden and osteolytic bone destruction of the models with the supplemental aim to establish

those as tools for compound screening.

To test the effect of a promising drug candidate, to show suitability of the models for compound screening and the use of imaging modalities as screening tools, an efficacy study was performed with sagopilone, a fully synthetic epothilone in clinical development investigated by Bayer Schering Pharma AG, exemplarily for the MDA-MB-231(SA)/luc model. The compound, sagopilone, was selected as previous studies indicated high antiproliferative potency of this drug on tumor cells both *in vitro* and *in vivo* as well as antiresorptive effects on osteoclasts in preliminary *in vitro* studies. Thus, these characteristics are promising that sagopilone might be effective in treating bone metastasis by interruption of the vicious cycle on two different positions, on tumor cell and osteoclast stages. Such compounds are rare on the market. To verify that sagopilone as a microtubule stabilizer has not only antiproliferative effects on tumor cells but also a direct antiresorptive effect on osteoclasts, a mouse model of ovariectomy-induced osteoporosis was established to study the effect of sagopilone on bone loss in non-tumor bearing mice.

These studies should contribute to reveal sagopilone as a drug effective in patients with bone metastasis and possibly also in other diseases with increased bone resorption such as osteoporosis by investigating its role in bone metastasis mouse models and its potential in exerting direct effects on osteoclasts *in vitro* and *in vivo*.

2 MATERIALS AND METHODS

2.1 Cell lines and culture

2.1.1 MDA-MB-231 cell lines

The breast cancer cell line MDA-MB-231(SA), which strongly metastasizes to bone (Mbalaviele et al., 1996), was a gift from Professor T. Guise (University of Virginia, VA, USA). Cells were cultivated in high glucose DMEM (Biochrom AG, Berlin, Germany) containing 10% heat-inactivated FCS (Biochrom AG), 2% glutamine (PAA Laboratories GmbH, Pasching, Austria), and 1% non-essential amino acids (PAA Laboratories). Injection of the cells into the left ventricle of nude mice results in the development of bone metastases. For intracardiac inoculations, cells were trypsinized and resuspended in PBS (Biochrom AG) to a final concentration of 5 x 10^5 cells / 100 µL (preventive model, chapter 3.3.3.1). The parental MDA-MB-231 cell line (from ATCC (American Type Culture Collection), Manassas, VA, USA) which was used for *in vitro* proliferation and subcutaneous tumor growth studies (chapters 3.3.1 and 3.3.2) was cultivated in the same medium as the MDA-MB-231(SA) cell line. For the therapeutic model (chapter 3.3.3.2), a MDA-MB-231(SA)/luciferase (luc) cell line was generated by stable transfection of the parental MDA-MB-231(SA) cell line with a pRev CMV_Luc2 vector. These cells were cultured with 250 µg/mL hygromycin B (Invitrogen Ltd, Carlsbad, CA, USA) and inoculated intracardially at a concentration of 1 x 10^5 cells / 100 µL.

2.1.2 786-O cell line

The human renal carcinoma cell line 786-O/luc generated by stable transfection with a pRev_CMV_Luc2 vector was cultivated in RPMI medium (Biochrom AG, Berlin, Germany) containing 10% heat-inactivated FCS (Biochrom AG), 2% glutamine (PPA Laboratories GmbH, Pasching, Austria), 4.5 g/l glucose (Sigma-Aldrich Chemie GmbH, Taufkirchen, Germany), 10 mM HEPES (Biochrom AG), 1 mM pyruvate (Biochrom AG) and 50 µg/ml hygromycin B (Invitrogen Ltd, Carlsbad, CA, USA). For intracardiac injections, cells were harvested from

subconfluent cell culture flasks and resuspended in PBS (Biochrom AG) to a final concentration of 5 x 10^5 cells / 100 µl.

2.2 Animal models

2.2.1 Animals

Animal studies were conducted in accordance to the German Animal Welfare Act of 1998 and with approval from the responsible authorities. Female athymic nude (nu/nu) mice (Harlan-Winkelmann GmbH, Borchen, Germany), female NMRI nude mice (Charles River, Sulzfeld, Germany) and C3H/HeN mice (Charles River) were maintained under pathogen-free, controlled conditions.

2.2.2 Human MDA-MB-231 breast cancer xenograft

3 x 10^6 MDA-MB-231 breast cancer cells, obtained from cell culture, were implanted s.c. in the inguinal region of female NMRI nude mice in 100 µl 1:1 medium / matrigel (BD Biosciences, San Jose, CA, USA) (7 mice / group). Treatment was started when the tumors were approximately 20 mm² in size and continued until progression of the tumors. Experimental groups were vehicle, sagopilone (8 mg/kg, single i.v dose) and paclitaxel (12 mg/kg, 5 x once daily, i.p.). In addition to the bolus injection, the sagopilone treatment group obtained a maintenance dose of 0.3 mg/kg for 4 consecutive days. Every two weeks a new treatment cycle started depending on the body weight as a parameter for drug related toxicity. Body weights were measured weekly during the treatment period. Tumor area was determined by caliper measurements weekly.

2.2.3 Treatment of bone metastases *in vivo* - MDA-MB-231(SA) model

Two treatment scenarios were evaluated in the mouse breast cancer bone metastasis model, MDA-MB-231(SA) (see also Strube et al., 2009). The first scenario (preventive model) simulated the adjuvant treatment of a breast cancer patient with a high risk of developing bone metastases and the second (therapeutic model), treatment of a patient with advanced metastatic breast

cancer and established osteolytic lesions.

In the preventive treatment model, mice were inoculated with a tumor cell suspension of MDA-MB-231(SA) cells on day 0 (Fig. 7). For intracardiac inoculations, 5-week-old female athymic nude mice were anesthetized with an intraperitoneal application of 5% Rompun (Bayer HealthCare AG, Leverkusen, Germany) / 10% Ketavet (Pfizer, Karlsruhe, Germany) in 0.9% NaCl, 0.1 ml / 10 g body weight. Using an insulin syringe (BD Micro-Fine+Demi U-100, Becton Dickinson GmbH, Heidelberg, Germany), 5 x 10^5 MDA-MB-231(SA) (preventive model) or 1 x 10^5 MDA-MB-231(SA)/luc (therapeutic model) cells in 100 µl PBS were inoculated into the left cardiac ventricle of anesthetized mice. Treatment with sagopilone (10 mg/kg, single i.v. dose) or vehicle was initiated on day 5, by which time tumor cells were expected to have spread to bone (Yoneda, 2000). Animal body weights were monitored daily from day 13 and at sacrifice (day 19), animals were assessed by radiography, and hind limbs, kidneys and adrenal glands were collected for histologic examination. Details of analytical methods are given below.

In the therapeutic model, after inoculation of MDA-MB-231(SA)/luc tumor cells at day 0 and X-ray randomization into treatment groups according to lesion size on day 12, treatment was initiated on day 13 with vehicle, sagopilone (10 mg/kg single dose i.v., day 13) or paclitaxel (9 mg/kg in 0.9% NaCl i.p. once daily, days 13-17) (Bristol-Myers Squibb GmbH & Co KGaA, Munich, Germany) (Fig. 7). Body weight and the onset of paraplegia were monitored daily from day 13. Before sacrifice (day 22), bone lesions were assessed by radiography and micro-computed tomography (micro-CT) under Rompun/Ketavet anesthesia. In addition, cancer cell dissemination was analyzed by bioluminescence imaging (BLI), also on day 22. Bones (hind limbs) and soft tissues (kidneys, adrenal glands) were collected for histologic analysis and serum samples were collected for analysis of biochemical markers of bone turnover. Whole blood was collected via the vena cava under anesthesia and the tartrate-resistant acid phosphatase 5b (TRACP 5b) concentration was determined in serum obtained by centrifugation of blood samples (10000 x g for 3 minutes) using serum-gel tubes (Sarstedt, Nümbrecht, Germany). Methods used for imaging and histologic analyses are detailed below.

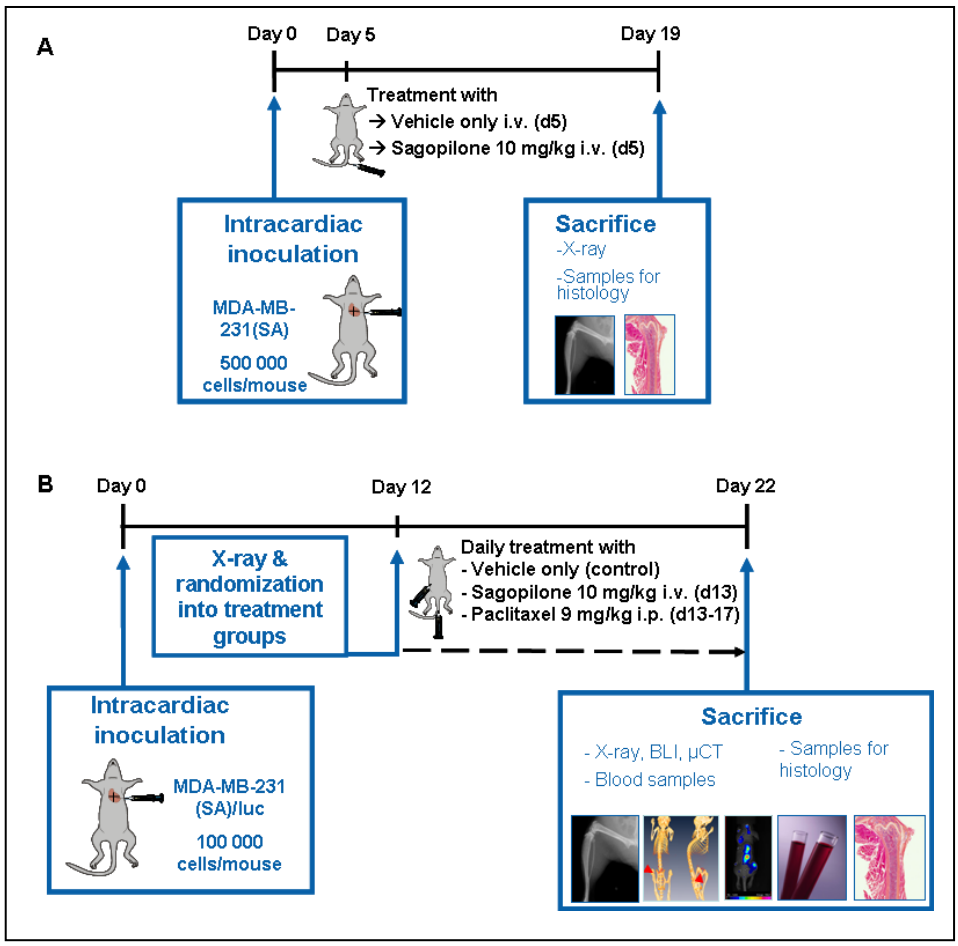

Figure 7. Treatment timelines for bone metastases experiments. (A) Preventive setting (B) Therapeutic setting.

2.2.4 *In vivo* selection of 786-O/luc cells from osteolytic bone lesions

Mice with osteolytic lesions in the hind limbs, caused by i.c. inoculation of 786-O/luc cells and detected by radiography, were sacrificed and the affected hind limb was separated from the body. Skin and muscles were removed and the hind limb was mushed with a piston through a sieve in a petridish containing 10 ml of 786-O/luc medium. Tumor cell suspension was collected from the petridish into a T-75 flask. On the next day, cells were washed twice with PBS to wash off mouse bone marrow cells that did not attach to the plate. After two to three weeks, a population of human cancer cells was obtained. These subpopulations were again inoculated into the left cardiac ventricle of anesthetized female athymic nude mice as in more detail described in chapter 2.2.3.

2.2.5 Ovariectomy (OVX)

Surgical OVX and SHAM operations were performed using a dorsal approach as described by Peng et al., 1994. Before operations, animals were randomized to groups according to their body weight. The ages of the mice were 3 months at the time of operations. For OVX, C3H/HeN mice were anesthetized with an intraperitoneal application of 5% Rompun (Bayer HealthCare AG, Leverkusen, Germany) / 10% Ketavet (Pfizer, Karlsruhe, Germany) in 0.9% NaCl, 0.1 ml / 10 g body weight. Ovaries were removed together with oviducts and a small portion of uterus. Post operative analgesia was performed using Temgesic® (0.1 mg/kg s.c.; Schering Plough, Kenilworth, NJ, USA) administered in association with the surgical operations and when necessary. Treatment was started at day 4 after surgical OVX and SHAM operations with either sagopilone (8 mg/kg i.v., single injection every 14 days) or estrogen (as pellet 0.01 mg / 60 days (Innovative Research of America, Sarasota, FL, USA)). Body weights were determined three times a week. At sacrifice (day 42) body weights and uterine weights were determined. In addition, hind limbs were collected to measure bone mineral density by pQCT measurements (chapter 2.4.3).

2.3 *In vivo* analytical methods

2.3.1 Radiography and measurement of osteolytic lesion area

Hind limbs of animals were X-rayed under 5% Rompun / 10% Ketavet anesthesia of mice using a Digital Faxitron small animal X-ray cabinet (Faxitron X-Ray, Wheeling, IL, USA) at 35 kV tube voltage, 0.3 mA current and 3 s exposure time. Quantitation of lesion area in hind limbs was performed using image analysis software (analySIS, Soft Imaging System GmbH, Münster, Germany). Radiography measurements were used for monitoring and quantitation of osteolytic lesions in the MDA-MB-231(SA)/luc (chapters 3.1.1, 3.3.3.1.2 and 3.3.3.2.2) and the 786-O/(luc) bone metastasis models (chapters 3.2.1 and 3.2.4).

2.3.2 Micro-computed tomography (micro-CT)

Micro-CT imaging was performed using a TomoScope micro-CT scanner (VAMP GmbH, Erlangen, Germany) in high-quality mode (40 kV tube voltage, 90 s scan time, 80 µm spatial resolution), without application of a contrast agent and under 5% Rompun / 10% Ketavet anesthesia of mice. Femur and tibia bone volume was calculated from reconstructed micro-CT images using Amira® image analysis software (Mercury computer systems Inc., Chelmsford, MA, USA). Micro-CT measurements were performed for 3D visualization of osteolytic lesions in the MDA-MB-231(SA)/luc (chapter 3.1.1) and 786-O/luc model (chapter 3.2.2) as well as for quantitation of bone volume in the MDA-MB-231(SA)/luc model (chapter 3.3.3.2.2).

2.3.3 Bioluminescence Imaging (BLI)

Noninvasive, whole-body imaging was performed to monitor luciferase-expressing MDA-MB-231(SA)/luc and 786-O/luc cells (chapters 3.3.3.2.3 and 3.2.2) using a cooled CCD camera (NightOWL LB, Berthold Technologies, Bad Wildbad, Germany). Before analysis, mice were injected i.v. with 100 µL luciferin (45 mg/mL in PBS, Synchem OHG, Felsberg/Altenburg, Germany) and anesthetized with 1–3% isofluran (CuraMED Pharma GmbH, Karlsruhe, Germany). Photon emission was measured over an integration time of 1 minute (MDA-MB-231(SA)/luc) or 1 second (786-O/luc cell lines) and recorded as pseudo-color images that were quantified using WinLight software (Berthold Technologies).

2.3.4 Positron emission tomography/computed tomography (PET/CT)

PET/CT acquisition in the 786-O/luc model was performed using the preclinical, small animal Siemens Inveon Scanner (Siemens, Erlangen, Germany) under 1.5-2.5% isoflurane / O_2 anesthesia of the mice. Mice were intravenously injected with 15.4 Mbq of ^{18}F-fluoride and scanned for 20 minutes, starting at 70-90 minutes post-injection. All images were reconstructed using Inveon-Research-Workplace (IRW) software (Siemens).

2.4 *Ex vivo* analytical methods

2.4.1 TRACP 5b measurement

Serum concentrations of osteoclast-derived TRACP 5b were measured using a solid phase immunofixed enzyme activity (MouseTRAP^{TM}) assay according to the manufacturer's instructions (Immunodiagnostic Systems GmbH, Frankfurt am Main, Germany).

2.4.2 Bone histology and histomorphometry

At sacrifice, hind limbs were fixed in 4% neutral buffered formalin (Merck & Co. Inc, Whitehouse Station, NJ, USA) for 2–3 days, decalcified in 10% EDTA (Sigma-Aldrich, Munich, Germany), dehydrated and embedded in paraffin. Tissue sections (4 µm) were stained with hematoxylin and eosin (H&E), orange G, and phloxine B using standard protocols. Total tumor area was determined in longitudinal midsections of tibiae and femora without knowledge of experimental groups. Histomorphometric analyses were performed using Soft Imaging System CellF (Olympus Soft Imaging GmbH, Münster, Germany).

For TRACP staining, 4 µm sections were incubated in substrate solution (naphthol AS-BI phosphate in ethylene glycol monoethyl ether, Sigma-Aldrich) and staining solution (sodium nitrite and pararosaniline chloride, Sigma-Aldrich) and were counterstained with hematoxylin. Osteoclast number / mm tumor-bone interface was determined in longitudinal midsections of tibiae and femora without knowledge of experimental groups.

CD31 immunostaining was performed using the Dako Autostainer (Universal Staining System, model LV-1). 5µm paraffin sections were deparaffinized and hydrated. Proteolytic enzymes were blocked with proteinase K ready-to-use solution (15 min, RT) (Dako, Hamburg, Germany) and endogenous peroxidase activity was blocked with 0.3% H_2O_2 for 15 min at RT. To inhibit non-specific staining during IHC detection, sections were incubated for 10 min at RT in protein block (serum-free, ready-to-use (Dako)) followed by incubation with biotinylated primary anti-CD31 antibody (1:100, PECAM-1, monoclonal, rat anti-mouse, BD Biosciences Pharmingen, San Jose, CA, USA) and extravidin-

peroxidase (1:300, 30 min, Sigma-Aldrich Chemie GmbH, Taufkirchen, Germany). The immunostaining was performed using the liquid DAB + substrate chromogen system according to the manufacturer's instructions (Dako). The slides were counterstained with hematoxylin (1 min) and washed with water (10 min).

2.4.3 Peripheral quantitative computed tomography (pQCT)

Mineral density of bone was measured from tibial metaphysis (especially trabecular bone) and diaphysis (especially cortical bone) using pQCT. The pQCT measurements were performed *ex vivo* after sacrifice of OVX and SHAM operated mice (chapter 2.2.5). For metaphyseal measurements, the site of CT scan was at the proximal end of tibia approximately 1.6 mm distally from the articular surface. For diaphyseal measurements, the site of CT scan was at the tibial shaft approximately 10 mm distally from the articular surface. The following parameters were determined: total density, trabecular density (metaphysis) and cortical density (diaphysis).

2.5 *In vitro* analytical methods

2.5.1 Osteoclast activity and differentiation assay

The osteoclast activity assay was performed by Pharmatest Services Ltd., Turku, Finland (www.pharmatest.fi). Human osteoclast precursor cells were cultured for 7 days without test compounds to allow osteoclast differentiation. The amount of TRACP 5b released into the culture medium was determined at day 7 as an index of the number of osteoclasts formed (Fig. 8). Sagopilone (2.5–50 nM) or paclitaxel (2.5–200 nM) was added at day 7 and mature osteoclasts were cultured for an additional 3 days, allowing them to resorb bone. The level of carboxy-terminal cross-linking telopeptide of type I collagen (CTX) is a measure of the collagen degradation activity of human osteoclasts and was measured at day 10 to determine bone resorption during days 7–10. Cytotoxicity was determined by the level of dying cells in the culture medium at day 10 using Toxilight® BioAssay Kit (Lonza, Verviers, Belgium). Trans-

epoxysuccinyl-L-leucylamido-(4-guanidino)butane (E64), a cysteine protease inhibitor that shows selectivity for cathepsin B and is known to inhibit osteoclast activity (Everts et al., 1992), was used as a control compound at 1.0 µM.

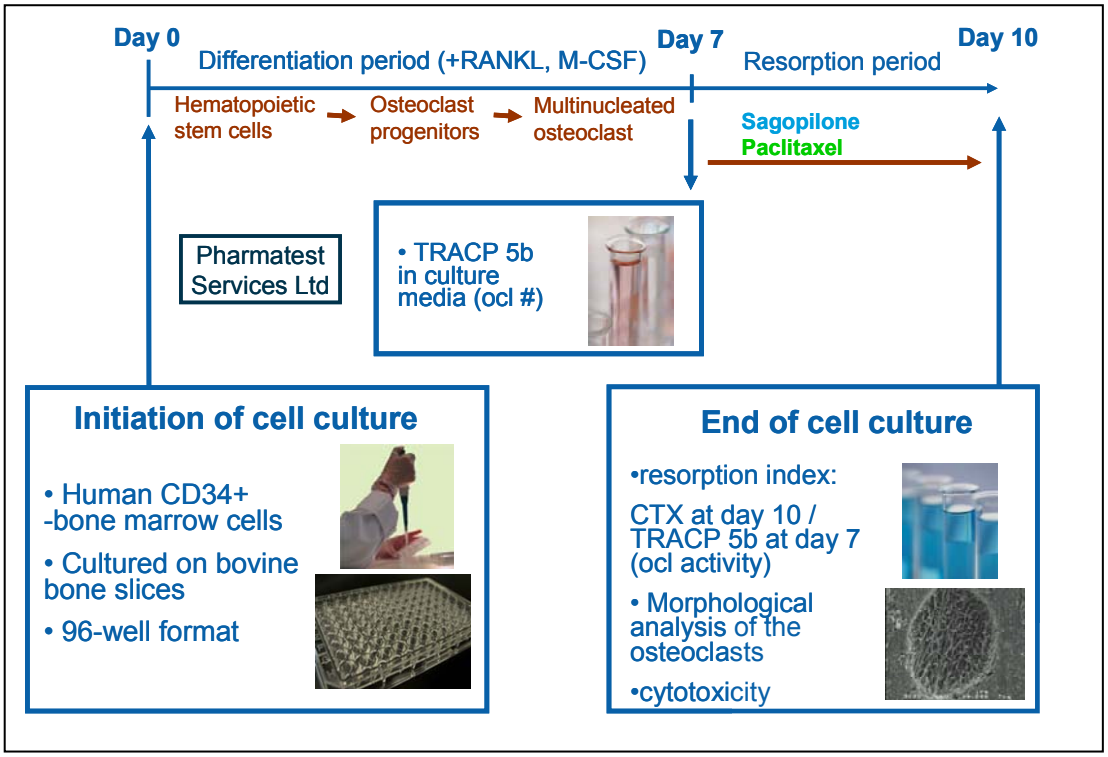

Figure 8. *In vitro* bone resorption assay. Osteoclast precursors were allowed to differentiate into mature osteoclasts (ocl). At day 7, when differentiation was complete, test (sagopilone or paclitaxel) or control (E64 cathepsin inhibitor, not shown) compounds were added and mature osteoclasts were cultured for an additional 3 days to allow bone resorption. The mean osteoclast activity is expressed as the resorption index (CTX concentration at day 10 / TRACP 5b concentration at day 7). Cytotoxicity was determined by quantifying the number of dying cells in the culture medium at day 10. The assay was performed at Pharmatest Services Ltd (www.pharmatest.fi).

Furthermore, we tested the short-term effects of sagopilone and paclitaxel on human osteoclast differentiation and activity to mimic the low pharmacokinetic in mice. The osteoclast activity assay was performed as described above with the difference that the compounds were added only for 2 hours at day 7 and not for the whole resorption period. The following concentrations were tested: 10, 50, 20 and 50 nM sagopilone; 20, 50 , 100, 200 nM paclitaxel. After 2 hours of incubation, the compounds were washed away by removing the culture medium and adding new medium without test compounds into the well. E64 (1 µM) was again used as a reference inhibitor of osteoclast activity and added into the cultures at day 7.

In the osteoclast differentiation assay, sagopilone and paclitaxel were added into the cultures at day 0 and washed away after 2 hours as described above. The following concentrations were tested: 0.1, 0.5, 1, 5, 10 nM sagopilone; 0.5, 1, 5, 10, 20 nM paclitaxel. Osteoprotegerin (OPG, 100 ng/ml) was used as a reference inhibitor of osteoclast differentiation and also added into the cultures at day 0. TRACP 5b activity was measured from the culture medium collected at day 7 as an index of the number of osteoclasts formed in each well during the differentiation period. CTX was measured from the culture medium collected at day 10 to quantitate bone resorption during days 7-10. TRACP staining, to visualize osteoclasts and to evaluate cytotoxic effects of the compounds on osteoclasts, was performed as described by Rissanen et al., 2008.

2.5.2 Western Blot

Cells were harvested by trypsinization, rinsed with PBS and lysed with M-Per buffer (Pierce Biotechnology Inc., Bonn, Germany) supplemented with protease inhibitor (Pierce). SDS-PAGE was performed in a 4-12% Bis-Tris gel (Invitrogen). Following protein transfer to a PVDF membrane (Invitrogen), the blot was incubated with a polyclonal antibody against CXCR4 (1:1500, abcam, Cambridge, UK). After incubation with a secondary horseradish-peroxidase (HRP)-conjugated anti-goat antibody (1:5000, Dako, Hamburg, Germany), the blots were developed using an enhanced chemiluminescence (ECL) detection kit (Invitrogen).

2.5.3 Quantitative determination of growth factors

The production and secretion of VEGF, TGF-α, EGF and bFGF by the parental 786-O/luc cell line and two subpopulations were determined in cell culture supernatants after 48 hours of culture using a quantitative sandwich enzyme immunoassay technique (ELISA) according to manufacturer´s instructions (R&D Systems GmbH, Wiesbaden-Nordenstadt, Germany). 0.8 x 10^6 cells were seeded in 2 ml medium, cell culture supernatants were collected after 48 hours of culture.

2.5.4 Proliferation assay

For determination of the proliferation of tumor cells the Alamar Blue assay was used. Alamar Blue detects cell viability by utilizing a blue and nonfluorescent dye resazurin, which is converted to a pink and fluorescent dye resorufin in response to chemical reduction of growth medium resulting from cell growth (Ahmed et al., 1994). Reduction related to growth causes the REDOX indicator to change from the oxidized form (nonfluorescent, blue) to the reduced form (fluorescent, pink). The fluorescent and colorimetric signal generated from the assay is proportional to the number of living cells in the sample.
MDA-MB-231 and MDA-MB-231(SA)/luc cells were seeded in 100 µl of medium at 5000 cells per well in 96-well plates. After 24 hours sagopilone (10 nM) was added in fresh medium and cells were incubated for 4-5 days. Every 12 hours Alamar Blue (Biosource, Solingen, Germany) was added to the wells in a final concentration of 10%. Proliferation was monitored after two hours of incubation (37°C) by measuring the fluorescence (excitation 528 nm, emission 590 nm) emitted by the REDOX indicator using a microtiter well plate reader (Victor^3, PerkinElmer Life Sciences, Massachusetts, USA).

2.5.5 Apoptosis assay

5000 MDA-MB-231 and MDA-MB-231(SA)/luc cells were seeded per well in 96-well plates. After 24 hours sagopilone (10 nM) was added in fresh medium and cells were incubated for 3 days. To measure sagopilone induced apoptosis, the Caspase-Glo® 3/7 assay (Promega) was applied. According to manufacturer´s instructions, 100 µl of Caspase-Glo® 3/7 Reagent was added to the wells. After 2 hours of incubation at room temperature the luminescence of each sample was measured using a plate-reading luminometer (Victor^3, PerkinElmer Life Sciences, Massachusetts, USA). Simultaneously, a 96-well plate was prepared to measure Alamar Blue based proliferation (chapter 2.5.4) for normalisation of the caspase values by the cell number.

2.6 Statistical methods

The results are reported as mean ± standard deviation (SD).

For the bone metastasis efficacy study, comparisons to control and comparisons sagopilone vs. paclitaxel were performed by exact Wilcoxon tests. An alpha-level of 0.05 was employed. Because of the exploratory nature of the study, no adjustments for multiplicity were made.

For the OVX study, statistical analysis was performed using one-way analysis of variance (ANOVA). Because statistically significant differences were observed, the results of group 1, 3 and 4 were compared separately with the results of group 2 using t-test.

The statistics for the 786-O/luc model development (*in vitro* assays, lesion size measured by radiography, BLI signal intensity, body weight) were performed using t-test to directly compare metastatic subpopulations with the parental cell line.

For the *in vitro* osteoclast assays, one-way analysis of variance (ANOVA) was used to study if the values obtained between different groups were statistically different (with $p<0.05$). If a statistically significant difference was observed in ANOVA, the results of the test and control groups were compared separately with the results of the baseline group using t-test.

To determine correlation between two parameters, linear regression analysis was performed using SigmaStat program (version 3.0, SPSS Science Software GmbH, Erkrath, Germany).

3 RESULTS

3.1 Characterization of the MDA-MB-231(SA) model

In the MDA-MB-231(SA) bone metastasis mouse model, $1x10^5$ breast cancer cells were inoculated in the left cardiac ventricle as described in chapter 2.2.3. The mice developed osteolytic lesions in 3 weeks after injection of the cells. At the end of the study, the mice suffer from paraplegia and cachexia as a result of the aggressive nature of the lesions and tumor burden. At first occurrence of these symptoms the mice were sacrificed immediately. For the simultaneous monitoring of tumor burden and osteolytic lesions bioluminescence imaging (BLI), histomorphometry, radiography and micro-computed tomography (micro-CT) were used. The tumor burden and tumor cell localisation (metastasis) were determined using bioluminescence imaging and histological examination (H&E staining) whereas tumor-induced bone destruction was assessed using radiography and micro-computed tomography as in more detail described in the materials and methods section. All measurements were performed at sacrifice.

3.1.1 Detection of osteolytic lesions

Whole-body micro-CT measurements revealed osteolytic lesions almost throughout the whole skeleton of the mice. Besides the hind limbs, the spine, pelvis, forelimbs, scapula and the skull were regions that were most affected by tumor-induced bone destruction (Fig. 9A and 9B).

A good correlation between radiography and micro-CT measurements, both X-ray based methods which were employed to monitor bone destruction in this model, was observed. Whereas radiography displayed a two-dimensional view of the hind limbs, micro-CT measurements more accurately reflected morphological changes in bone in a three-dimensional manner. However, the localisation of osteolytic lesions exactly correlated with both methods as depicted in Figure 9C. Osteolytic lesions were evident in proximal tibia and distal femur. To point out the correlation between both method, lesion area and bone volume were determined in 17 mice and the correlation coefficient r and the p-value P were calculated (Fig. 9D). Values of r = 0.719 and P = 0.001

indicate a good correlation between radiography and micro-CT data.

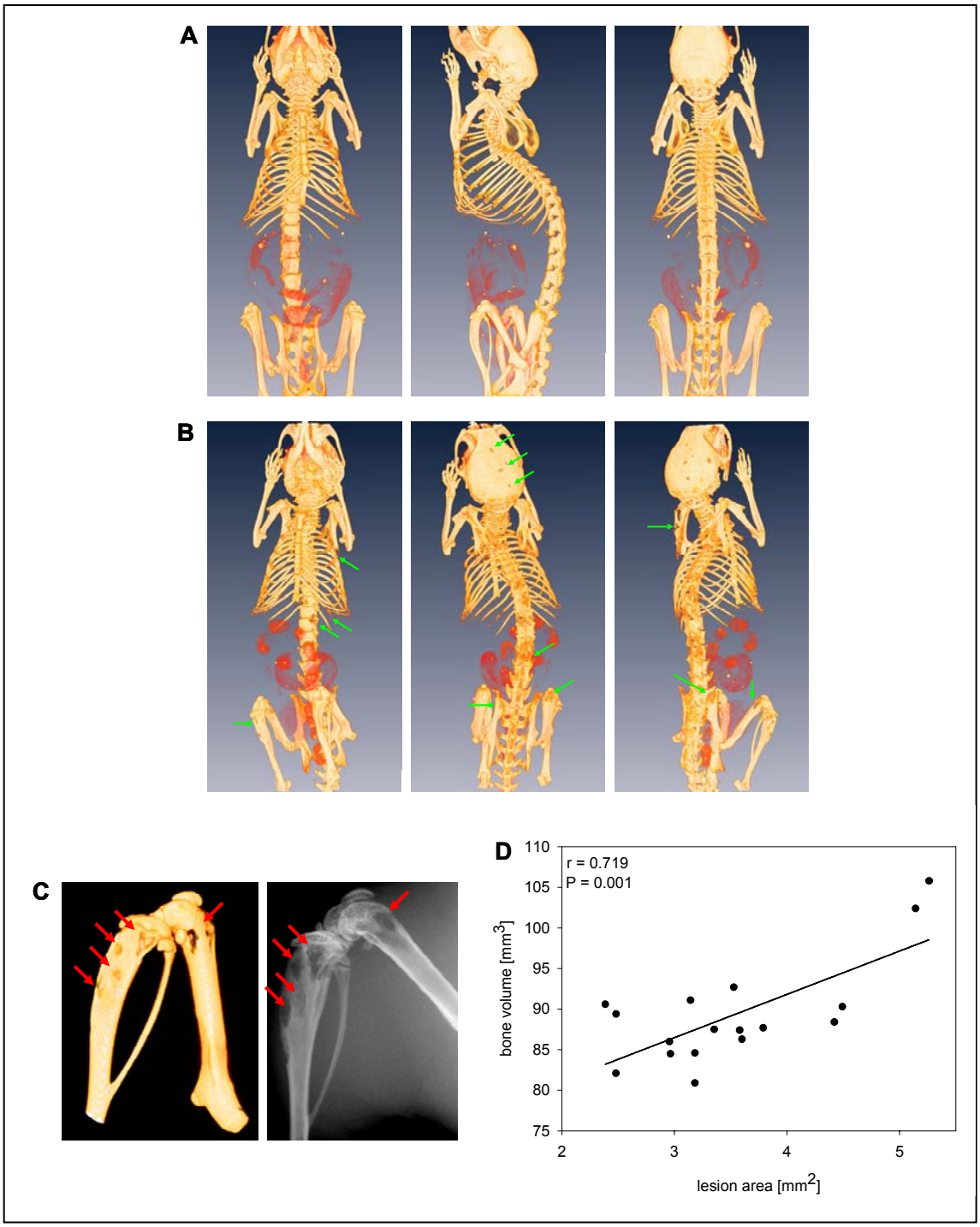

Figure 9. Skeletal changes in the MDA-MB-231(SA)/luc bone metastasis mouse model. Representative whole-body micro-CT images of (A) control and (B) tumor cell inoculated animals. Arrows indicate osteolytic lesions in hind limbs, forelimbs, spine, pelvis, scapula and calvaria. (C) Correlation of micro-CT and radiography data in a hind limb of the same mouse inoculated with MDA-MB-231(SA) cells. Arrows indicate osteolytic lesions in femur and tibia. (D) Bone volume of hind limbs determined by micro-CT vs. lesion area of hind limbs measured by radiography indicating good correlation between both methods, n=17 mice (r=0.719 (correlation coefficient), P=0.001 (p-value)).

To determine severity of bone destruction, quantitation of lesion area of the radiography data was performed using image analysis software (Fig. 10A and 10B). Similarly, total bone volume of hind limbs was calculated from reconstructed micro-CT images using Amira® image analysis software (Fig. 10C and 10D). The quantitation of osteolytic lesion area and bone volume respectively allows for the use of these imaging techniques as tools for compound screening (chapter 3.3.3.2.2).

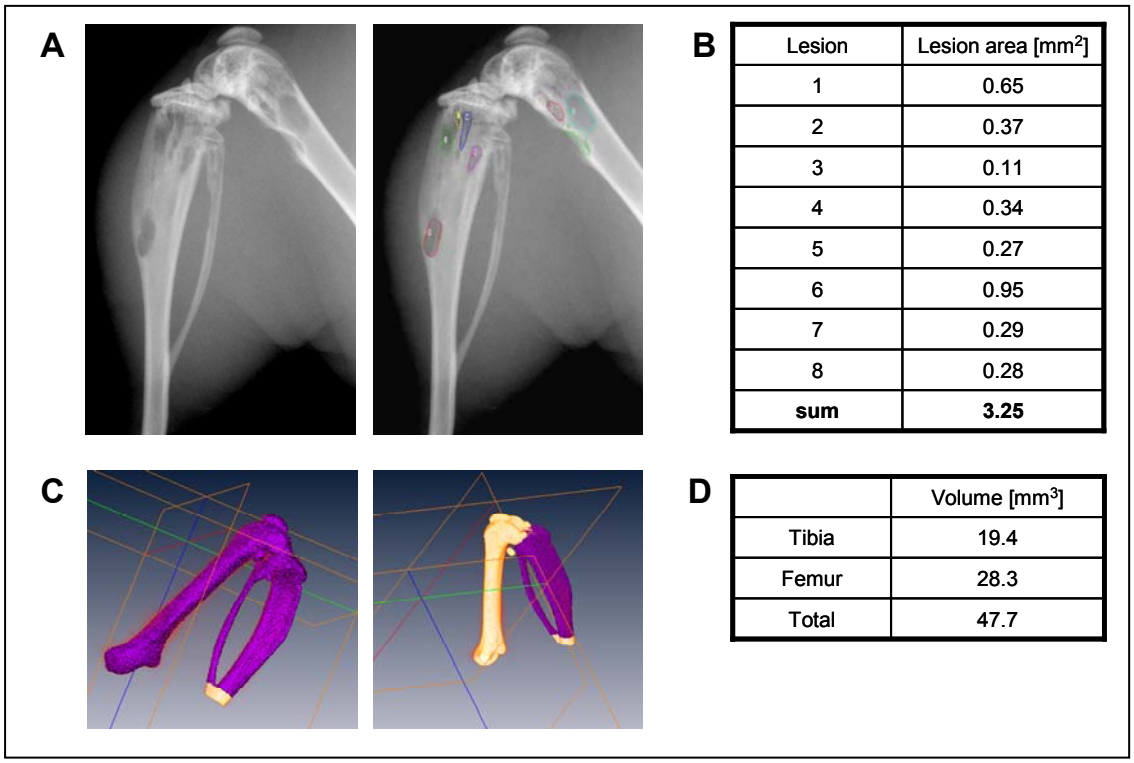

Lesion	Lesion area [mm²]
1	0.65
2	0.37
3	0.11
4	0.34
5	0.27
6	0.95
7	0.29
8	0.28
sum	**3.25**

	Volume [mm³]
Tibia	19.4
Femur	28.3
Total	47.7

Figure 10. Quantitation of bone destruction in the hind limbs of mice. (A) Representative radiography images and determination of osteolytic lesions in femur and tibia. (B) Calculation of osteolytic lesion area by addition of all lesions in one hind limb. (C) The violet colour represents calculated total volume of tibia and femur (left) and only tibia (right) in one hind limb. (D) Determination of bone volume by image segmentation tools of Amira software.

3.1.2 Detection of tumor burden

Bioluminescence imaging allowed visualization of the tumor cell dissemination. The bioluminescence signal indicated metastasized tumor cells in the region of hind limbs, forelimbs, spine and skull (Fig. 11A). BLI reflects dissemination of luciferase labelled tumor cells throughout the whole body of the animal.

In contrast, histomorphometry allows more detailed evaluation of structural

changes in bone. Histological examination revealed that the tumors were primarily located within the bone and in some animals tumor totally replaced the bone marrow cavity. High tumor burden resulted in cortical destruction of bone (Fig. 11B, animal 4). In addition, there was a strong correlation between BLI signal intensity, lesion and tumor area determined by histomorphometry, indicated by a concomitant increase of BLI signal intensity, lesion and tumor area in individual animals (Fig. 11A-D). In general, it could be observed that the higher the tumor burden, the larger the osteolytic lesions detected.

The strong correlation between methods determining the location and severity of tumor burden (BLI and histology) and bone destruction (radiography) cannot only be visualized but also expressed mathematically by the correlation coefficient r (Fig. 12). r measures the strength between two variables and can assume values between -1 and 1 (Bland and Altman, 1986). The closer the correlation coefficient is to 1 (increasing linear relationship) and -1 (decreasing linear relationship), the stronger the correlation between the variables. Consequently, a good correlation could be observed between lesion area determined by radiography and tumor histology data with $r = 0.782$ and $P<0.001$ (Fig. 12B) as well as between radiography and BLI data ($r = 0.667$, $P<0.001$) (fig. 12C). The correlation was less strong between methods measuring tumor burden such as BLI and histology with a correlation coefficient of $r = 0.511$ and a p-value of $P = 0.008$ (Fig. 12A).

The estimation of BLI signal intensity, tumor area, lesion area and bone volume allows not only qualitative, but also quantitative analysis of osteolytic changes and tumor burden in bones. Thus, these technologies are helpful tools to determine efficacy of compounds in a therapeutic setting (chapter 3.3.3.2).

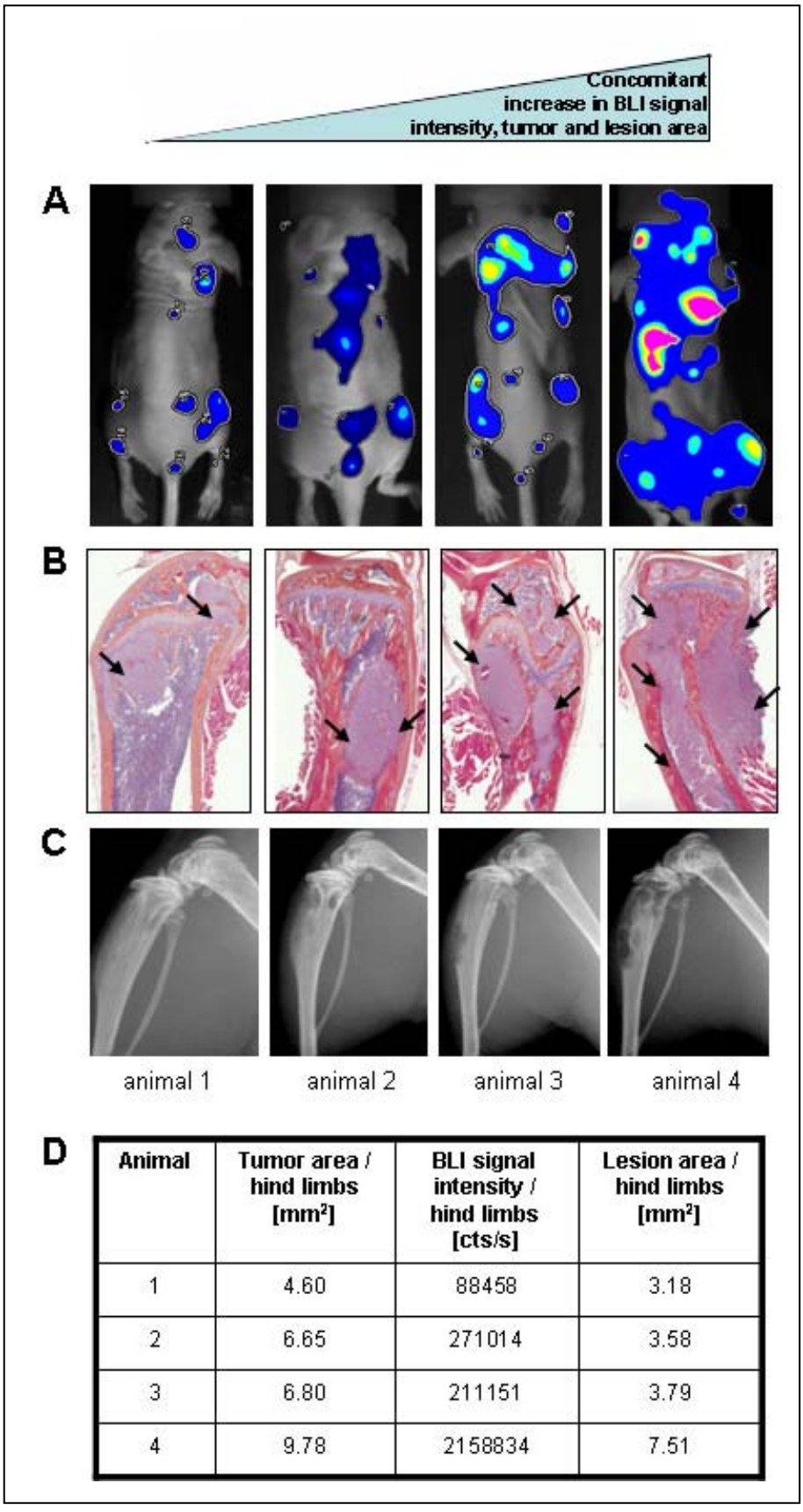

D

Animal	Tumor area / hind limbs [mm²]	BLI signal intensity / hind limbs [cts/s]	Lesion area / hind limbs [mm²]
1	4.60	88458	3.18
2	6.65	271014	3.58
3	6.80	211151	3.79
4	9.78	2158834	7.51

Figure 11. BLI signal intensity, tumor and lesion area concomitantly increased in mice inoculated i.c. with MDA-MB-231(SA)/luc cells. (A) Bioluminescence images and (B) H&E stained bone sections indicating tumor burden (C) Radiographs indicating osteolytic lesions (D) Corresponding quantitation of bioluminescence signal intensity, tumor and lesion area in bone.

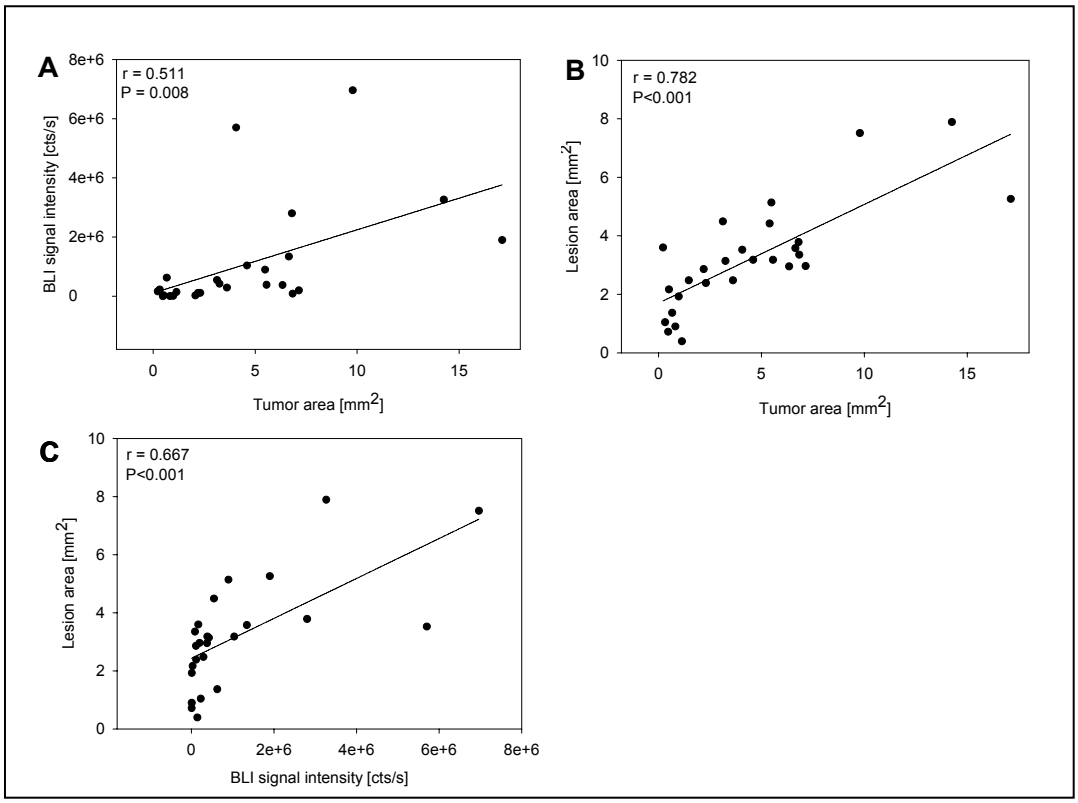

Figure 12. Correlation between different imaging techniques. Calculation of correlation coefficients indicate good correlation between (A) BLI and histology (r = 0.511, P = 0.008) and (B) high correlation between radiography and histology data (r = 0.782, P<0.001) as well as (C) between radiography and BLI data with r = 0.667 and P<0.001. (n = 26 (A), n = 27 (B), n = 25 (C), Animals from the therapeutic efficacy study described in chapter 2.2.3 were used (vehicle, sagopilone and paclitaxel treated mice).

3.2 Development and characterization of the 786-O model

This part of the thesis aimed to develop a RCC bone metastasis mouse model which are uncommon to better understand the biology of RCC bone metastasis, to have a possibility for compound testing and thus improve therapy options.

3.2.1 Time course of osteolytic lesions

After 786-O/luc tumor cell inoculation, the animals developed aggressive osteolytic bone destruction as monitored by radiography and micro-CT scans with the endpoint at a mean of 60 days. All of the mice developed similar osteolytic lesions. No osteoblastic lesions were observed. First lesions occurred at 4 weeks after tumor cell inoculation. Figure 13A shows the time course of the development of osteolytic lesions monitored weekly from day 28 until day 56 by

radiography. The determination of mean lesion size from the X-ray images indicated a steady increase of the osteolytic lesion area (Fig. 13B). The site and number of bone metastases are shown in Table 1. The observed extensive bone destructions were similar to those noted in clinical settings and mainly occurred in tibia, femur, jaw, forelimbs, pelvis and sometimes in scapula and spine as detected by whole body micro-CT imaging (Table 1).

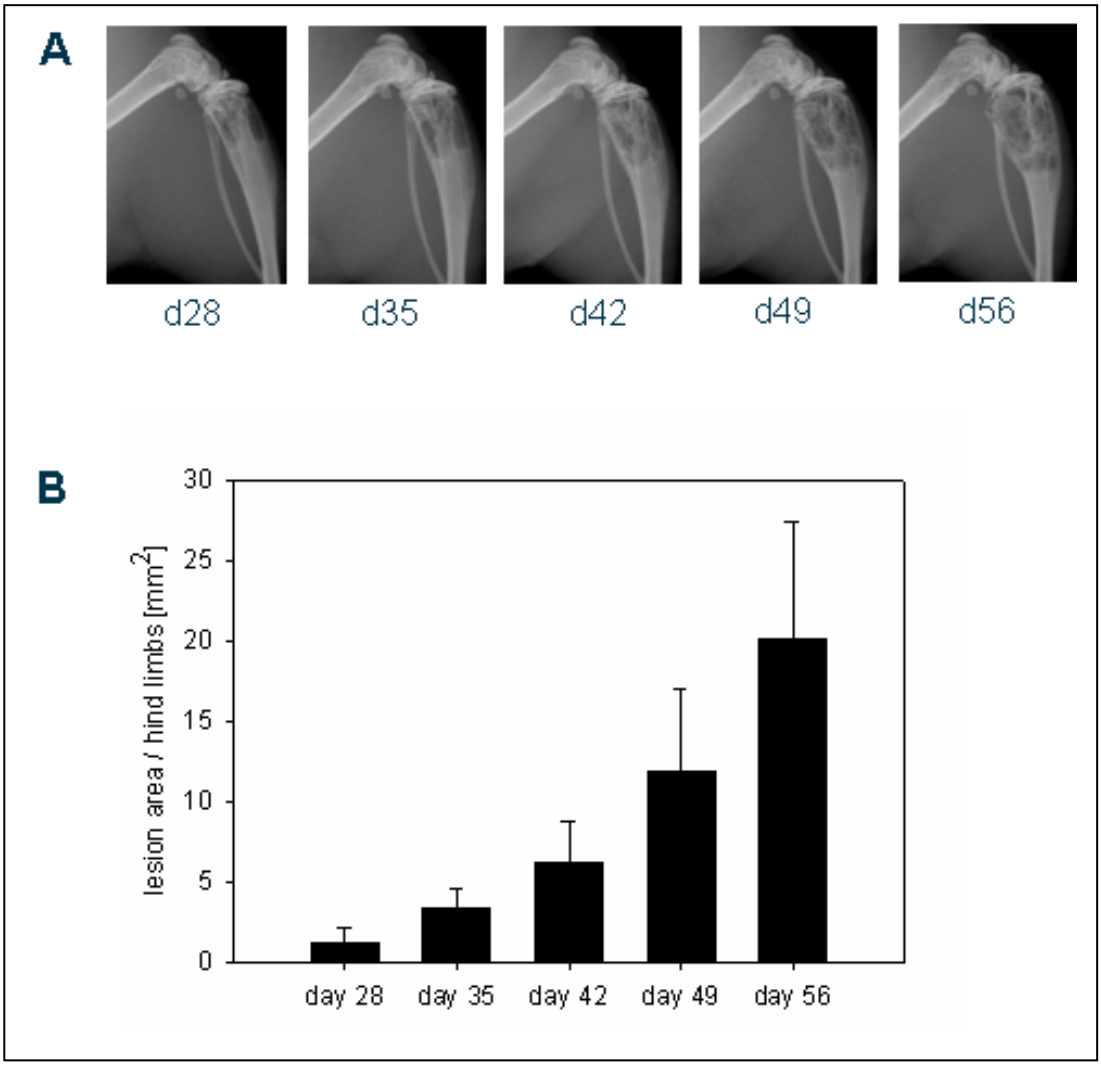

Figure 13. The growth of osteolytic lesions constantly increased in the 786-O/luc bone metastasis model. (A) Representative radiographs of hind limbs monitored weekly from week 4 until week 8. (B) Mean osteolytic lesion area of hind limbs during the course of the study (n = 10). Mean + SD values shown.

Site	No. of animals (%)
Tibia/Fibula	100
Jaw	100
Femora	90
Pelvis	80
Humeri	80
Scapula	70
Spine	50
Ulna	40
Ribs	30
Skull	20
Finger	20

Table 1. Distribution and number of bone metastases in the 786-O/luc RCC bone metastasis model determined by whole-body micro-CT measurements. Tibia/fibula, jaw, femora, pelvis and humeri are the most affected areas of the skeleton.

3.2.2 Multimodal imaging

Figure 14 shows representative images of osteolytic lesions and tumor in the hind limb of a mouse inoculated intracardially with 786-O/luc cell line monitored by different imaging techniques (radiography, micro-CT, BLI) and histology (H&E staining of a hind limb). The localisation of tumor cells monitored by BLI correlated with affected areas of the skeleton as measured by whole-body micro-CT. BLI images show spread of cancer cells in the regions of hind limbs and forelimbs. No soft tissue metastases in kidneys, adrenal glands, heart and lungs were detected either by BLI or by histomorphometry using H&E staining.
As shown by histological examination, the tumors were primarily located within the bone and resulted in cortical destruction of bone by tumor that replaced the marrow cavity.

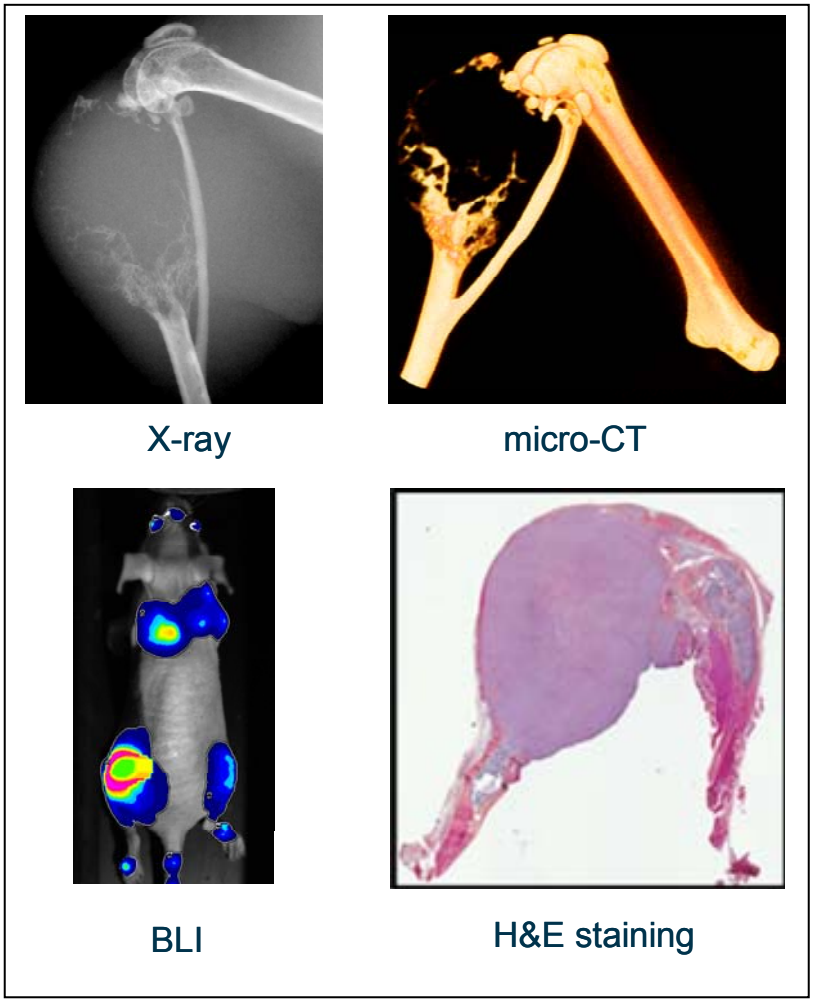

Figure 14. Characterization of the 786-O/luc RCC bone metastasis model by different imaging techniques and histology. X-Ray and micro-CT images of the same leg showing strong osteolytic lesions, H&E stained bone section of the same leg as measured with radiography and micro-CT revealing cortical destruction of bone by tumor that replaces the marrow cavity. BLI images showing spread of cancer cells in the regions of hind limbs and forelimbs.

The PET/CT technology was used to localize skeletal metabolic activity in the 768-O/luc bone metastasis mouse model. The PET/CT scan with ^{18}F-fluoride, a non-specific bone tracer, revealed abnormal high accumulation of ^{18}F-fluoride in lytic lesions, especially in hind limbs, spine, scapula and skull, compared to the uptake in normal bone. There was a good correlation of ^{18}F-fluoride accumulation and pathologic appearance of osteolytic lesions by CT (Fig. 15). The strong signal in the bladder of the mouse is due to rapid excretion of ^{18}F-fluoride by the kidneys (Fig. 15, middle and right).

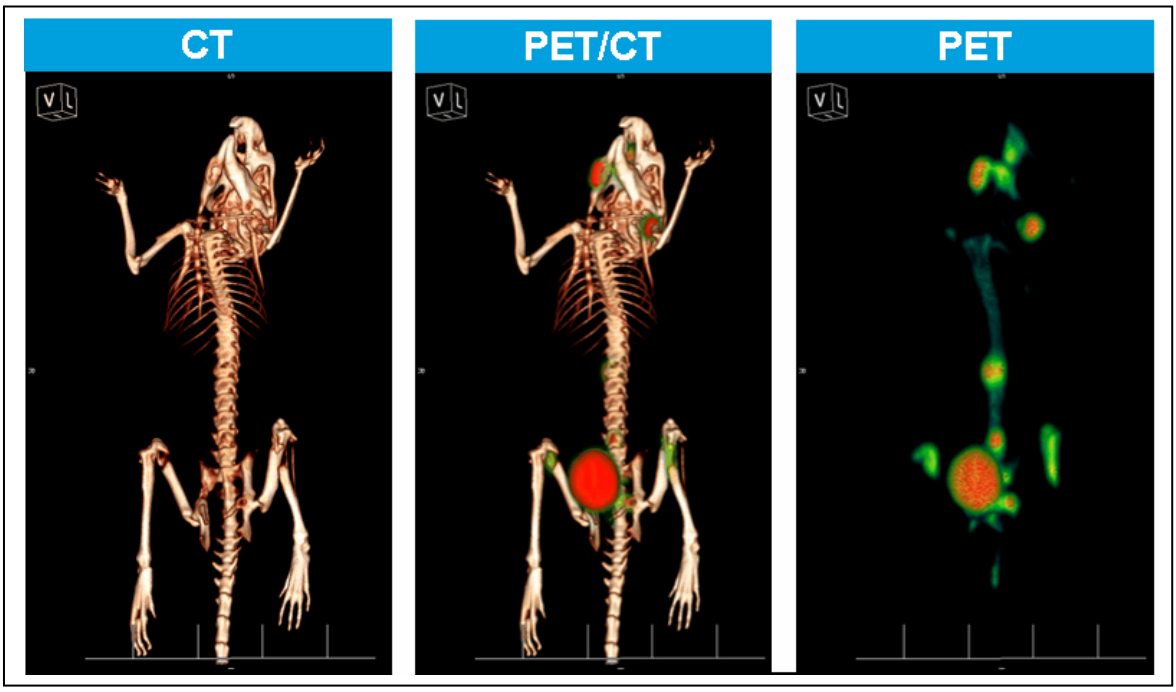

Figure 15. Simultaneous monitoring of osteolytic lesions and skeletal metabolic activity by ^{18}F-fluoride PET/CT imaging of the same mouse. CT scan indicating osteolytic lesions (left), PET scan showing ^{18}F-fluoride signals in the skeleton (right) and combined PET/CT image (middle).

3.2.3 Osteoclast involvement

To clarify whether bone destruction is a result of osteoclast activation by 786-O/luc tumor cells or caused by demolition of bone by tumor growing within the hind limb, TRACP staining was performed to highlight activated osteoclasts in the hind limbs (Fig. 16A). A lower number of active osteoclasts was observed in animals with small tumors compared to animals with large tumors. A correlation was observed between number of osteoclasts and tumor area indicated by a correlation coefficient of r = 0.879 and a p-value of P = 0.004 (Fig. 16B). The larger the tumor area, the higher the number of active osteoclasts indicating that bone destruction is osteoclast-mediated.

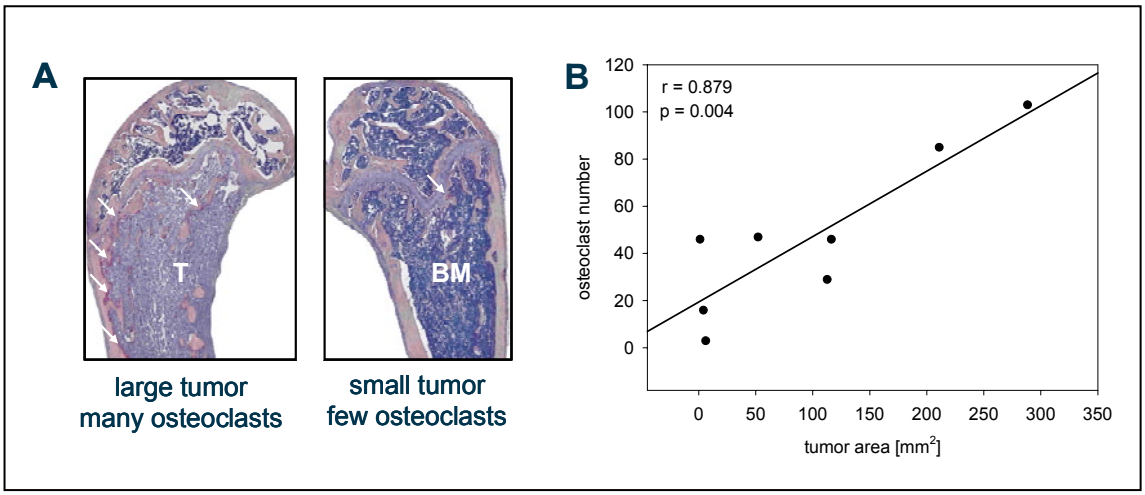

Figure 16. Osteoclast activation is higher in animals bearing large tumor in bone. (A) Representative TRACP staining indicating the level of activated osteoclasts (arrows indicate osteoclasts; T, tumor, BM, bone marrow). (B) A correlation was observed between number of osteoclasts and tumor area (n = 8 mice). The larger the tumor area, the higher the number of active osteoclasts. (r, correlation coefficient)

3.2.4 *In vivo* screening of highly metastatic 786-O/luc subclone

Tumor cell populations are heterogeneous and have different abilities to metastasize to secondary organs. Therefore, the *in vivo* selection approach was used to isolate highly metastatic subpopulations that have the special characteristic to home preferably to bone (Fig. 17A). A highly metastatic (HM) subclone, 786-O(HM)/luc, could be isolated resulting in the almost 3-fold induction of osteolytic lesion area compared to the parental cell line on day 49 and consequently in a much faster development of osteolytic lesions (Fig. 17B and 17C). Another isolated subclone, 786-O(LM)/luc (LM: low metastatic), didn´t result in a more metastatic phenotype and showed osteolytic lesion sizes in the range of the parental cell line. The osteolytic lesion area was statistically significant higher in 786-O(HM)/luc cell line compared to both parental ($P = 0.002$, day 49) and low metastatic cell line ($P<0.001$, day 49) whereas there was no statistical difference in lesion area between parental and 786-O(LM)/luc cell line ($P = 0.082$, day 49).

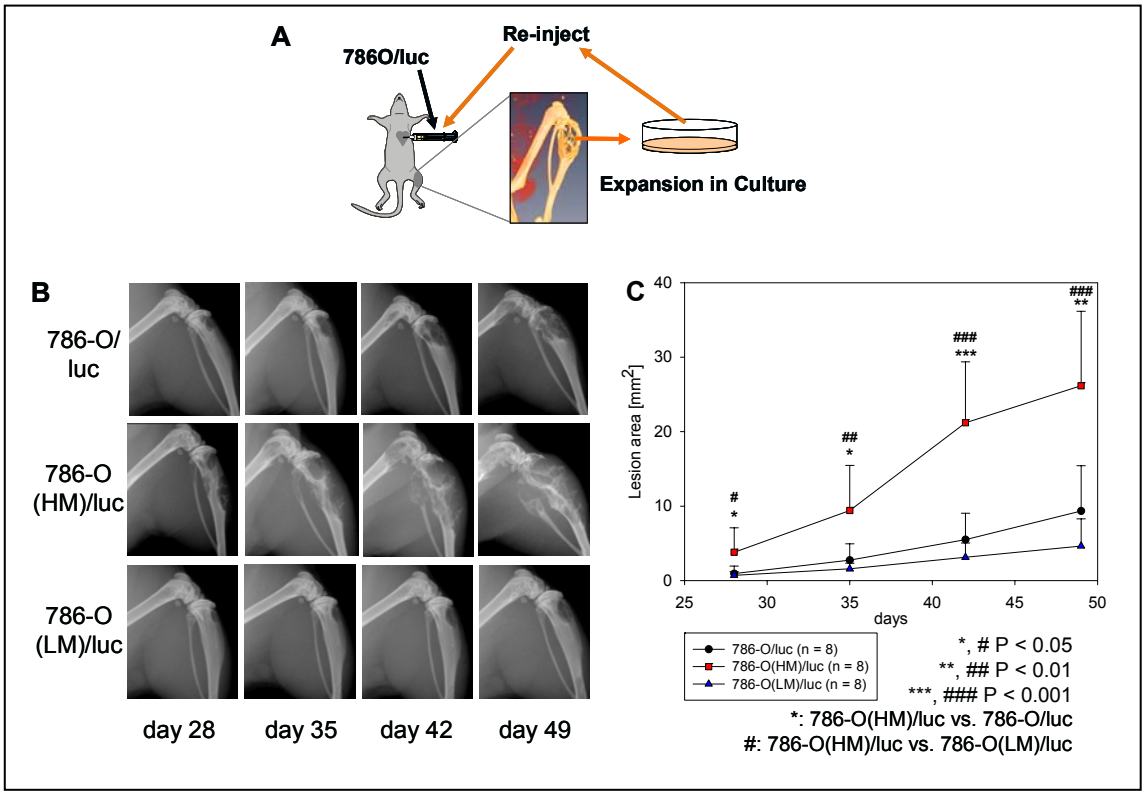

Figure 17: Growth of osteolytic lesions in the parental and two *in vivo* selected 786-O/luc cell lines. (A) Schematic representation of the *in vivo* selection process. 786-O/luc cells were injected into the left cardiac ventricle of nude mice. Tumor cells were isolated from bone metastases and reinoculated after expansion in culture. (B) Representative radiographs of hind limbs showing the development of osteolytic lesions from day 28 to day 49. (C) Quantitation of osteolytic lesion area depending on the time indicating significantly higher osteolytic lesion area in animals inoculated with 786-O(HM)/luc cell line compared to the parental cell line. Mean + SD values shown.

In addition to increased lesion area in 786-O(HM)/luc inoculated animals, the tumor burden at day 49 was also much higher indicated by statistically significant increased BLI signal intensity compared to mice inoculated with the parental cell line (P = 0.015) (Fig. 18B). Consequently, the 786-O(HM)/luc inoculated mice suffer more from tumor-induced cachexia as shown by significantly reduced body weights compared to the parental 786-O/luc cell line (P<0.001) (Fig. 18A). Inoculation of the low metastatic cell line, 786-O(LM)/luc, in mice resulted in body weights and tumor burden on the level of the parental cell line as expected in accordance with the osteolytic lesion size and tumor burden and consequently no statistically significant differences compared to the parental cell line.

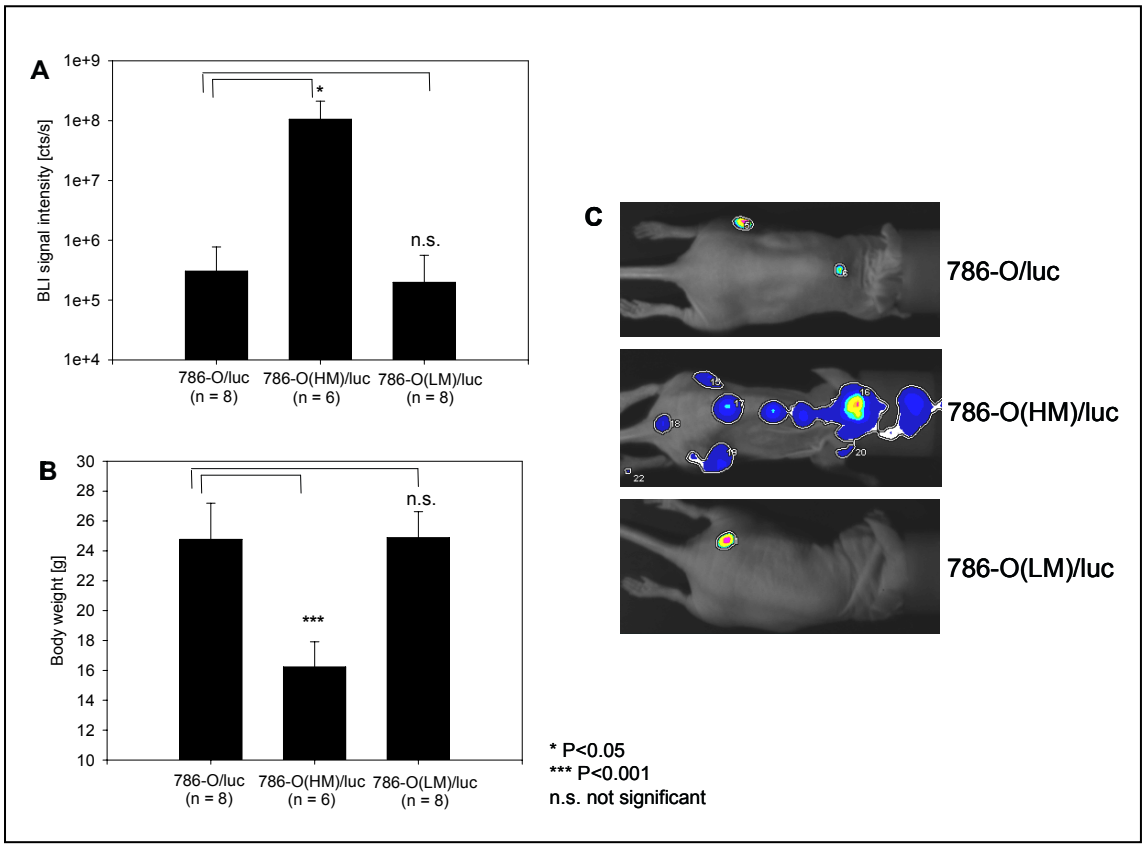

Figure 18: Tumor-induced cachexia and tumor burden in the parental and two *in vivo* selected 786-O/luc cell lines at day 49 (sacrifice). (A) Body weights were statistically significant lower in the highly metastatic 786-O(HM)/luc cell line compared to the parental cell line due to tumor-induced cachexia. (B) Inoculation of the 786-O(HM)/luc cell line resulted in higher tumor burden as indicated by statistically significant increased BLI signal intensity. Mean + SD values shown. (C) Representative BLI images of mice inoculated with the parental, high or low metastatic cell line to visualize tumor burden.

3.2.5 *In vitro* characterization of highly metastatic 786-O/luc subclone

Two different human RCC subpopulations with high and low metastatic potential *in vivo* (chapter 3.2.4) were selected from bone metastases caused by 786-O/luc cells characterized by different expressions of growth factors playing a role in RCC bone metastasis. The subpopulation with high metastatic potential, 786-O(HM)/luc, showed induction or similar expression of all analyzed factors compared to the parental cell line (Fig. 19). TGF-α, known to be involved in the RCC-stimulated osteoclast-mediated bone destruction (Takahashi et al., 1986), was on the same level in the 786-O(HM)/luc cell line as in the parental cell line ($P = 0.178$) but significantly decreased in the low metastatic 786-O(LM)/luc cell line after one cycle of *in vivo* selection ($P < 0.001$) (Fig. 19A). Pro-angiogenic factors such as VEGF and bFGF were significantly induced only in the highly

metastatic 786-O(HM)/luc *in vivo* selected cell line compared to the parental cell line (VEGF, P = 0.008; bFGF, P = 0.024) (Fig. 19B and 19C) which is in line with the hypervascularity of RCC bone metastases noted clinically (Durr et al., 1999). This was confirmed by histological examination. CD31 staining indicated huge blood-vessels and high micro vessel (MVD) density in RCC bone tumors (Fig. 19D, I-III). CD31 staining of a 786-O s.c. tumor showed similarly high MVD (Fig. 19D, IV). EGF could not be detected in 786-O/luc cell lines. Protein expression of CXCR4, a bone-homing factor, was present but no difference in CXCR4 levels could be observed in 786-O/luc cell lines (Fig. 19E).

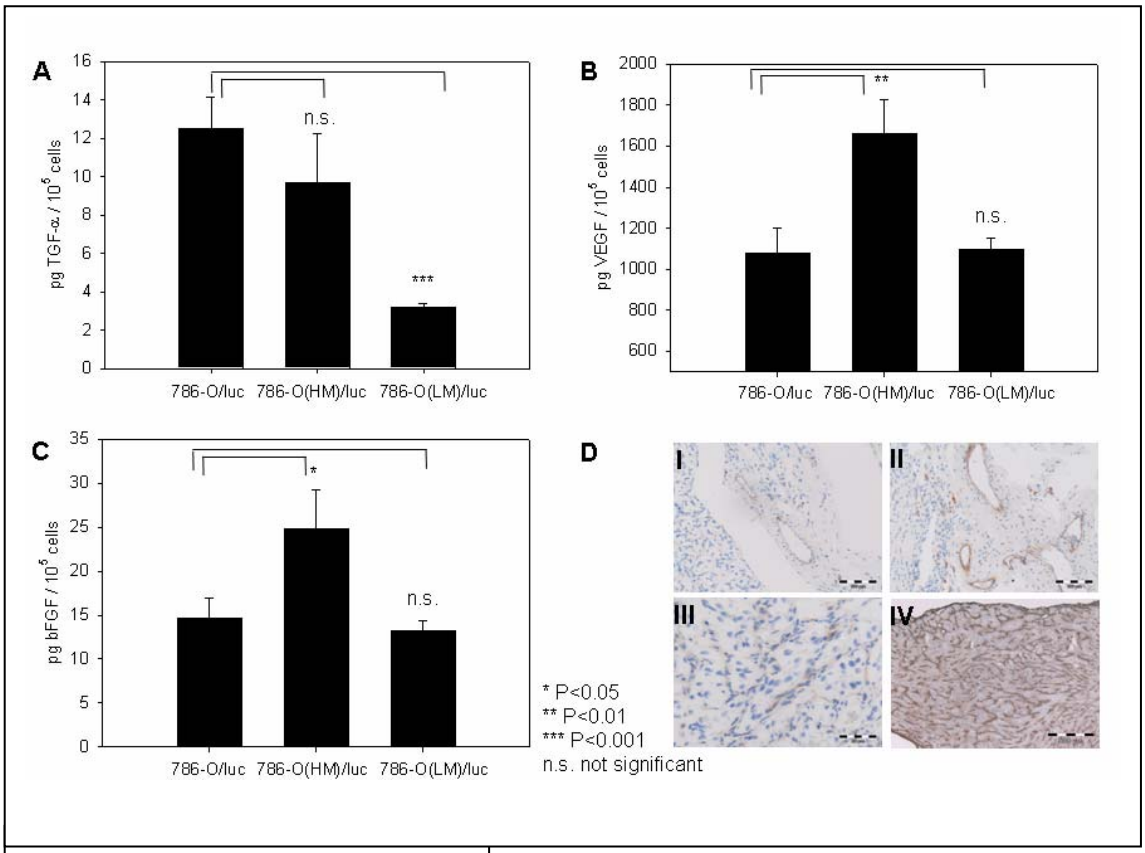

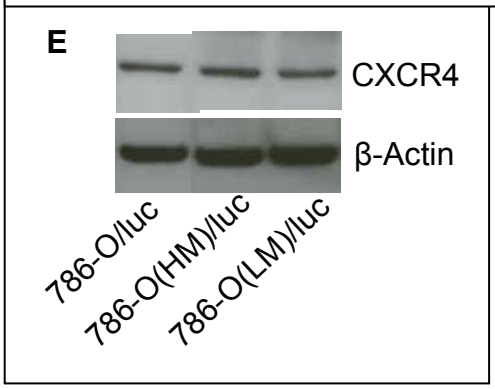

Figure 19. *In vitro* characterization of *in vivo* selected cell lines. To confirm their metastatic activity, different selected subpopulations were characterized by quantitative ELISA of (A) TGF-α, (B) VEGF and (C) bFGF which are known to be important factors in RCC bone metastasis. Subpopulation 786-O(HM)/luc showed induction of the pro-angiogenic factors VEGF and bFGF compared to the parental cell line. Mean + SD values shown. (D) CD31 staining of bone sections showing similar high micro vessel density compared to a 786-O s.c. tumor kindly provided by Nicole Kahmann. (magnification X 20 (I, II), X 40 (III), X 2.5 (IV)). (E) Western Blot of CXCR4 showing no differences in CXCR4 protein expression in different 786-O/luc cell lines.

3.3 The effect of sagopilone on tumor growth and bone resorption

Previous results indicated that sagopilone exerts cytotoxic effects against a panel of tumor models (Klar et al., 2006). As drugs that are effective against bone metastasis are rare on the market, the potential of sagopilone to inhibit tumor burden and the consequent bone destruction was determined. Here we additionally investigate the mechanisms underlying the inhibitory activity of sagopilone on tumor cells and osteoclasts. In summary, we showed that sagopilone inhibits breast cancer bone metastasis and bone destruction due to simultaneous inhibition of both tumor growth and bone resorption. Moreover, we show that sagopilone is far more effective than paclitaxel, another microtubule stabilizer, in preventing symptoms of bone metastases.

3.3.1 Inhibitory effect of sagopilone on MDA-MB-231 cell growth *in vitro*

To study the effects of sagopilone treatment on MDA-MB-231 and MDA-MB-231(SA)/luc tumor cell growth *in vitro* an alamar blue proliferation assay (chapter 2.5.4) and a caspase 3/7 assay (chapter 2.5.5) were performed (Fig. 20). The highly bone-metastatic subclone MDA-MB-231(SA)/luc grows around 2.2 times faster compared to the parental cell line. However, the effect of 10 nM sagopilone is similar on both cell lines inducing a strong antiproliferative effect. Sagopilone as a cytotoxic compound, which is able to inhibit the depolymerization of microtubules, blocks the cell cycle and then the cell undergoes apoptosis. This was confirmed by a caspase 3/7 assay showing increased caspase 3/7 activity in both cell lines while proliferation again is decreased.

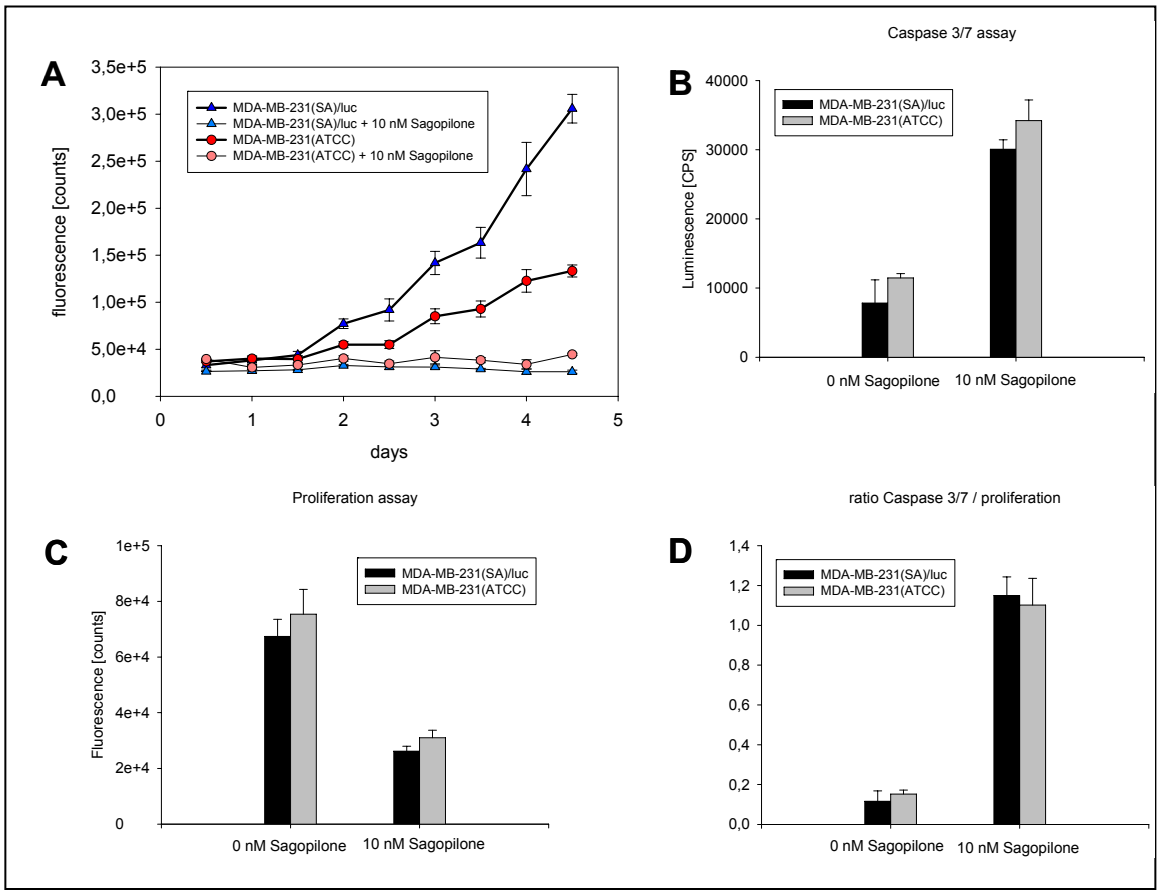

Figure 20. *In vitro* effects of sagopilone on MDA-MB-231 cells. (A) Inhibition of MDA-MB-231 and MDA-MB-231(SA) tumor cell proliferation by sagopilone treatment. Alamar blue proliferation assay showing anti-proliferative effect of sagopilone on both cell lines at a concentration of 10 nM over a period of 4 days. (B) Caspase 3/7 assay indicating induction of apoptosis after sagopilone treatment (10 nM), (C) Proliferation after 10 nM sagopilone treatment and (D) Normalization of caspase 3/7 assay on proliferation.

3.3.2 Inhibitory effect of sagopilone on MDA-MB-231 tumor growth *in vivo*

The *in vivo* efficacy of sagopilone was investigated by evaluation of the tumor-inhibiting effect of sagopilone in the human breast cancer model MDA-MB-231, xenografted in NMRI nude mice, based on tumor area during the study which was measured weekly with calipers. To compare the antiproliferative activity of sagopilone with a chemotherapeutic drug which is currently used in breast cancer treatment regimes, a paclitaxel treated group was included. The MDA-MB-231 cell line is tumorigenic in nude mice, forming poorly differentiated adenocarcinoma (grade III) and is widely used for the characterization of new cytotoxic drugs for breast cancer therapy. This model is rather moderate sensitive to the treatment with most cytotoxic drugs and therefore used for the

characterization of new compounds. Treatment with the epothilone derivative sagopilone with the maximum tolerated dose resulted in an inhibition of the tumor proliferation. The response rate after sagopilone treatment was similar to the reference compound paclitaxel. Sensitivity of the MDA-MB-231 model to sagopilone and paclitaxel treatment is shown by a complete inhibition of tumor growth in comparison to the progressive growth in the untreated control (Fig. 21). The response after sagopilone and paclitaxel treatment was significant to the control ($P<0.05$) (Fig. 21). It was found that sagopilone (8 mg/kg) and paclitaxel (12 mg/kg) were well tolerated with a body weight decrease of less than 10 % (Fig. 22).

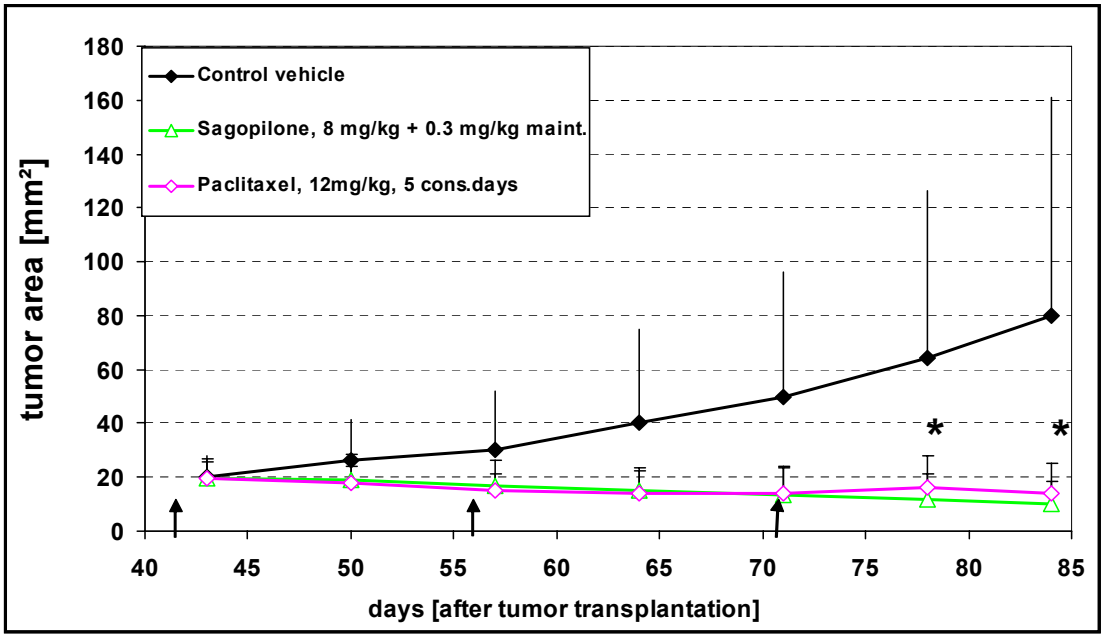

Figure 21. Evaluation of tumor growth inhibition by treatment with sagopilone and paclitaxel based on tumor area during the study. During the treatment period the tumor area was measured weekly with calipers. The changes of the tumor area in correlation with the time is shown. Start of treatment cycles are indicated by arrows. n = 7 for vehicle and sagopilone, n = 6 for paclitaxel group. Mean + SD values shown. * $P<0.05$ for vehicle vs. sagopilone and vehicle vs. paclitaxel using Dunn´s test.

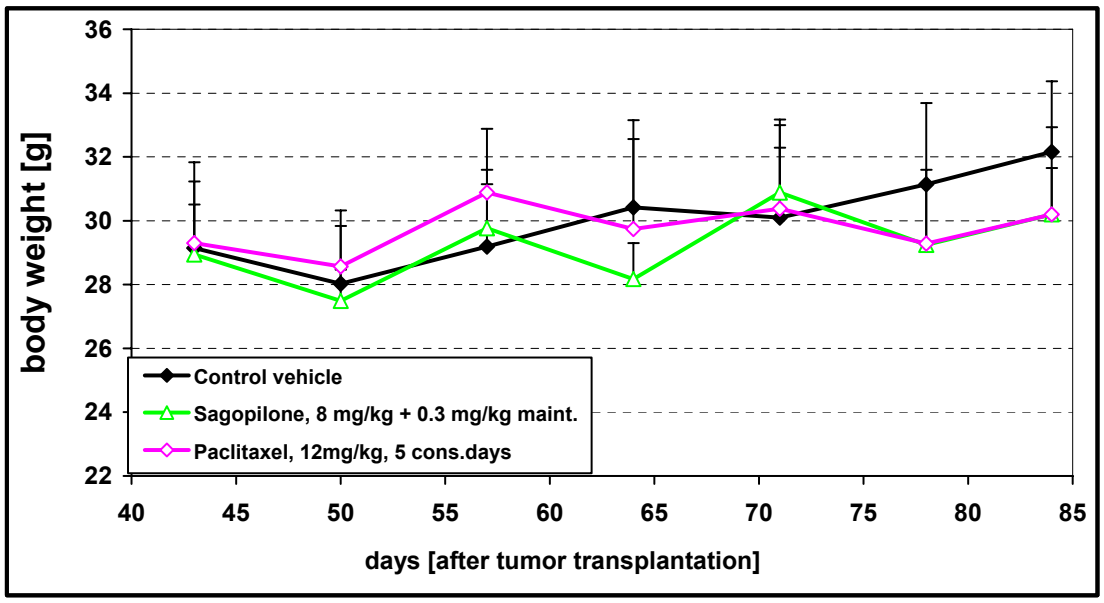

Figure 22. Evaluation of body weight as parameter for drug related toxicity during treatment with sagopilone. During the treatment period the body weight was measured weekly. n = 7 for vehicle and sagopilone, n = 6 for paclitaxel. Mean + SD values shown.

3.3.3 Efficacy of sagopilone in the MDA-MB-231 bone metastasis model

Sagopilone inhibits the growth of breast cancer cells *in vitro* and *in vivo* as exemplified by MDA-MB-231 tumor cells in chapter 3.3.1 and 3.3.2. In this study, we evaluated the activity of sagopilone or paclitaxel compared with vehicle treatment against osteolytic lesions and bone metastases in a human xenograft model of breast cancer bone metastasis, MDA-MB-231(SA), which was described in more detail in chapter 3.1, using treatment models simulating the adjuvant (preventive) and metastatic (therapeutic) settings in the clinic (Strube et al., 2009).

3.3.3.1 Effect of sagopilone in a preventive setting on

3.3.3.1.1 Tumor-induced cachexia

Sagopilone treatment was analyzed in a preventive setting in the MDA-MB-231(SA) model, simulating adjuvant treatment of a breast cancer patient at risk of bone metastases. To follow drug related toxicity, body weight of the mice was measured during the treatment period starting on day 5 until sacrifice on

day 19. Sagopilone treated mice (10 mg/kg) lost body weight until day 12 due to the cytotoxic effect of the drug but then recovered and benefit from the treatment. In contrast, body weight of the vehicle animals was stable until day 12 and then rapidly decreased due to tumor-induced cachexia (Fig. 23A). At the end of the study, mice treated with sagopilone had significantly higher body weights, with a mean of 22.3 ± 2.1 g compared with 20.1 ± 2.8 g in the vehicle group (P = 0.0433), indicating a significant reduction in tumor-induced cachexia (Fig. 23B).

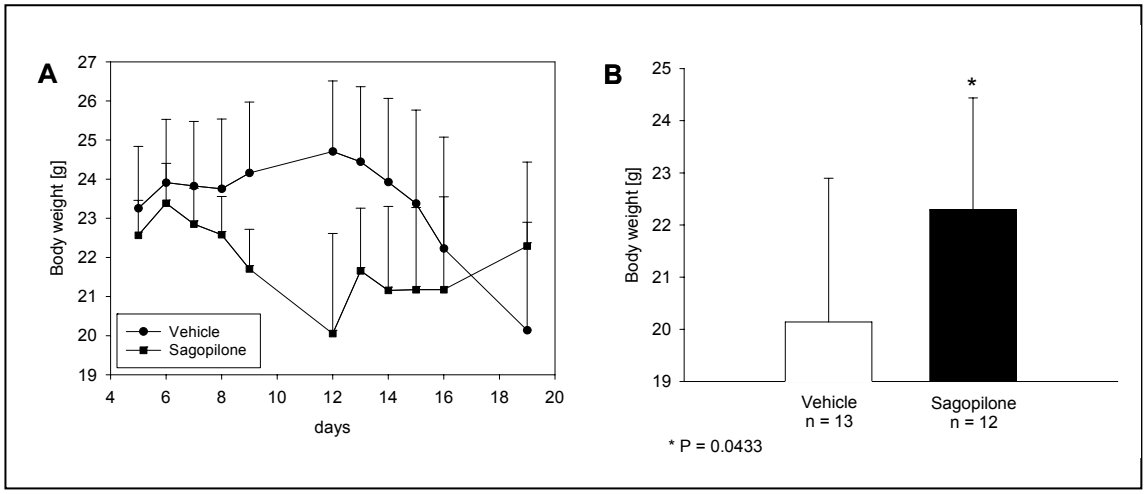

Figure 23. Evaluation of body weight in the preventive MDA-MB-231(SA) bone metastasis model as parameter for drug related toxicity and as indicator for tumor-induced cachexia during treatment with 10 mg/kg sagopilone. (A) Time course of the body weight of the mice during the treatment period. (B) Mean body weight of the mice at the end of the study (day 19). Mean + SD values shown.

3.3.3.1.2 Osteolytic lesions

Sagopilone treatment in this model also significantly reduced the area and number of osteolytic lesions compared with vehicle treatment, as measured by radiography (Fig. 24A). Untreated mice had a mean osteolytic lesion area of 8.1 ± 4.8 mm^2 compared with 0.1 ± 0.2 mm^2 in sagopilone-treated animals (P < 0.001) (Fig. 24B). The mean number of lesions was 21.2 ± 11.9 in vehicle-treated mice compared with 0.7 ± 0.9 in sagopilone-treated mice (Fig. 24C). Additionally, none of the mice in the sagopilone group (n = 15) had visceral metastases, compared with 5 of the vehicle group animals (n = 15) (data not shown).

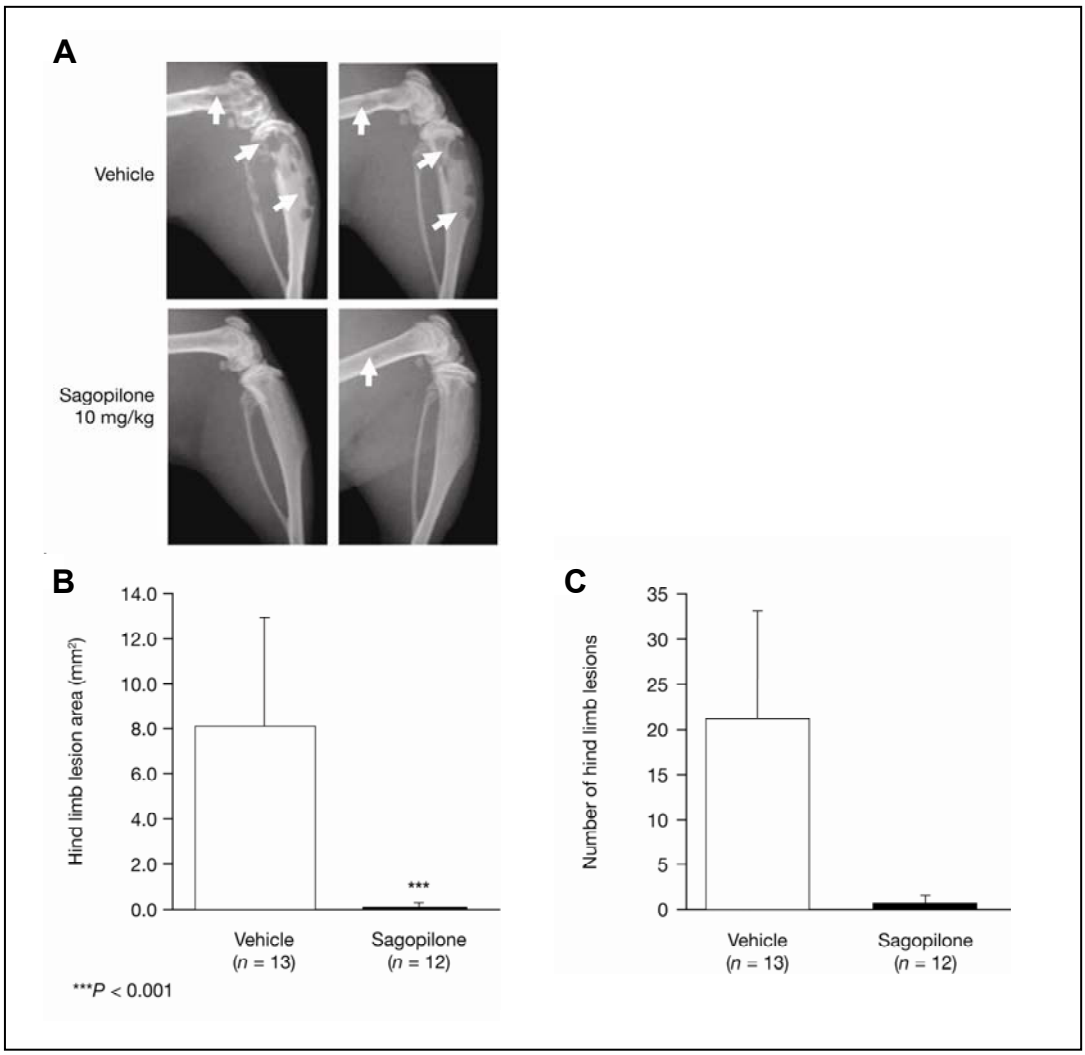

Figure 24. Sagopilone significantly reduces osteolytic lesions in a preventive MDA-MB-231(SA) treatment model of breast cancer bone metastasis. (A) Representative radiographs of hind limbs of vehicle- and sagopilone-treated animals 19 days after tumor cell inoculation (arrows indicate the extent of osteolytic lesions). Osteolytic lesion area (B) and lesion number (C) in hind limbs. Mean + SD values shown.

3.3.3.1.3 Tumor growth in bone

Sagopilone completely inhibited tumor growth in bone in this setting, as assessed by histomorphometry (Fig. 25). In vehicle-treated mice, tumors fill the bone marrow cavity, replace normal cellular elements and eventually lead to the destruction of cortical bone (Fig. 25A). Sagopilone treatment resulted in a complete inhibition of mean tumor growth compared with a tumor size of 6.3 ± 5.5 mm^2 in the vehicle group (Fig. 25B).

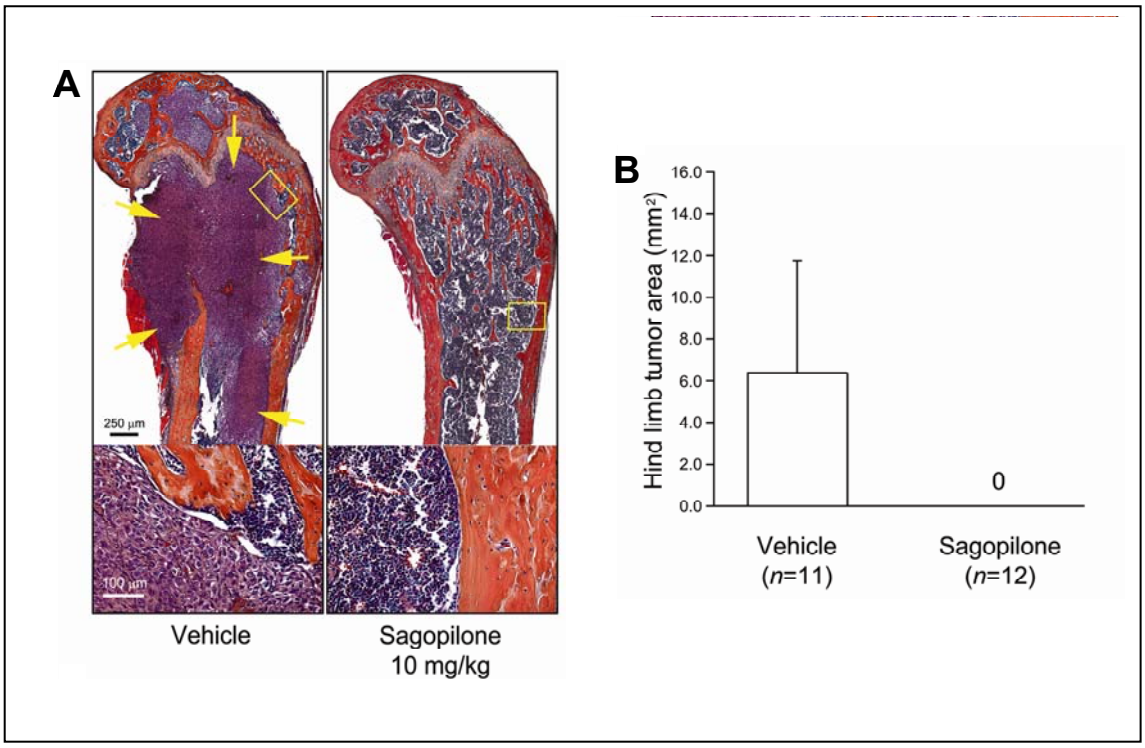

Figure 25. Sagopilone eradicates tumor growth in bone in a preventive MDA-MB-231(SA) treatment model of breast cancer bone metastasis. (A) Representative H&E-stained bone sections of femurs of vehicle- and sagopilone-treated animals (arrows indicate the extent of the tumor, for visualization of the bone and tumor morphology see insets, magnification X 10, insets X 20). (B) Tumor area in the hind limbs of vehicle- and sagopilone-treated animals. Mean + SD values shown.

3.3.3.2 Effect of sagopilone and paclitaxel in a therapeutic setting on

3.3.3.2.1 Tumor-induced paraplegia and cachexia

A second schedule was evaluated in the MDA-MB-231(SA) model to simulate the therapeutic treatment of a patient with advanced metastatic breast cancer involving osteolytic bone lesions. Similar to the results observed with sagopilone in the preventive treatment model, sagopilone or paclitaxel treatment also showed a trend for reduced tumor-induced cachexia in this therapeutic setting, with mean ± SD body weights of 18.8 ± 2.2 g and 19.3 ± 1.7 g in the sagopilone and paclitaxel groups, respectively, compared with 17.6 ± 1.8 g for vehicle-treated animals (Fig. 26A). There is not a statistically significant difference (P = 0.136). Both agents also considerably reduced the number of paraplegic animals compared with vehicle treatment, with approximately 10% of animals in the sagopilone or paclitaxel treatment groups affected versus 70% of vehicle-treated animals (Fig. 26B).

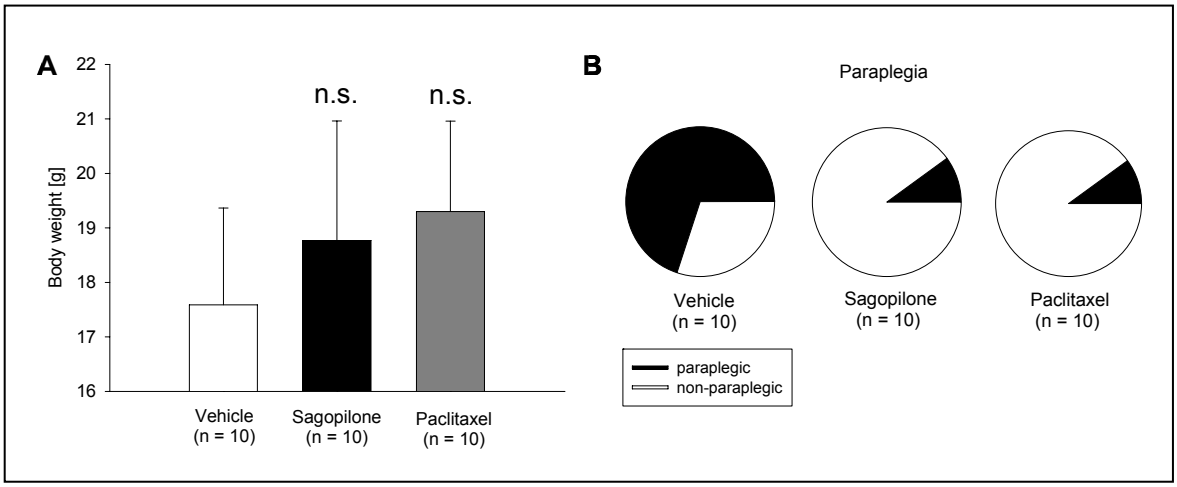

Figure 26. Sagopilone and paclitaxel reduce symptoms of tumor burden in the MDA-MB-231(SA) breast cancer bone metastasis model. Mice inoculated with MDA-MB-231(SA) cells and treated with sagopilone or paclitaxel had (A) a higher body weight and (B) much lower incidence of paraplegia than vehicle animals. Mean + SD values shown, n.s. not significant.

3.3.3.2.2 Osteolytic lesions

Radiography assessments performed 22 days after tumor inoculation in the therapeutic model indicated that sagopilone significantly reduced osteolytic lesions compared with vehicle group (Fig. 27A and 27B). The mean area of hind limb osteolytic lesions was significantly lower in sagopilone treated animals (1.16 ± 0.84 mm^2) compared with vehicle group (4.23 ± 2.06 mm^2; $P < 0.001$) and compared with paclitaxel treated animals ($P = 0.002$) (Fig. 27B). Paclitaxel also reduced lesion area (2.78 ± 0.83 mm^2) when compared with vehicle treatment, although this decrease was not statistically significant (Fig. 27B).

The analysis of skeletal changes, as measured by micro-CT, closely correlated with the radiography results (Fig. 27C and 27D). Bone destruction was again mainly evident at the proximal ends of femora and tibiae (Fig. 27C) and whole body images also revealed lesions in the hips, spine, forelimbs, scapula, and calvaria of tumor-bearing animals. Quantitation of hind limb total bone volume using micro-CT data (Fig. 27D) indicated that bone destruction in sagopilone-treated animals (bone volume 94.06 ± 5.57 mm^3) was significantly reduced compared with vehicle-treated animals (bone volume 87.85 ± 3.70 mm^3; $P = 0.03$) and paclitaxel-treated animals (bone volume 86.16 ± 3.19 mm^3; $P<0.001$). In contrast, bone destruction in the paclitaxel-treated group appeared to be similar to the vehicle group (bone volume 86.16 ± 3.19 mm^3; $P > 0.05$).

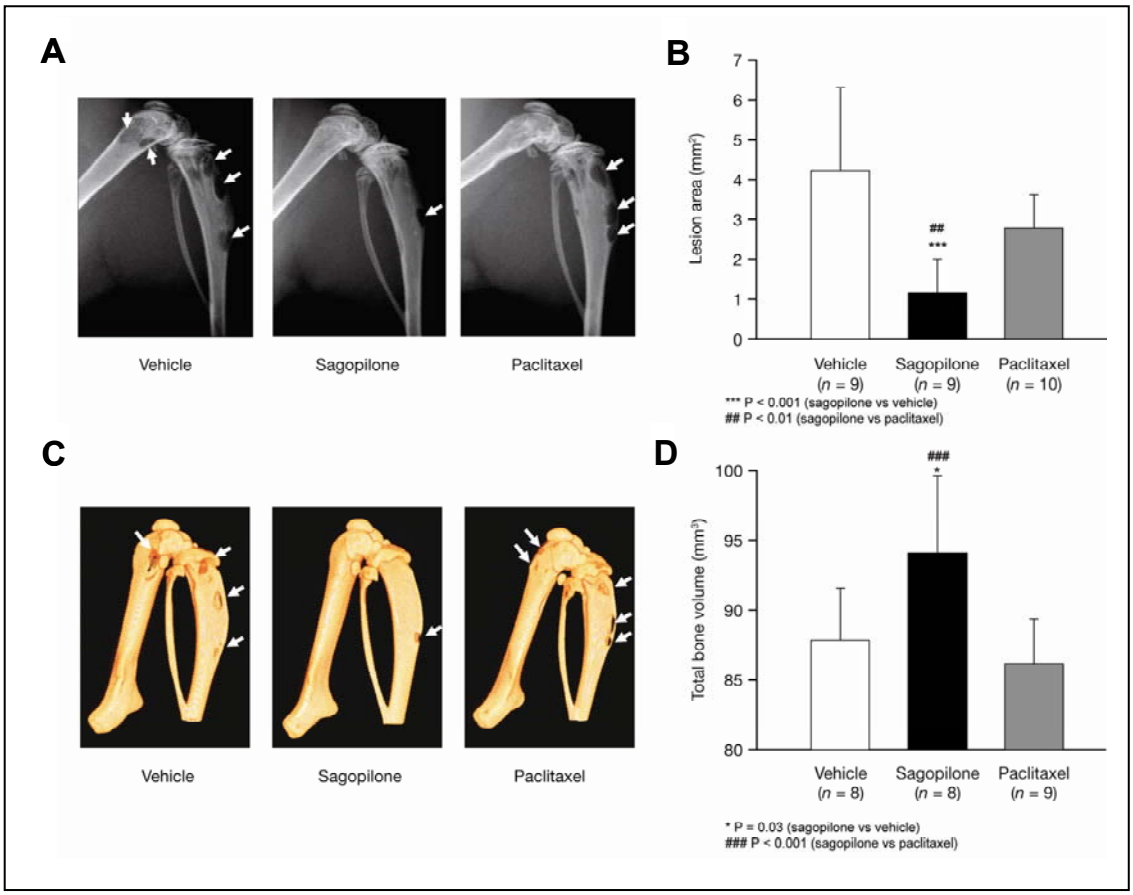

Figure 27. Sagopilone significantly reduces osteolytic lesion area and loss of bone volume compared with paclitaxel in the MDA-MB-231(SA) model when used as therapeutic treatment. (A) X-rays taken at day 22 after tumor cell inoculation (arrows indicate the extent of osteolytic lesions) and (B) corresponding lesion area. (C) Micro-CT scans showing representative three-dimensional images and (D) corresponding quantitation of total bone volume of both hind limbs. Mean + SD values shown.

3.3.3.2.3 Tumor growth in bone

Assessment of luciferase-expressing tumor cells by BLI at sacrifice (day 22) was used to measure tumor progression in bone, as well as the spread of tumor cells in other tissues. The bioluminescence signal indicated tumor cells in the region of hind limbs, forelimbs, spine, and brain (Fig. 28A). A significant decrease in bioluminescence signal intensity was observed in the sagopilone treatment group (167551 ± 205993 cts/s) as well as in the paclitaxel-treated group (366622 ± 258612 cts/s) compared with the vehicle group (2604798 ± 2372678 cts/s) ($P = 0.011$ for vehicle versus paclitaxel and $P < 0.002$ for vehicle versus sagopilone) (Fig. 28B), indicating that both treatments reduced tumor burden.

The bioluminescence data were confirmed by histologic examination of tumors

in bone (Fig. 28C and 28D) and visceral organs, confirming a correlation between both methods. In paclitaxel- and vehicle-treated mice, tumor area in bone extended throughout the marrow cavity and replaced normal cellular elements (Fig. 28C). Quantitation of tumor size in multiple sections revealed a significantly lower tumor area in bone in the sagopilone-treated animals ($1.27 \pm 0.98\ mm^2$) compared with the vehicle group ($8.16 \pm 5.22\ mm^2$) ($P < 0.001$) and compared with paclitaxel-treated animals ($P = 0.005$), thus reflecting the antitumor effect of sagopilone in bone metastases (Fig. 28D). The tumor area in bone of paclitaxel-treated animals ($4.52 \pm 2.33\ mm^2$) was not statistically lower than in the vehicle group. In addition, a lower number of sagopilone-treated animals (20%), and no paclitaxel-treated animals, exhibited adrenal gland metastases compared with the vehicle group (43%) (data not shown).

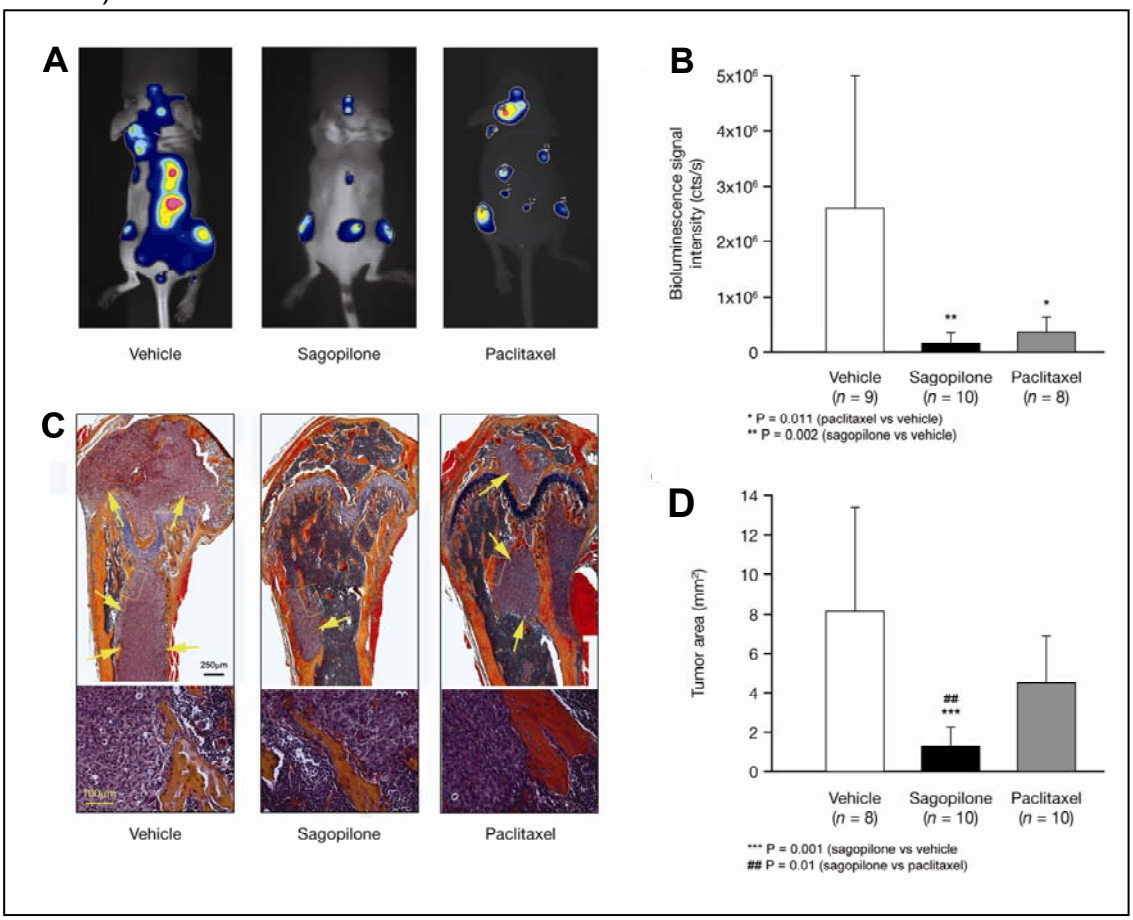

Figure 28. Sagopilone and paclitaxel considerably reduce tumor burden in a therapeutic MDA-MB-231(SA) treatment model of breast cancer bone metastasis. (A) Bioluminescence images indicating the tumor burden and (B) corresponding bioluminescence intensity quantitation. (C) Representative H&E-stained bone sections of femurs of vehicle-, sagopilone- and paclitaxel-treated animals (arrows indicate the extent of the tumor, for visualization of the bone and tumor morphology see insets, magnification X 10, insets X 20) and (D) corresponding tumor area in bone quantitation. Mean + SD values shown.

3.3.3.2.4 Activation of osteoclasts *in vivo*

TRACP 5b is expressed in bone-resorbing osteoclasts and is therefore considered to be a useful marker of bone resorption rate (Alatalo et al., 2003). We measured the serum TRACP 5b concentration and analyzed TRACP staining in hind limbs (Fig. 29A), where it correlates with the number of activated osteoclasts. The osteoclast cell count indicated a statistically significant increase of activated osteoclasts in the vehicle (10.57 ± 2.42) group compared with paclitaxel-treated (7.40 ± 2.94; P = 0.002) and sagopilone-treated animals (3.67 ± 2.20; *P* < 0.001) (Fig. 29B). Additionally, serum TRACP 5b concentrations were significantly lower in sagopilone-treated mice (5.59 ± 0.96 U/L) and paclitaxel-treated mice (5.24 ± 0.48 U/L) compared with the vehicle group (8.93 ± 1.76 U/L; P < 0.001 in both cases) (Fig. 29C), suggesting a considerable reduction in the bone resorption rate after sagopilone or paclitaxel treatment. There is no statistically significant difference between sagopilone and paclitaxel treatment groups.

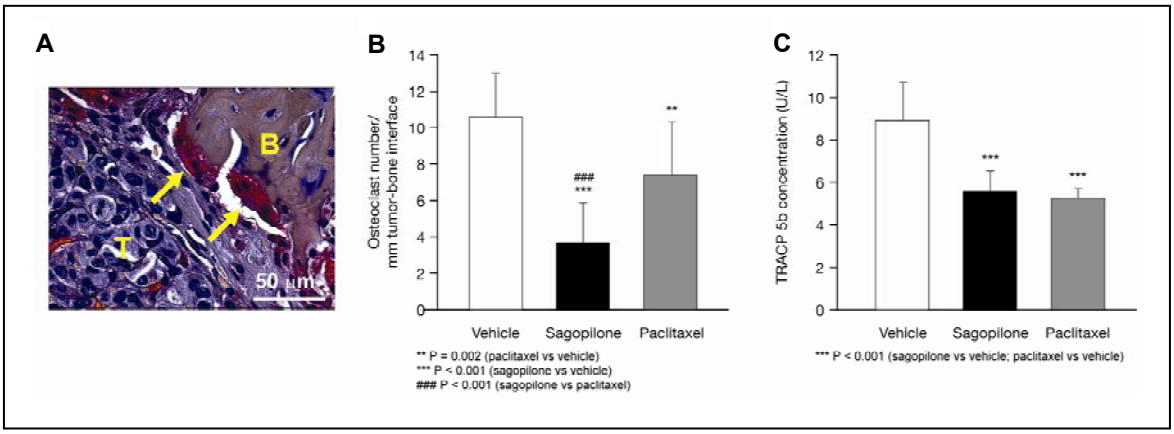

Figure 29. Sagopilone-treated animals have a significantly lower number of activated osteoclasts and bone resorption rate compared with vehicle- and paclitaxel-treated mice. (A) TRACP staining of bone showing active multinucleated osteoclasts resorbing bone in the tumor-bone interface (arrows indicate osteoclasts; B, bone; T, tumor; magnification X 40). (B) Osteoclast number / mm tumor-bone interface calculated in TRACP-stained sections. (C) Serum TRACP 5b concentration. Mean + SD values shown. TRACP 5b, serum tartrate-resistant acid phosphatase 5b.

3.3.3.3 Anti-resorptive effect of sagopilone *in vitro*

Sagopilone significantly inhibited osteoclast activity in a dose-dependent manner in an *in vitro* human osteoclast activity assay (Fig. 30A), but was not cytotoxic to osteoclasts (Fig. 30B). In comparison, while paclitaxel also showed an inhibitory effect on osteoclast activity, although to a lesser extent (Fig. 30C), this was associated with significant cytotoxic effects at several dose levels (Fig. 30C). The reference inhibitor E64 significantly inhibited osteoclast activity and showed no cytotoxic effects, demonstrating that the results obtained are reliable.

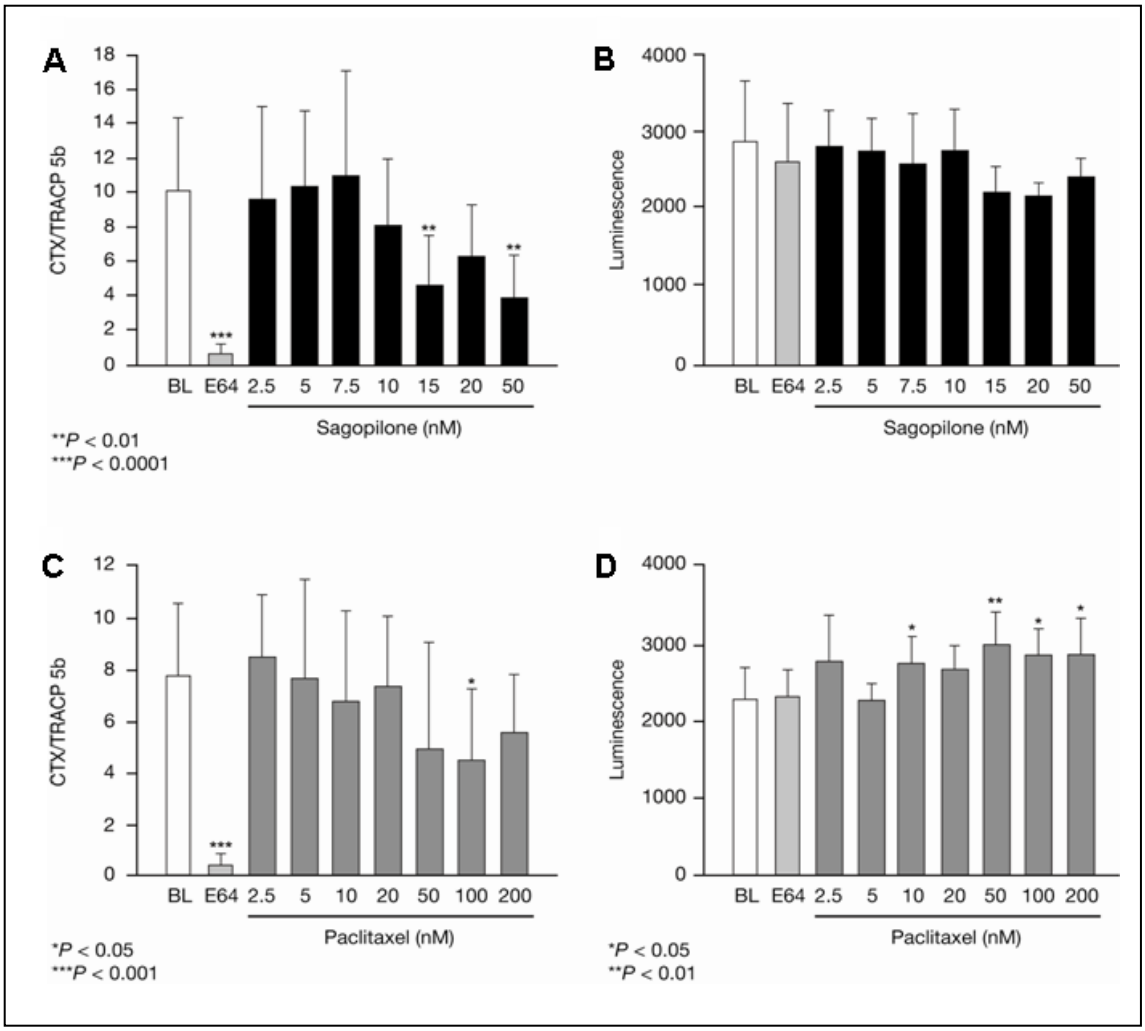

Figure 30. Sagopilone reduces the resorption activity of human osteoclasts with no cytotoxic effects in a human osteoclast activity assay. The mean osteoclast activity in sagopilone-treated (A) and paclitaxel-treated (C) cells expressed as the resorption index (CTX concentration at day 10 / TRACP 5b concentration at day 7). Cytotoxicity in sagopilone-treated (B) and paclitaxel-treated (D) cells determined as the luminescence released from dying cells during the culture period. Mean + SD values shown. BL, baseline.

Both compounds, sagopilone and paclitaxel, showed short-term inhibitory effects in the osteoclast differentiation assay (Fig. 31A and 31C), but had no effects in the osteoclast activity assay (Fig. 31B and 31D). Sagopilone inhibited osteoclast differentiation at 5 nM and 10 nM concentrations, whereas paclitaxel showed inhibitory effects only at 20 nM concentrations. Based on microscopic evaluation both compounds didn´t show clear cytotoxic effects in the osteoclast differentiation and activity assay after short-term treatment of compounds (Fig. 32 and 33).

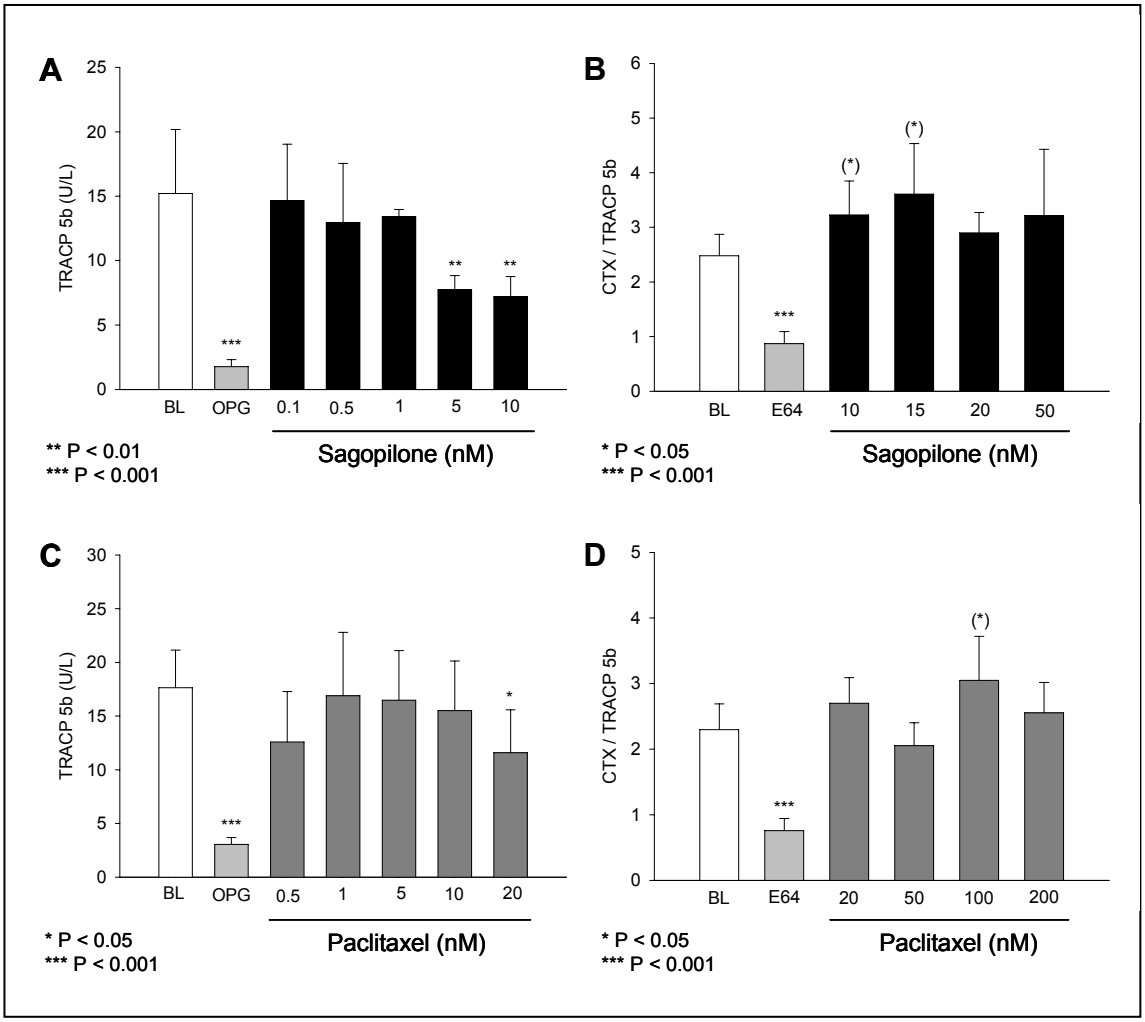

Figure 31. Short-term effects of sagopilone and paclitaxel on human osteoclast differentiation and activity *in vitro*. Effects of sagopilone (A) and paclitaxel (C) on osteoclast differentiation at day 7 shown as TRACP 5b activity (U/L) secreted into the culture medium during the differentiation period (days 1-7). Effects of sagopilone (B) and paclitaxel (D) on osteoclast activity at day 10 expressed as the resorption index (CTX concentration at day 10 / TRACP 5b concentration at day 7). Mean + SD values shown. BL, baseline.

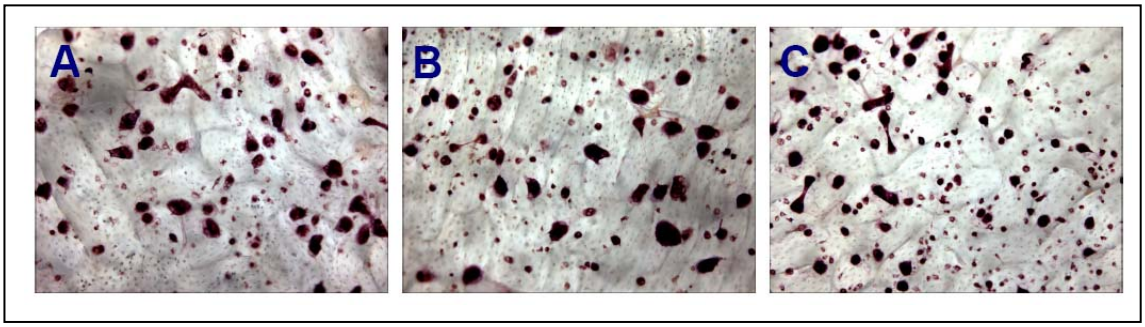

Figure 32. Microscopic evaluation of cytotoxicity in human osteoclast differentiation assay. Representative microscopical images of the effects of sagopilone and paclitaxel in human osteoclast differentiation assay. TRACP staining at day 7 (magnification X100). (A) Cells from the baseline group. (B) Cells from the group treated with 10 nM sagopilone. (C) Cells from the group treated with 20 nM paclitaxel.

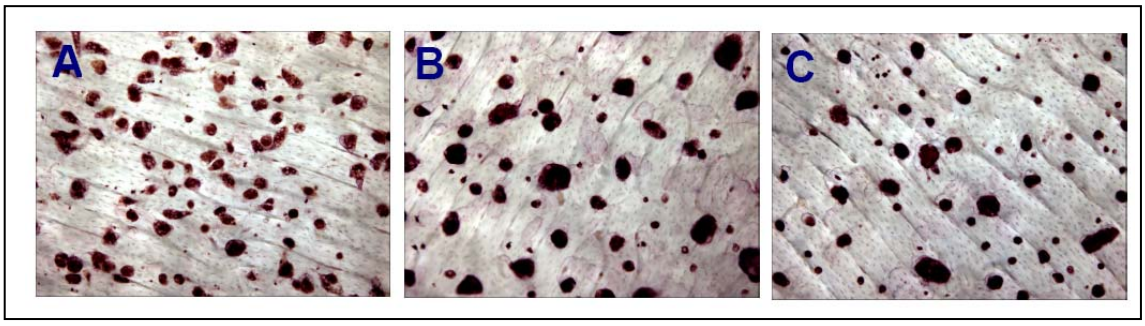

Figure 33. Microscopic evaluation of cytotoxicity in human osteoclast activity assay. Representative microscopical images of the effects of sagopilone and paclitaxel in human osteoclast activity assay. TRACP staining at day 10 (magnification X100). (A) Cells from the baseline group. (B) Cells from the group treated with 50 nM sagopilone. (C) Cells from the group treated with 200 nM paclitaxel.

3.3.3.4 Anti-resorptive effect of sagopilone *in vivo*

To study the effect of sagopilone on bone resorption *in vivo* in the absence of tumor, a preclinical mouse model of ovariectomy (OVX)-induced osteoporosis was established in C3H/HeN mice. These mice suffer from bone loss after estrogen withdrawal and mimic the situation of postmenopausal women suffering from osteoporosis. Thus, this model allows for investigating the direct effects of sagopilone on activated osteoclasts *in vivo*. To determine if the model is working, ANOVA was done showing that there is a statistically significant difference between control and OVX groups and no difference between control and OVX+E2 groups with regard to body weight and uterine weight. As a consequence, these parameters (body weight and uterine weight) indicate that the operations and dosings were performed successfully. Then the groups were

compared separately to OVX group using t-test.

As depicted in Figure 34, body weights significantly increased after OVX ($P < 0.001$) (Fig. 34A) whereas uterine weights significantly decreased ($P < 0.001$) when OVX group is compared to control (sham-operated) group (Fig. 34B). Estrogen replacement by E2 (17β-estradiol) pellets prevented the effects caused by OVX and resulted in body weights and uterine weights at the same level as the control group. Thus, a statistically significant difference could be observed between OVX and OVX+E2 treated animals (body weights, uterine weights: $P = 0.003$). Body weights of sagopilone treated animals were significantly lower compared to the OVX animals ($P = 0.002$), whereas uterine weights were similar in these groups ($P = 0.157$).

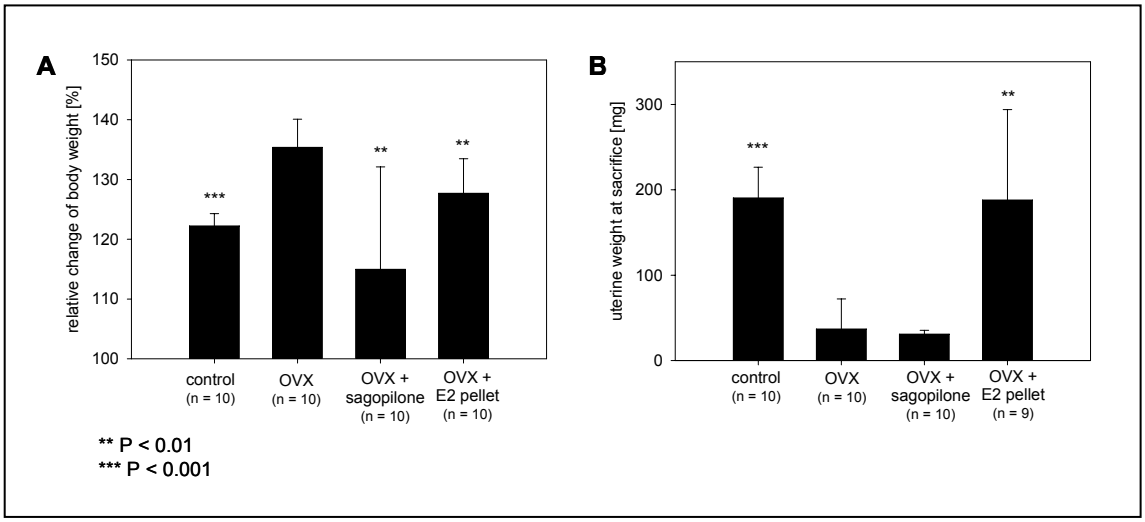

Figure 34: Body weights and uterine weights 42 days after OVX. (A) Body weights significantly increased after OVX, the effects were prevented by estrogen replacement. Sagopilone treatment significantly reduced body weights compared to the control group due to its antiproliferative effects on somatic cells. (B) Uterine weights significantly decreased after OVX, the effects were prevented by estrogen replacement. Sagopilone resulted in reduced uterine weights. Mean + SD values shown. Statistics: All groups were compared separately to OVX group using t-test.

Six weeks after surgery, osteoporotic changes were observed by pQCT and CT measurements (Fig. 35 and 36). OVX caused significant bone loss compared to sham-operated animals ($P = 0.001$) indicated by reduced bone mineral density (BMD) in the tibial metaphysis as determined by pQCT measurements (Fig. 35A). The effects of OVX on trabecular bone were prevented by estrogen replacement therapy ($P<0.001$ for OVX vs. OVX+E2). Sagopilone treatment

resulted in significantly increased trabecular BMD in the tibial metaphysis compared to OVX mice (p = 0.009) suggesting an inhibitory effect of sagopilone on activated osteoclasts *in vivo* (Fig. 35A). No differences in cortical BMD in the tibial diaphysis were observed between the groups (Fig. 35B).

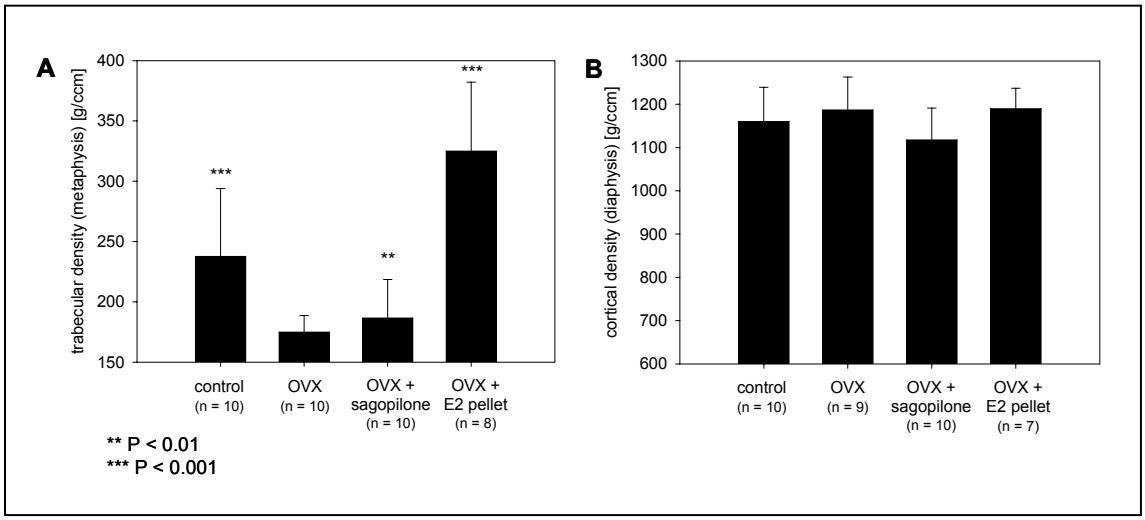

Figure 35: Trabecular and cortical bone mineral density 42 days after OVX. (A) Trabecular bone mineral density (BMD) in the tibial metaphysis significantly decreased after OVX as measured by pQCT, the effects were prevented by estrogen replacement. Sagopilone significantly increased BMD compared to OVX animals. (B) No differences in cortical BMD in the tibial diaphysis were observed between the groups. Mean + SD values shown. Statistics: All groups were compared separately to OVX group using t-test.

High resolution (20 µm) CT scans visually illustrate osteoporotic changes in bone. OVX animals show clearly reduced trabecular density in the metaphysis of the tibia compared to the sham-operated mice as indicated by decreased grey scale values in both axial and saggital sections of the bone (Fig. 36). Sagopilone inhibited the effects of ovariectomy-induced bone loss resulting in a slightly more distinct trabecular network visible in saggital isosurface images.

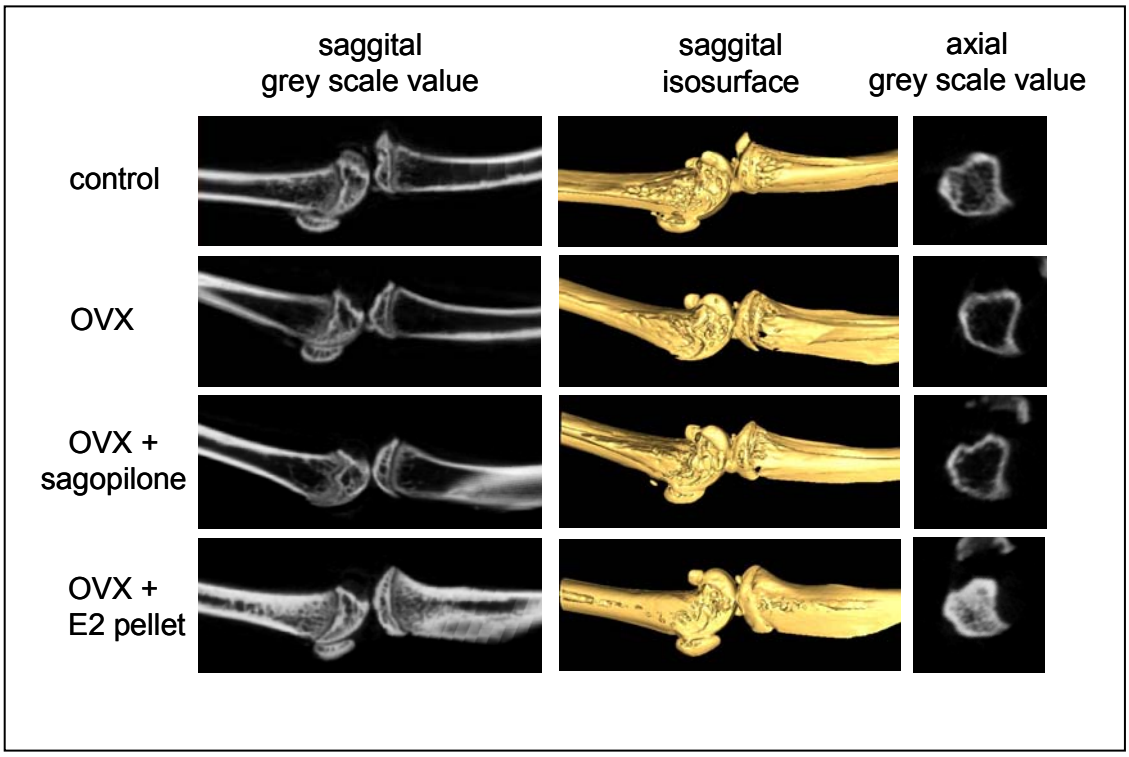

Figure 36: High resolution CT scan of osteoporotic changes in bone 42 days after OVX. Trabecular bone mineral density in the tibial metaphysis decreased after OVX as measured by CT (resolution 20 µm), the effects were prevented by estrogen replacement resulting in a distinct trabecular network. Sagopilone slightly increased BMD compared to OVX animals.

4 DISCUSSION

4.1 Development and characterization of bone metastasis mouse models

Cancer metastasis to bone is a severe, incurable disease. There is a high incidence of skeletal complications among metastatic breast cancer and RCC patients leading to a decline in the quality of life (Coleman, 1997). Patients suffer from the highly aggressive nature of the particularly osteolytic lesions causing intractable pain, hypercalcemia and increase of the fracture risk (Cameron et al., 2006; Zekri et al., 2001). Furthermore, treatment possibilities are limited and mainly palliative. Especially advanced RCC is difficult to treat because this tumor is highly resistant to systemic therapy (Milowsky and Nanus, 2003; Motzer et al., 1997; Vuky et al., 2006). In many cases a surgical resection of the tumor is the only proven modality of treatment and can result in prolonged survival (Leibovich and Blute, 2006). Moreover, very little is known to date about the underlying molecular mechanisms of RCC bone metastasis. Consequently, there is a crucial need for well-characterized animal models to mimic the clinical situation, to identify targets involved in cancer metastasis to bone and to evaluate and find new therapy approaches which can contribute to the reduction of the risk of developing skeletal complications.

Taken together, results presented in this thesis highlight the importance of the development and characterization of animal models for RCC and breast cancer bone metastasis. The 786-O and MDA-MB-231 model provide reliable situations of the clinical situation as they reproduce many of the features seen in patients despite significantly shorter duration and allow the design and optimization of more effective treatments by better understanding the biology that regulates RCC and breast cancer bone metastasis.

4.1.1 Breast cancer

The MDA-MB-231(SA) heart injection model in which 100,000 cancer cells are directly inoculated into the arterial circulation is a suitable model to study the mechanisms of bone metastasis as metastases preferentially and sometimes exclusively occur in bone and only to a less extent in lung, liver or other visceral

organs (adrenal glands, ovary, brain) (Yoneda, 1997). However, this model represents late stages in osteolytic metastasis. Consequently, the major disadvantage of this model is the lack of the early steps of the metastatic process including early growth of the primary site and intravasation of tumor cells (Céspedes et al., 2006). Additionally, tumor cell lines are often passaged for many generations which might not be representative of the tumor in its native state and might alter pathways that drive metastasis (Kamb, 2005). Furthermore, systemic inoculation requires large bolus injections of tumor cells which doesn´t accurately reflect the situation in patients with metastatic disease. In patients generally just few tumor cells enter the systemic circulation from the primary site. Finally, the use of immunocompromised animals doesn´t reflect the human situation either although studies in these mice are predictive of clinical responses (Kamb, 2005). However, the MDA-MB-231 model mimics crucial features of human disease. Especially, the availability of established preventive and therapeutic settings can specifically reflect early and late stage breast cancer bone metastasis. Of course, no single animal model of cancer is an exact surrogate for human disease, but the MDA-MB-231 model closely replicates histology, physiological effects and at least some of the biochemical pathways of breast cancer bone metastasis. Moreover, the MDA-MB-231 bone metastasis model is valuable for preclinical therapy and appropriate for evaluating compounds for several reasons: On the one hand, it allows for the routine and rapid screening of many compounds due to its short duration of only 3 weeks. On the other hand, there is a high incidence of animals affected by tumor burden and bone lesions with an almost ideal take rate of 100% which guarantees reproducibility. Another important point is the availability of objective and quantitative endpoints of therapeutic responses, such as paraplegia, cachexia, osteolytic lesion area or tumor area, which allows reliability in determining potency of different compounds.

Despite the almost 100% take rate in the MDA-MB-231(SA) model presented in this thesis, a randomization based on osteolytic lesion size was performed before the start of treatment in the therapeutic setting (chapter 2.2.3). In contrast, other studies report that although animals were measured by radiography before start of treatment to confirm appearance of osteolytic

lesions, they were then divided into groups irrespective of lesion size (Peyruchaud et al., 2001; Canon et al., 2008). However, the occurrence of osteolytic lesions depends on technical skillfulness (Yoneda et al., 2000) and can therefore vary between animals. The randomization as done in the efficacy study presented in this thesis ensures that mean osteolytic lesion size per treatment group is almost the same at start of treatment and that animals without osteolytic lesions can be excluded. Furthermore, the day of randomization differs between different studies presented in the literature. Regarding the MDA-MB-231 heart injection model, a study reported randomization at day 7 and median survival time of 27 days (Canon et al., 2008) whereas randomization in the study presented in this thesis was done at day 12 and sacrifice at day 22 (see Fig. 7). Late randomization makes the model more aggressive and more difficult to show efficacy of compounds in this setting. Instead of randomization by osteolytic lesion area, the randomization by tumor burden measured by BLI is reported at day 3 after inoculation of the tumor cells (Buijs et al., 2007). However, as discussed in more detail in chapter 4.2.3, BLI is a semi-quantitative method so that X-ray randomization is preferred when osteolytic lesions are already visible and measurable. On the other hand, BLI randomization on day 3 after tumor cell inoculation is useful as there are no osteolytic lesions visible by radiography yet. Instead of BLI the use of fluorescence imaging using a bone-metastatic GFP-labeled subclone of the MDA-MB-231 cell line is reported (Peyruchaud et al., 2001). Fluorescence imaging allowed the detection of bone metastases approximately one week before the occurrence of radiologically distinctive osteolytic lesions indicating that fluorescence imaging is a modality to detect early events during formation of bone metastases (Peyruchaud et al., 2001).

A model that overcomes some limitations of the heart injection model mentioned above is the 4T1 orthotopic spontaneous bone metastasis model that better represents the whole metastatic process beginning from the primary site and as a consequence more closely resembles the situation in patients except that the tumor cells used are not of human origin. Furthermore, removal of the primary tumor is possible, comparable to the clinical situation where the tumor is surgically removed, and provides a model for adjuvant therapy of occult

metastasis (Killion et al., 1999). However, due to the murine origin of the 4T1 mammary cancer cells, that derive from a spontaneous carcinoma of a Balb/cfC3H mouse, this model allows the use of immunocompetent syngeneic female mice (Balb/c). Inoculation of 4T1 cells in the mammary fat pad of 4-6 week old mice causes primary tumor formation and metastases to multiple organs including bone within 4-5 weeks (Yoneda et al., 2000). One problem with this model is the low take rate with regard to the development of bone metastases. Bone metastases, which occur in approximately 70% of patients with metastatic breast cancer, arise spontaneously in this model (Lelekakis et al., 1999) so that the use in drug development is to test strategies which target the metastatic disease in general and not specifically bone metastases.

Especially in drug development, the use of mouse models is beneficial and inexpensive compared to rat models because less compound is needed due to the lower body weight of the mice. In addition, efficacy studies always require different study groups to test various compounds and several animals per group to minimize variability. Compared to rats, a huge number of mice can be housed in relatively little space because of their small body size. Additionally, mice are quicker to breed and easier to manipulate genetically (Lindblad-Toh, 2004). Both rats and mice grow rapidly, have relatively short lifespans, a rapid rate of reproduction, a well-characterized skeleton and are widely available. Thus, rodents have been proven to be not only good models in bone metastasis but in cancer research in general (Rosol et al., 2003; Bibby, 2004). However, especially in biomarker or pharmacokinetic studies which require serum for multiple biochemical measurements, the rat model is preferred due to higher blood volume. Moreover, rats are physiologically more similar to humans than mice. Thus, rats are superior in toxicological studies because humans and rats share more of the detoxifying P450 genes compared to humans and mice (Lindblad-Toh, 2004).

4.1.2 Renal cell cancer

Whereas breast cancer bone metastasis models are quite popular, so far, experimentally induced models of RCC bone metastasis are rare (Rosol et al.,

2003). The only available mouse model for RCC bone metastasis was developed in the group of Kristy Weber and utilizes the bone-derived RBM1 cell line which was isolated from a bone metastasis of a patient with advanced RCC (Weber et al., 2002). These cells are inoculated intratibially and develop osteolytic lesions similar to those in patients.

According to our knowledge, the 786-O/luc mouse model characterized in this thesis is the first model available using a RCC cell line derived from a primary clear cell adenocarcinoma that causes bone metastasis after intracardiac inoculation. This model develops severe osteolytic lesions in hind limbs, forelimbs, spine, hips and sometimes in the scapula and the spine similar to those noted in the clinical setting. Bone lesions in patients associated with RCC are typically osteolytic (Zekri et al., 2001). The lesions that developed in the mice inoculated with 786-O/luc cells resemble those in patients and were highly destructive and of osteolytic nature leading in some cases to long-bone fractures, a feature also observed in patients (Zekri et al, 2001). The particularly osteolytic character of the lesions was confirmed by the correlation between tumor area and number of activated osteoclasts indicating an osteoclast-mediated bone resorption. The hypervascularity of RCC bone tumors noted clinically (Durr et al., 1999) is also evident in our model and indicated by high micro-vessel density in CD31 stained bone sections, which was similarly high compared to a 786-O s.c. tumor (Fig. 19D, IV). The less intense staining of bone tumors is due to paraffin embedding which is unfavourable for the CD31 antibody used compared to frozen sections of the s.c. tumor. Taken together, this model provides a good reproduction of the disease in patients and might help to find and evaluate effective treatment possibilities.

A disadvantage of the original 786-O/luc bone metastasis model for its use in preclinical therapy was the long duration until the development of bone metastasis as well as the varying endpoint between different animals (50-80 days after inoculation). To establish a model that is suitable for therapeutic testing, including short duration and equal time of sacrifice, an *in vivo* selection can be done with the aim to accelerate the development of osteolytic lesions in the 786-O/luc model. Using this approach, we were able to isolate a high and a low metastatic subpopulation, 786-O(HM)/luc and 786-O(LM)/luc respectively,

compared to the parental cell line. The increased metastatic ability of *in vivo* selected cells doesn´t result from a faster growth rate but rather from the acquisition of specific metastasis-promoting functions and the ability to mobilize and recruit host osteoclasts. In general, cancer cell populations are heterogeneous and consist of a mixture of cells with different abilities to metastasize to different secondary sites (Fidler and Kripke, 1977). The aim of the *in vivo* selection approach is to isolate highly bone metastatic subpopulations from the original mixture. The ability to form aggressive bone metastases is in turn associated with a characteristic gene expression profile. As hypervascularity is associated with RCC bone metastasis, we analyzed pro-angiogenic factors and could find that those are overexpressed in the highly metastatic 786-O(HM)/luc *in vivo* selected subpopulation compared to the parental and the low metastatic 786-O/luc cell line (chapter 3.2.5). Among those factors are VEGF and bFGF which are reported to be crucial for angiogenesis, proliferation, survival and spread of cancer cells (Dvorak, 2002; Rini and Small, 2005). As reported, the induction of proangiogenic factors in the majority of RCC is due to the inactivation of the von Hippel-Lindau (VHL) tumor suppressor gene, which is also deficient in 786-O cells (Gorospe et al., 1999). The loss of VHL leads to stabilization of hypoxia-inducible factor-1α (HIF-1α) which in turn results in the expression of many proangiogenic factors such as VEGF (Semenza, 2002). VEGF is the most important angiogenic cytokine and its overexpression contributes to the typical hypervascular histology of clear cell RCC (van Spronsen et al., 2005). Thus, it is not surprising that tumor growth of the 786-O(HM)/luc cell line is favored by increased angiogenesis resulting in a more active stimulation of osteoclasts and consequent bone destruction as noted *in vivo* (chapter 3.2.4). Furthermore, besides its stimulating effect on tumor growth in bone, both VEGF and bFGF exert direct effects on osteoclasts as well. VEGF is reported in osteolytic bone metastasis of hepatocellular carcinoma (HCC) to act on osteoclasts thereby stimulating bone resorption and contributing to the high incidence of bone metastasis in HCC of 13% (Iguchi et al., 2002). It was also demonstrated that VEGF enhances survival, differentiation and resorptive activity of osteoclasts (Yang et al., 2008). bFGF is described to induce osteoclast formation in bone marrow cultures of C57BL/6

mice (Hurley et al., 1998). In summary, not only published data but also the elevated levels of both factors in the highly metastatic *in vivo* selected cell line indicate a role of VEGF and bFGF in both tumor growth and bone resorption in the 786-O/luc model but clarification of the processes involved needs further investigations. To confirm their role in bone resorption, VEGF and bFGF could be tested in the osteoclast differentiation and activity assay (chapter 2.5.1) if increased activity and possibly differentiation are observed. Investigations if VEGF downstream targets are activated by increased bone resorption in osteoclasts, for example PI3-kinase → Akt or MEK → ERK pathways, would give further insight into the involvement of VEGF in bone resorption. Furthermore, the efficacy of angiogenesis inhibitors in the 786-O model, such as PTK/ZK (Bayer Schering Pharma AG and Novartis Pharma) which selectively blocks VEGF receptor tyrosine kinase signaling from all known VEGFs, followed by thorough analysis of CD31, VEGF and bFGF immunohistochemical stainings in bone sections as well as serum levels of these factors would clarify the importance of angiogenic factors in the 786-O model.

To analyze the metastatic potential of the selected cell lines *in vivo*, the different subclones were again i.c. inoculated resulting in the almost 3-fold increased development of osteolytic lesions of the 786-O(HM)/luc subclone compared to the parental 786-O/luc cell line (chapter 3.2.4). In addition to the *in vitro* studies, the more aggressive nature of osteolytic lesions confirms as well that the selection process was successful. However, the 786-O(LM)/luc subclone didn´t result in the development of more destructive lesions compared to the parental cell line indicating that such selection procedures do not always yield cells with increased metastatic ability (Ling et al., 1985; Stackpole et al., 1991). These studies and also my study show that some metastatic properties are not stably maintained within the tumor cell population but exert transient functions to promote metastasis. Finally, the s.c. tumor growth of the high metastatic, low metastatic and parental 786-O/luc cell lines needs to be evaluated and compared with tumor growth in a bone metastasis study. Equal s.c. tumor growth of the three cell lines definitely confirms that the *in vivo* selection approach was successful. This means that the accelerated growth of bone

metastases is not due to increased proliferation of the 786-O(HM)/luc cell line but to the acquisition of bone metastasis promoting factors. However, also accelerated growth of the highly metastatic subclone compared to the parental cell line would indicate successful *in vivo* selection with both high expression of proliferation- and bone metastasis-promoting factors.

However, the mechanisms involved in 786-O/luc tumor cell-induced bone destruction are still unclear but seem to be similar to those known to be important in RCC bone metastasis (Weber et al., 2007). The molecular pathways of RCC bone metastasis are different from those identified in breast and prostate cancer bone metastasis. PTHrP, one of the most important factors in the vicious cycle of breast cancer bone metastasis (Guise et al., 2005; Guise et al., 2002), doesn´t play a key role in RCC stimulated bone destruction although this factor is expressed by bone-derived RCC cells (Weber et al., 2007). However, this needs to be confirmed for the 786-O/luc model presented in this thesis. As reported, 786-O cells also express large amounts of PTHrP and its receptor PTH1R (Massfelder et al., 2004). Anti-PTHrP treatment (N-terminal PTHrP neutralizing antibody or PTH1R antagonist) induced tumor regression of s.c. implanted 786-O cells in 70% of mice (Massfelder et al., 2004). It needs to be investigated if in the 786-O bone metastasis model PTHrP contributes to autocrine growth of 786-O cells (Burton et al., 1990) or promotes osteoclast differentiation like in breast cancer bone metastasis (Guise et al., 1996). First, PTHrP and PTH1R protein levels in 786-O/luc parental and 786-O(HM)/luc cell lines could be analyzed to give first evidence of possibly increased expression in the highly bone-metastatic subclone. Second, to investigate the role of PTHrP in the 786-O bone metastasis model in *vivo*, PTHrP bone plasma concentrations of affected hind limbs need to be measured as described by Guise et al., 1997. Elevated PTHrP levels in bone plasma compared with blood plasma would indicate enhanced production of PTHrP by tumor cells in the bone microenvironment. If elevated PTHrP bone plasma levels are measured, a study with anti-PTHrP treatment in the 786-O model needs to be performed which could confirm a role of PTHrP in bone resorption if decreased osteolytic lesion area would be observed. Although the role of PTHrP in the 786-O model is still unclear, there is evidence that 786-O/luc

tumor cells stimulate the activation of osteoclasts (chapter 3.2.3) possibly via VEGF and bFGF. The number of osteoclasts is in turn increased by TGF-α that stimulates the proliferation of osteoclast precursors (Takahashi et al., 1986). As a consequence, a vicious cycle of RCC bone metastasis as depicted in Fig. 37 can be assumed although there are still a variety of other factors involved.

To more clearly clarify processes and reveal new targets of RCC bone metastasis an extensive gene expression study between the highly metastatic 786-O(HM)/luc and the parental cell line would be helpful as described for the validation of genes important in breast cancer bone metastasis (Kang et al., 2003). A microarray study could identify bone-homing, metastasis- or osteolysis-promoting factors that might be important in RCC bone metastasis. As shown, the bone-homing factor CXCR4 is expressed by 786-O/luc cells but doesn´t seem to play a major role showing the same protein expression in high metastatic, low metastatic and parental 786-O/luc cell lines (chapter 3.2.5). Instead of CXCR4, bone sialoprotein (BSP) and osteopontin (OPN), two bone matrix proteins with significant roles in normal bone metabolism, have both been proposed to play a role in metastatic homing to bone (Carlinfante et al., 2003). The expression of these adhesive proteins varies between different tumor cell types causing bone metastasis and might facilitate the interaction with the bone surface. One other factor possibly important in 786-O induced osteolysis could be macrophage inflammatory protein-1δ (MIP-1δ or CCL15), originally called leukotactin-1, which was identified as a novel osteoclast stimulatory factor produced at elevated levels in human RCC bone metastasis tissues relative to primary RCC tissues and bone marrow from healthy adults. MIP-1δ also enhanced osteoclast differentiation in response to RANKL (Kominsky et al., 2008). Moreover, there is evidence that the expression of matrix metalloproteinase-13 (MMP-13), playing a role in tumor-induced osteolysis, is increased in RCC bone metastasis compared to primary and adjacent normal kidney tissue and regulated by TGF-β1 (Kominsky et al., 2008). TGF-β1 in turn is a known RCC bone metastasis-promoting factor and TGF-β1 stimulation of RCC bone metastasis cells plays a role in promoting tumor growth and osteolysis *in vivo* (Kominsky et al., 2007). However, as reported, the 786-O cell line expresses high amounts of TGF-β1 but no TGF-β type II

receptor (Ananth et al., 1999). Due to the abrogation of the TGF-β type II receptor expression, 786-O cells are resistant to the antiproliferative effects of TGF-β1 (Ananth et al., 1999). Moreover, it has been shown that TGF-β1 stimulates angiogenesis (Massagué et al., 1992). To investigate the role of TGF-β1 in angiogenesis in 786-O cells, the effect of a TGF-β neutralizing antibody on VEGF and bFGF levels *in vitro* could be analyzed. As a consequence, in the 786-O/luc model presented in this thesis, other bone-derived growth factors than TGF-β1 might exert effects on tumor cells, such as BMPs, PDGFs or IGFs. This could be analyzed by investigating *in vitro* cell proliferation or levels of for example proangiogenic factors or cytokines in 786-O/luc cells after treatment with the corresponding growth factor and vehicle respectively.

Taken together, the development of the 786-O/luc bone metastasis model and the consequent *in vivo* selection approach presented in this thesis are the basis for the identification of targets implicated in RCC bone metastasis, to substantiate the proposed vicious cycle of RCC bone metastasis (Fig. 37) and improve therapeutic interventions.

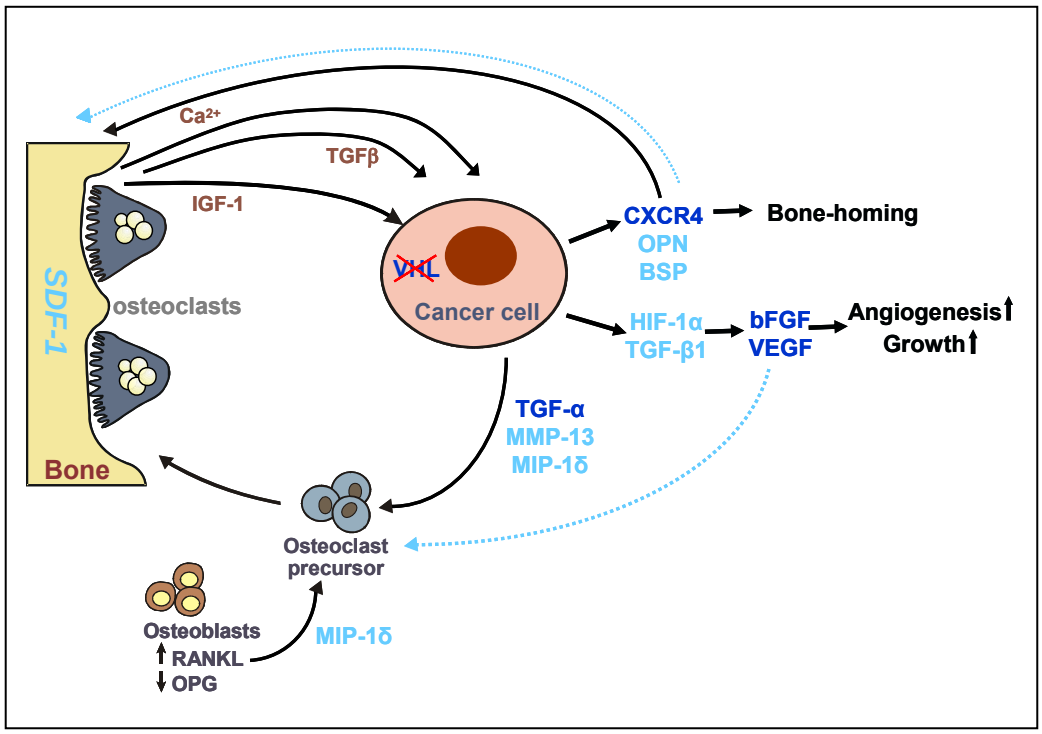

Figure 37. Proposed vicious cycle of RCC bone metastasis. Possible mechanisms involved in RCC metastasis to bone as described in more detail in the text (chapter 4.1.2). According to the results presented in this thesis, factors shown in dark blue are suggested to play a role in 786-O/luc induced bone metastasis. Factors shown in light blue needs to be validated for the 786-O/luc model.

4.2 Small animal imaging technologies in bone metastasis models

4.2.1 Impact on the 3 Rs

Chapters 3.1 and 3.2 describe thorough characterizations of mouse models of tumor metastasis using a variety of imaging technologies and histological examination. In a bone metastasis model, tumor size cannot be assessed *in vivo* using conventional methods such as the caliper. Thus, imaging is a necessary tool to avoid the sacrifice of animals at given time points to assess tumor size at necropsy. As a consequence, without these technologies substantially more animals would need to be used which means that the combination of different imaging technology has the potential to substantially contribute to the 3 Rs, especially to the reduction of animals used per experiment and refinement of the experimental design (Hagelschuer et al., submitted). Since assessment of tumor size is terminal, a group of mice needs to be sacrificed at every time point of interest. Whereas repeated measurements in individual animals minimize variability, a higher number of mice per group are required using conventional techniques (= Reduction). That means reduction of animals is achieved by reducing variability: as animals are followed over time, each animal serves as its own control. Consequently, inter-individual variability is eliminated, and higher statistical power is obtained, allowing the number of animals per group to be reduced. Furthermore, the quality of data obtained from an animal experiment can be enhanced by performing imaging studies. BLI or PET imaging for example allow for a longitudinal monitoring of tumor cell localization and for the detection of whole-body tumor burden (Chang et al., 2006) which would be very difficult using conventional methods requiring for instance the time-consuming and cumbersome histological analysis of all tissues and bones. Thus, luminescent and PET imaging provide substantially more information from the same number of animals than conventional methods (= Reduction and Refinement). The same is true for radiography and micro-CT measurements allowing observations of bone destruction over time. However, when performing longitudinal X-ray measurements the exposure to radiation needs to be considered which might exert therapeutic effects on tumor and consequently on

lesions (Taschereau et al., 2006). Furthermore, because tumor burden can typically be quantified at earlier stages, due to the high sensitivity of luminescent imaging and PET technology (McCaffrey et al., 2003; Schirrmeister, 2007), a shorter overall time course of experiment is possible, thus minimizing the strain on the animals (= Refinement). Refinement can be achieved by making it possible to define earlier, less stressful time points and milder degrees of disease. A complete replacement of bone metastasis experiments is not possible due to the complex mechanisms involved including manifold interactions between for example the bone microenvironment, osteoclasts, osteoblasts, tumor cells, immune cells, stroma and vasculature. To date, there are no cell and tissue culture models or computer simulations available for studying the processes in a whole living system (Festing, 2007). Not only in bone metastasis but in many instances, animal experiments are the only method to answer complex biological questions, and are not likely to be replaceable by other methods in the near future. Hence, it is an important goal to adapt and refine existing methods in order to minimize strain on the laboratory animals; luminescent imaging, PET, micro-CT and radiography have already been proven by the studies presented in this thesis to improve animal welfare by contributing to this important goal. In conclusion, imaging modalities contribute to animal welfare by reducing and refining *in vivo* experiments. As optical imaging technology progresses, further advances are likely that will result in further improvements of animal experiments.

4.2.2 Impact on animal model development

For the 786-O/luc model development, a combination of different imaging modalities was used. The 786-O/luc-labelled cell line allowed for the monitoring of tumor burden and dissemination of cancer cells by BLI. This technique is especially useful for the localisation of tumor cells but less applicable for quantitative analysis because it is a semi-quantitative method depending as in more detail described in chapter 4.2.3 for example on the depth of the tumor in the body or oxygen availability for the luciferin-luciferase reaction (Sadikot and Blackwell, 2005). In contrast, histological examination displays structural

changes in bone including cortical destruction of bone or replacement of bone marrow by tumor. However, histological examination can only be assessed at sacrifice and not *in vivo* by longitudinal measurements as it is for example possible with BLI. To histologically determine tumor burden at different time points, more study groups would be needed which would be in turn unfavourable in terms of the 3R concept (see chapter 4.2.1). In addition, although histology allows for accurate quantitative examination of tumor area in bone, always only one level of bone is examined. As a tumor is a three-dimensional object, the quantitation is consequently not an exact reflection of the whole tumor. Anyway, the choice of a longitudinal midsection of each bone guarantees that the method can be reliably used for quantitation. To improve the accuracy of the method, several slides could be examined and quantified. Although BLI is measured in the whole animal, it cannot be used for the three-dimensional quantitation of the tumor either. The BLI signal intensity is reduced from a 3D object (=tumor) to a 2D signal, one of the reasons why BLI is a semi-quantitative method (Sadikot and Blackwell, 2005). However, for characterization of unknown mouse models, whole-body BLI is a fast and beneficial method for tumor cell detection. To overcome limitations of quantitation of tumor, PET imaging could be performed followed by quantitation of the signal which accurately displays the 3D structure of the tumor. However, for a large number of animals the use of this techniques is impossible due to long measurement times.

As for the assessment of skeletal changes, radiography and micro-CT measurements nicely correlated in terms of structure and localisation of osteolytic lesions (chapter 3.1.1 and 3.2.2). Quantitation of osteolytic lesions by radiography was, however, better applicable to the MDA-MB-231 model as the osteolytic lesions are well-defined on the radiography images. In contrast, osteolytic lesions caused by 786-O/luc tumor appeared diffuse on the radiography images due to much more extensive osteolysis compared to the MDA-MB-231 model. The large tumor in bone in the 786-O/luc model expands the bone so that the lesion area measured was larger than the bone itself and depended on the size of the tumor (chapter 3.2.1, Fig. 13). A possibility to avoid difficulties in measuring osteolytic lesion area in the 786-O model, would be to

determine a region of interest (ROI) at earlier time points of the study, for example after 4 weeks of tumor cell inoculation when the tumor and osteolytic lesions are relatively small. The ROI should reflect the original area of tibia and femur respectively. At later time points of the study, osteolytic lesion area should only be determined within the ROI irrespective of possible bone destructions outside of the ROI. However, as a consequence, for the 786-O model, the quantitation of bone volume by micro-CT measurements, as validated for the MDA-MB-231 model (chapter 3.3.3.2.2), seems to be more suitable and should be used in future studies. This technique allows the measurement of the bone volume that is not degraded irrespective of the dimension of the tumor and is consequently more reliable for determination of osteolytic lesions in the 786-O model.

Moreover, a good correlation was observed between whole-body BLI and radiography measurements (chapter 3.1.2, Fig. 12) indicating that bone destruction increases with the extent of tumor burden. These observations are in line with the well-known theory about the development of bone metastases caused by breast cancer cells stating that bone destruction is the result of an increase of osteoclast activation induced by breast cancer cells (reviewed in Käkönen and Mundy, 2003). As depicted in Figure 12C, the mice cluster in 2 groups both with very low or no BLI signal intensity. One group is characterized by very small osteolytic lesion area. These animals reflect the sagopilone treated mice indicating, as investigated in this thesis, the strong antiproliferative and antiresorptive activity of this drug compound. The other group shows higher osteolytic lesion area. These animals belong to the group treated with paclitaxel, a compound with also high antiproliferative but less antiresorptive effects compared to sagopilone as reported in this thesis as well. However, BLI measures whole-body tumor burden whereas X-ray and histology measurements determine osteolytic lesion area and tumor burden respectively only in the hind limbs. In addition to this fact, also the semiquantitative character of BLI might contribute to decrease the degree of correlation between these methods.

The regions of bone destruction in turn are areas of high metabolic activity compared to the normal bone. These can be easily detected by ^{18}F-fluoride

PET/CT measurements which accurately reflect the localisation of high bone turnover as well as bone destruction. The very high uptake of ^{18}F-fluoride in lytic breast cancer metastases is already known from previous studies (Petren-Mallmin et al., 1998). In patients, imaging studies are indispensable to detect asymptomatic RCC more frequently and at an early stage of disease as well as in the early stages of metastatic dissemination. Especially the high sensitivity of PET-imaging contributes to the detection of early and consequent small metastases (Eubank and Mankoff, 2005). This was clearly observed in a PET-study of the 786-O model using a tracer in clinical development of Bayer Schering Pharma AG in which each metastasis detected by PET could be histologically verified (data not shown). The Research-Workplace (IRW) software (Siemens) used for analysis of the PET/CT data also allows quantitation of PET signal intensity so that this imaging modality might be used for monitoring therapy.

4.2.3 Impact on compound screening

Another fundamental application of imaging modalities is the combination of these technologies as helpful tools in determining the efficacy of pharmacological compounds in a therapeutic setting (Strube et al., 2009). In the bone metastasis study described in chapter 3.3.3.2, the efficacy of sagopilone against bone metastases *in vivo* was assessed using a combination of different imaging techniques: BLI to monitor dissemination of cancer cells and tumor burden, X-ray for quantitative analysis of bone lesions, and micro-CT, which accurately reflects a three-dimensional view of the skeleton, for morphologic changes. We found that micro-CT also allows quantitative analysis of tumor volume in bone, similar to its use in other studies to accurately quantify bone loss (Barck et al., 2004; von Stechow et al., 2003). Treatment effects determined by micro-CT measurements in the sagopilone and paclitaxel treatment groups correlated with the X-ray data (chapter 3.3.3.2.2). Consequently, both methods can be used for quantitation but the radiography measurements are generally preferred due to time saving reasons, especially if a large number of animals needs to be analyzed. Nevertheless, the method of

choice is dependent on the animal model and the characteristics of the lesions analyzed as described in chapter 4.2.2. To conclude, for the MDA-MB-231 model radiography measurements are probably sufficient to reliably determine osteolytic lesion size whereas for the 786-O model and also models with osteoblastic bone metastasis micro-CT measurements are probably the better if not only option to obtain reliable data.

In terms of measuring efficacy against tumor burden, BLI and histologic examination also showed a good correlation in this study (chapter 3.3.3.2.3). Histologic examination is essential for measuring structural bone changes, including cortical destruction and effects on bone marrow. Furthermore histology is useful for clarifying mode of action of compounds. To cite an example, TRACP staining in bone sections revealed inhibitory effects of sagopilone on activated osteoclasts as shown in this thesis. Another example is an immunohistochemistry staining for active caspase 3 which can confirm apoptotic effects of compounds in tumor tissue sections (Ottewell et a., 2008). In contrast, BLI is suitable for semi-quantitative assessment of tumor progression in bone. More precisely, although BLI is a commonly used, powerful and relatively cost-effective technology, several issues need to be considered when using this imaging tool. First, the luciferase reaction is a complex interaction of several molecules. If one of these molecules for example oxygen is not abundantly present which is the case in hypoxic tumor areas, light emission doesn´t represent the luciferase activity as well as the biologic effect. Second, the transmission of light through animal tissue is limited and wavelength-dependent resulting in loss of photon intensity coming from signals in deep tissues. This is also one of the reasons why optical imaging is not readily applicable to diagnostic imaging in patients, because most organs of interest would be out of reach; additionally firefly luciferase is not of human origin. Third, optical imaging is based on two-dimensional planar images. Thus, to interpret the planar light signals obtained, depth of the light source, tissue penetration and scattering must be taken into consideration. Consequently, these issues contribute to the fact that BLI signal intensity provides semiquantitative information and needs validation for specific applications (Sadikot and Blackwell, 2005).

In the clinic, imaging techniques for early detection of metastases are indispensable because most serum markers, such as the bone resorption marker TRACP 5b, are insufficiently sensitive to detect early bone metastases, although they can serve as early indicators of treatment response (Chao et al., 2004).

4.3 Dual action of sagopilone in the treatment of bone metastases

In the efficacy studies described in chapter 3.3, it was shown that sagopilone, the first fully synthetic epothilone in clinical development, has high activity and is well tolerated *in vivo* in the MDA-MB-231(SA) breast cancer bone metastasis xenograft model when used as both a preventive and therapeutic treatment against bone metastases. The action of sagopilone against bone metastases appears to be two-fold, combining the inhibition of tumor cell growth with the inhibition of osteoclast activation and bone resorption. In the development of breast cancer bone metastases tumor growth leads to bone resorption and vice versa (Guise et al., 2005), and compounds that can inhibit the process at both stages, such as sagopilone, may therefore provide a promising therapy option against bone metastases.

4.3.1 Preventive model

In our preventive treatment model, tumor cells had already spread to the bone but treatment was started before the development of osteolytic lesions. This scenario aimed to simulate the adjuvant setting in the clinic, with local or distant breast cancer progression without diagnosed bone metastases. Patients with a high risk of developing bone metastases include those with positive lymph node status or immunocytochemical evidence of bone marrow involvement (Alexandrova et al., 2003; Colleoni et al., 2000). Our *in vivo* data suggests that sagopilone may increase metastasis-free survival by reduction of cancer dissemination, combined with an almost complete eradication of metastatic tumors in bone and the inhibition of osteolysis. The effects of this treatment include reduced tumor-induced cachexia, which can impact on quality of life.

Thus, adjuvant treatment with sagopilone may be effective in patients who have an aggressive tumor with high risk of bone metastasis and could signal a possible trend towards fewer pathologic fractures, reduced bone pain and less need for radiotherapy treatment. The results of the preventive study gave a first evidence of the dual action of sagopilone on osteoclasts and tumor cells and of efficacy of sagopilone in bone metastasis at all. This could not be assumed because sagopilone doesn´t have a bone-binding moiety such as bisphosphonates. Autoradiography studies in female rats revealed medium and low sagopilone concentrations in bone and bone marrow (data not shown). Thus, the compound was tested in the more aggressive therapeutic setting in comparison to paclitaxel which was approved for the treatment of metastatic breast cancer in 1994 (Gueritte, 2001).

4.3.2 Therapeutic model

In the therapeutic MDA-MB-231(SA) breast cancer bone metastasis model, tumor growth in bone was already severe and osteolytic lesions were clearly visible by radiography, indicating an extremely active vicious cycle. This model resembles the clinical situation of a patient with advanced metastatic breast cancer exhibiting severe osteolytic lesions and tumor growth in bone. In the clinic, therapy for patients with established bone metastasis is mainly palliative and aims to increase quality of life by reducing factors such as tumor-associated cachexia (Rubin, 2003), which has been noted as an indicator of poor prognosis in various indications, including lung and pancreatic cancer (Bachmann et al., 2008; Kim et al., 2004; Sakuragi et al., 1996). Skeletal complications, including spinal compression, also increase the degree of morbidity and impact on quality of life (Coleman, 1997) and can lead to permanent neurological damage, including paraplegia (Jung et al., 2004; Sakuragi et al., 1996). Sagopilone substantially reduced cachexia and paraplegia *in vivo*. This suggests a potential for increased quality of life also in the clinic with the use of sagopilone.

In the therapeutic model, sagopilone treatment again significantly reduced overall tumor burden compared with both vehicle and paclitaxel treatment

whereas the reduction seen with paclitaxel compared with the vehicle group was not significant. The strong antitumor effect is particularly due to the pharmacokinetic profile of sagopilone. It is quickly taken up by the cells and incorporates more efficiently in the tumor cells as compared to paclitaxel (Hoffmann et al., 2008). Inhibition of tumor cell growth in sagopilone-treated animals, indicated by BLI and histomorphometry assessments, led to a subsequent decline in bone resorption compared with the vehicle group, with significantly reduced osteoclastic lesion area and bone destruction monitored by radiography and micro-CT. Regarding osteolytic lesion area and bone volume, sagopilone had a significantly better effect on reducing bone destruction when compared to paclitaxel. In contrast, osteolytic lesion area and bone volume in paclitaxel-treated animals did not differ significantly from vehicle-treated animals. Sagopilone treatment also resulted in significant reduction of activated osteoclasts in TRACP-stained bone sections compared with vehicle and paclitaxel-treated animals as well as reduced serum TRACP 5b levels compared with the vehicle group, indicating decreased bone resorption. The reduced serum TRACP 5b concentration in paclitaxel-treated animals may be due to the destruction of osteoclasts outside the tumor-bone interface. Our *in vitro* results, which indicate that paclitaxel is cytotoxic to osteoclasts, also provide an explanation for the decrease in overall bone resorption rate with paclitaxel treatment. The inhibition of bone resorption by paclitaxel is therefore likely to be a result of non-specific cytotoxic effects on osteoclasts, unrelated to osteoclast activation by tumors. As a sensitive and specific marker for bone resorption, TRACP 5b is used in the clinic to monitor treatment response in breast cancer patients with bone metastases (Chung et al., 2006). However, as reported, secreted TRACP 5b is a reliable marker of osteoclast number whereas CTX reflects the resorbing activity of osteoclasts (Rissanen et al., 2008). In patients with breast cancer-induced osteolysis, CTX has been shown to decrease markedly after pamidronate treatment and is thus considered to have potential for monitoring therapy (Body et al., 1997).

In conclusion, these results suggest that sagopilone effectively interrupts the vicious cycle at two different positions inhibiting both tumor growth and bone resorption (Fig. 38), whereas paclitaxel appears to mainly interrupt the cycle by

inhibiting tumor growth. The dual action of sagopilone was confirmed by both *in vitro* and *in vivo* data. On the one hand, inhibition of tumor cell proliferation (chapter 3.3.1), inhibition of s.c. tumor growth (chapter 3.3.2) and bone metastases (chapters 3.3.3.1.3 and 3.3.3.2.3) indicate the effect of sagopilone on cancer cells, on the other hand osteoclast activity and differentiation assays (chapter 3.3.3.3), reduced lesion area in the bone metastasis model (chapters 3.3.3.1.2 and 3.3.3.2.2), TRACP staining and serum TRACP 5b levels (chapter 3.3.3.2.4) suggest an antiresorptive effect of sagopilone. To exclude that this is not an indirect effect of reduced tumor cell growth, which would lead to an interruption of the vicious cycle as well, the OVX study was performed which confirmed in non-tumor bearing animals that sagopilone has direct inhibiting effects on osteoclasts indicated by increased bone mineral density compared to OVX animals (chapter 3.3.3.4).

Together, the tolerability and efficacy data for the therapeutic treatment model suggest a great promise for sagopilone as a treatment for patients with advanced metastatic breast cancer and bone involvement.

Despite promising results with bisphosphonates (Coleman, 2004), a broader spectrum of compounds to treat and prevent bone metastases is needed. A study which directly compares sagopilone with clodronate in the MDA-MB-231 bone metastasis model shows similar effects of both compounds on bone and additional effects of sagopilone on tumor (Hoffmann et al., 2006). Also other therapeutic interventions against bone metastasis currently in clinical trial program, such as RANKL or cathepsin K inhibitors, target solely osteoclasts in the vicious cycle and are efficient in reducing markers of bone turnover in patients with breast cancer bone metastasis (Lipton et al., 2007; Jensen et al., 2008).

For sagopilone, proof-of-concept has already been demonstrated in Phase II trials of patients with platinum-resistant ovarian cancer (Rustin et al., 2007) and prostate cancer (Graff et al., 2008). Results presented here highlight the potential of sagopilone for the treatment of patients with advanced metastatic breast cancer including bone metastases, and also those with breast or other cancers who have a high risk of developing bone metastases. These potentially include breast and prostate cancer patients, particularly those treated with

aromatase inhibitors or androgen deprivation therapy respectively, who suffer from skeletal complications including fractures (Ahlborg et al., 2008). The ongoing sagopilone Phase II clinical trial program will clarify how the dual action of sagopilone against both tumor growth and osteoclast activity *in vivo* translates into efficacy and tolerability in the clinic.

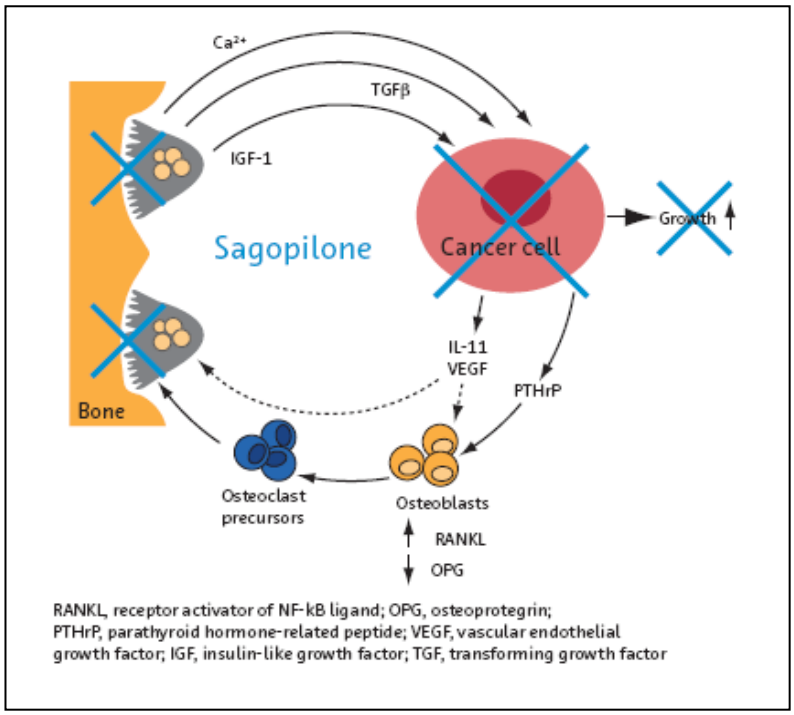

Figure 38: Mechanism of action of sagopilone. The proposed mechanism of action of sagopilone suggests two points of inhibition in the cycle of bone metastasis formation (Strube et al., 2008).

4.4 Effect of sagopilone on bone resorption

4.4.1 *In vitro*

The *in vivo* inhibition of bone resorption demonstrated by sagopilone was mirrored *in vitro*, in a bone resorption assay using human osteoclasts. However, the exact molecular mechanism behind this activity is still unknown and requires further studies. The doses of the *in vitro* assay were chosen according to the pharmacokinetic data in mice. As we don´t have any evidence that sagopilone accumulates in osteoclasts, it was assumed that the sagopilone concentration in bone is around the same as in the serum. The serum levels of the compounds in mice quickly decrease after i.v. application and the compounds

accumulate in the tumor. Sagopilone incorporates more efficiently in the cells compared to paclitaxel. It was reported that paclitaxel also has *in vitro* effects on osteoclastic bone resorption at therapeutically relevant concentrations, and that 10 µM paclitaxel had cytotoxic effects on osteoclasts (Hall et al., 1995). In contrast, the results presented in this thesis indicated cytotoxic effects of paclitaxel at 0.05 µM in the osteoclast activity assay. This difference in cytotoxic concentration of paclitaxel on osteoclasts might be due to the use of human osteoclasts in the assay described in this thesis compared to rat osteoclasts. Furthermore, the assays were performed differently, for example with longer incubation periods of paclitaxel in the assay reported in this thesis. Our *in vitro* assay with long-term treatment of compounds during the whole resorption period indicated that sagopilone inhibits human osteoclast activity and bone resorption to a greater extent than paclitaxel, but without the cytotoxic effects associated with paclitaxel treatment (chapter 3.3.3.3).

The inhibition of the growth and activity of non-proliferating end cells, such as osteoclasts, by sagopilone may partly be due to interference with non-mitotic microtubule-dependent functions, which include exocytosis, cell morphology, polarization and adhesion. Indeed, the inhibition of endothelial cell adhesion has previously been reported with paclitaxel (Davis et al., 2005). Normal adhesion is required for adequate osteoclast function because osteoclasts are activated by contact with the mineralized bone matrix (Jimi et al., 1996). Moreover, under non-adherent conditions, the formation of multinuclear osteoclasts is decreased, thus leading to coverage of a smaller area of bone and further reduction in activity (Miyamoto and Suda, 2003). The exocytosis of extracellular vesicles, important for several processes during normal bone resorption, including degradation of the bone matrix (Hall et al., 1995; Vaananen and Laitala-Leinonen, 2008) may also be blocked by sagopilone.

To more intensely study the molecular interactions between sagopilone and osteoclasts, it would be interesting to compare microtubule immunofluorescence tubulin stainings in sagopilone and vehicle treated osteoclasts in culture by laser scanning confocal microscopy to compare cytoskeletal organization. In addition the removal of osteoclast bone resorption products by transcytosis could be investigated between controls and sagopilone

treated osteoclasts as described by Salo et al., 1997. They reported that rat osteoclasts were cultured on biotin labeled bovine bone slices, and that the resorbed biotinylated material was visualized by FITC-conjugated streptavidin. This allows to follow the transport of degradation products of organic bone matrix during resorption and monitor osteoclasts in different stages of the resorption cycle. Moreover, the formation of the ruffled border membrane could be disturbed by sagopilone thereby inhibiting bone resorption. To study this, electron micrographs of bone sections of mice treated with either sagopilone or vehicle could be analyzed. To quantify the amount of resorbed bone, a pit formation assay could be performed *in vitro*. This assay measures the amount of resorption pits caused by resorbing osteoclasts on bone slices as well as the area of resorbed bone.

However, the inhibition of osteoclast activity might be important only in humans whose pharmacokinetic of sagopilone is higher compared to mice (data not shown). Therefore, osteoclasts might be exposed for a longer time to sagopilone that it can exert effects on osteoclast activity without cytotoxic effects as demonstrated *in vitro*. In contrast, a short loading dose of compound of 2 hours, as performed in the second setting of the osteoclast assay (Fig. 31), indicates no effects on osteoclast activity but on osteoclast differentiation. Consequently, in mice sagopilone appears to inhibit earlier processes of osteoclast fusion and differentiation. The counting of nuclei per osteoclast would clarify if sagopilone inhibits fusion of osteoclast precursors into mature osteoclasts.

In conclusion, the studies mentioned above could contribute to clarify the molecular mechanisms involved in inhibition of bone resorption by sagopilone.

4.4.2 *In vivo*

The *in vivo* inhibition of bone resorption was demonstrated in the MDA-MB-231 bone metastasis model by decreased osteolytic lesion area, increased bone volume, reduced serum TRACP 5b levels and reduced number of activated osteoclasts in TRACP stained bone sections of sagopilone treated animals compared to the vehicle group. However, it is still unclear if this effect is mainly

due to the anti-proliferative effect of sagopilone on tumor cells and consequent interruption of the vicious cycle at the tumor cell stage or to an additional, similarly strong inhibition of osteoclastic bone resorption or differentiation. First evidence of a direct anti-resorptive effect of sagopilone gave the osteoclast activity assay which was performed with human osteoclasts *in vitro* (chapter 3.3.3.3). A short loading dose of compound only inhibited osteoclast differentiation and not activity. Finally, the possibly anti-resorbing effects of sagopilone were confirmed *in vivo* using the OVX model of osteoporosis in mice. Here, sagopilone showed efficacy in preventing bone loss in OVX mice indicated by significantly increased trabecular bone mineral density (BMD) compared to OVX animals (chapter 3.3.3.4). These data suggest sagopilone as an agent with direct inhibitory effects on osteoclast activity or differentiation and thus confirm the hypothesis of mode of action that sagopilone´s efficacy in treating bone metastases is due to the interruption of the vicious cycle on both tumor cell and osteoclast stages (Fig. 38). However, in the OVX study a sagopilone dose (8mg/kg) was used which is effective in tumor-bearing animals. This dose might be too high and possibly inhibiting osteoblasts so that the effect on bone mineral density is not optimal. The possibly too high dose is also reflected by a significant decrease in body weight in sagopilone treated animals compared to OVX mice caused by drug-related toxicity (chapter 3.3.3.4) which is more evident in non-tumor bearing animals as no accumulation of the compound in tumor tissue occurs. As a consequence, in non-tumor-bearing mice fast-dividing somatic cells are possibly more affected by the compound compared to cells in tumor-bearing animals. The observed decrease in uterine weight at the end of the study (chapter 3.3.3.4) is caused by hypogonadism which all chemotherapeutic agents exert on the ovaries resulting in amenorrhea in patients (Mincey, 2003). However, the result of the pQCT measurements suggests that sagopilone is not at least reducing the bone density such as lots of other drugs (cancer treatment-induced bone loss (CTIBL)) (Pfeilschifter and Diel, 2000) and appears to compensate the hypogonadal state by a simultaneous inhibitory effect on osteoclasts. CTIBL is especially common in breast and prostate cancer patients treated for example with aromatase inhibitors (AIs) or androgen deprivation therapy respectively. As for AIs, they

also cause ovarian suppression thereby eliminating circulating estradiol levels (Brufsky, 2008) which is associated with bone loss similar as in postmenopausal osteoporosis. Patients with CTIBL are often treated with bisphosphonates (Saad et al., 2008).

In summary, an optimization of the sagopilone dose in the OVX model is necessary to obtain more potent effects of sagopilone on inhibition of osteoclast activation. To determine the most effective dose of sagopilone on BMD and to get more information about the effect of sagopilone on bone, a study on osteoblast activity using osteoblast cultures would be beneficial to find out the dose which kills osteoblasts. In addition, the studies performed on osteoclast activity and differentiation using a short loading dose of compound (2 hours) are helpful to mimic the low pharmacokinetic in mice and to find out which dose is sufficient to inhibit osteoclast activity or differentiation. Although no cytotoxic effects could be observed microscopically after a short loading dose of sagopilone and paclitaxel on osteoclasts, theses assays use human osteoclasts. The effect on mouse osteoclasts needs to be evaluated *in vivo* in the OVX model. However, based on these studies, the sagopilone dose could be optimized. According to the *in vitro* assays, osteoclast differentiation is inhibited at 5-10 nM (short loading dose of compound) whereas the lowest osteoclast activity inhibiting concentration is 15 nM (long loading dose of compound). These concentrations of sagopilone correspond to a concentration of 3-5 mg/kg *in vivo* compared to the 8-10 mg/kg dose effective in tumor-bearing animals. To follow the inhibition of bone resorption during the study, markers of bone turnover (such as CTX, TRACP 5b, PINP) could be measured in serum samples. PINP and CTX should increase and TRACP 5b should decrease at 2 weeks after OVX as reported by (Rissanen et al., 2008).

To conclude, the OVX study in mice showed evidence of a direct inhibitory effect of sagopilone on osteoclasts *in vivo*. The possibility that sagopilone is beneficial for bone, will strengthen the status of sagopilone as an anti-cancer compound compared to other microtubule stabilizing agents. Furthermore, it might be possible to develop sagopilone to treat osteoporosis and other diseases with increased bone resorption.

5 ACKNOWLEDGEMENTS

An dieser Stelle möchte ich mich bei allen bedanken, die mich bei der Erstellung dieser Arbeit unterstützt haben.

I am truly grateful to my supervisor, Sanna-Maria Käkönen, for her valuable contribution and her support during this work. Not only her immense knowledge in the field of bone metastasis and cancer biology but also her talent to motivate as well as her enthusiasm made this thesis possible. The confidence-based working atmosphere is greatly appreciated and gave me excellent conditions within which to work in the Department of TRG Oncology at BSP.

Prof. Petra Knaus danke ich herzlich für die Übernahme des Koreferates sowie für die stimulierenden „Symposien für externe Doktoranden“.

Besonders möchte ich vor allem allen Mitarbeitern des 6. OGs der TRG Onkologie für ihre geduldige Unterstützung, umfangreiche Hilfsbereitschaft und Einführung in diverse Methoden danken. Ein herzliches Dankeschön geht dabei an Bernd für die Hilfe bei den Herzinokulationen, Anica für die Unterstützung in der Zellkultur, Nicole und Silke für die Beantwortung sämtlicher Fragen bezüglich der Histologie, Willi und Andreas für die Bereitstellung der letzten Sagopilone-Vorräte sowie an alle fleißigen Helfer bei langwierigen Knochenaufarbeitungen: Karola, Ina, Natalie, Paul, Katrin, Angela. Ein ganz spezieller Dank gilt Maher und Karola nicht nur für ihre Unterstützung im Laboralltag sondern vor allem für die schönen Pausen zwischendurch. Besonderer Dank geht außerdem an Laura, meine liebe Büronachbarin, für ihr immer offenes Ohr: Mille grazie!

Außerhalb der Onkologie möchte ich mich ganz herzlich bei der Small Animal Imaging Unit (SAIU) von Bayer Schering Pharma AG für die gute Zusammenarbeit und die hohe Flexibilität bei der doch oft sehr kurzfristigen Planung bedanken: Herr Hauff, Liza, Tine und Nicole. Großer Dank gilt

außerdem Sabine Zitzmann-Kolbe und Norman Koglin sowie Eva-Maria Bickel und Jörg Jannsen von „Oncology Imaging Research“ für die beeindruckenden PET-Aufnahmen.

Dankeschön außerdem an Jens Hoffmann für wertvolle Ratschläge bei der Planung von Sagopilone-Studien sowie für das Korrekturlesen der Zusammenfassung dieser Arbeit. Richardus Vonk möchte ich herzlich für die ausgiebigen statistischen Analysen und Diskussionen sowie der sehr geschätzten Hilfe bei jeglichen statistischen Problemen danken.

I warmly thank the team of Pharmatest Services Ltd in Turku, Finland for performing the osteoclast activity and differentiation assays. I am especially grateful to Jussi Halleen and Jukka Rissanen for scientific discussions and valuable advices regarding the osteoclast assays as well as OVX studies. I also would like to thank Rami Käkönen for patient assistance with image processing and great help with reading and commenting my poster abstracts.

Weiterhin möchte ich allen Koautoren der originalen Publikationen für die gute Zusammenarbeit und Unterstützung beim Erstellen der Manuskripte danken.

Mein besonderer Dank geht an meine Familie, die mich uneingeschränkt unterstützt und mit aufmunternden Worten zum Erfolg dieser Arbeit beigetragen hat. Ohne Euch hätte es diese Arbeit nie gegeben.

Nicht zuletzt möchte ich mich auch für die finanzielle Unterstützung durch die Bayer Schering Pharma AG bedanken.

6 REFERENCES

Abrams, J. S., Vena, D. A., Baltz, J., Adams, J., Montello, M., Christian, M., Onetto, N., Desmond-Hellmann, S., Canetta, R., Friedman, M. A., and et al. (1995). Paclitaxel activity in heavily pretreated breast cancer: a National Cancer Institute Treatment Referral Center trial. J Clin Oncol *13*, 2056-2065.

Ahlborg, H. G., Nguyen, N. D., Center, J. R., Eisman, J. A., Nguyen, T. V. (2008). Incidence and risk factors for low trauma fractures in men with prostate cancer. Bone *43*, 556-560.

Ahmed, S. A., Gogal, R. M., Walsh, J. E. (1994). A new rapid and simple non-radioactive assay to monitor and determine the proliferation of lymphocytes: an alternative to [3H]thymidine incorporation assay. J Immunol Methods *170(2)*, 211-224.

Alatalo, S. L., Peng, Z., Janckila, A. J., Kaija, H., Vihko, P., Vaananen, H. K., and Halleen, J. M. (2003). A novel immunoassay for the determination of tartrate-resistant acid phosphatase 5b from rat serum. J Bone Miner Res *18*, 134-139.

Alexander, J. M., Bab, I., Fish, S., Muller, R., Uchiyama, T., Gronowicz, G., Nahounou, M., Zhao, Q., White, D. W., Chorev, M.*, et al.* (2001). Human parathyroid hormone 1-34 reverses bone loss in ovariectomized mice. J Bone Miner Res *16*, 1665-1673.

Alexander E. J. (2008). Sagopilone. Drugs of the Future *33(6)*, 496-505.

Alexandrova, E., Sergieva, S., Nikolova, V., and Danon, S. (2003). Bone marrow micrometastases as a prognostic factor in early breast cancer patients. J Buon *8*, 133-137.

Ananth, S., Knebelmann, B., Grüning, W., Dhanabal, M., Walz, G., Stillmann, I. E., Sukhatme, V. P. (1999). Transforming growth factor β1 is a target for the von Hippel-Lindau tumor suppressor and a critical growth factor for clear cell renal carcinoma. Cancer Res *59*, 2210-2216.

Aubin J.E., Lian J.B., Stein G.S. (2006). Bone Formation: Maturation and Functional Activities of Osteoblast Lineage Cells. In Favus M.J. (ed) Primer on the metabolic bone diseases and disorders of mineral metabolism, Lippincott-Raven, Philadelphia, pp 20-29.

Bachmann, J., Heiligensetzer, M., Krakowski-Roosen, H., Buchler, M. W., Friess, H., and Martignoni, M. E. (2008). Cachexia worsens prognosis in patients with resectable pancreatic cancer. J Gastrointest Surg *12*, 1193-1201.

Balls, M., and Straughan, D. W. (1996). The three Rs of Russell & Burch and the testing of biological products. Dev Biol Stand *86*, 11-18.

Barck, K. H., Lee, W. P., Diehl, L. J., Ross, J., Gribling, P., Zhang, Y., Nguyen, K., van Bruggen, N., Hurst, S., and Carano, R. A. (2004). Quantification of cortical bone loss and repair for therapeutic evaluation in collagen-induced arthritis, by micro-computed tomography and automated image analysis. Arthritis Rheum *50*, 3377-3386.

Bendre, M. S., Montague, D. C., Peery, T., Akel, N. S., Gaddy, D., and Suva, L. J. (2003). Interleukin-8 stimulation of osteoclastogenesis and bone resorption is a mechanism for the increased osteolysis of metastatic bone disease. Bone *33*, 28-37.

Bibby, M. C. (2004). Orthotpoic models of cancer for preclinical drug evaluation: advantages and disadvantages. Europ J Cancer *40*, 852-857.

Black, D. M., Cummings, S. R., Karpf, D. B., Cauley, J. A., Thompson, D. E., Nevitt, M. C., Bauer, D. C., Genant, H. K., Haskell, W. L., Marcus, R.*, et al.* (1996). Randomised

trial of effect of alendronate on risk of fracture in women with existing vertebral fractures. Fracture Intervention Trial Research Group. Lancet *348*, 1535-1541.

Blair, H. C., and Athanasou, N. A. (2004). Recent advances in osteoclast biology and pathological bone resorption. Histol Histopathol *19*, 189-199.

Bland, J. M., Altman, D. G. (1986). Statistical methods for assessing agreement between two methods of clinical measurement. Lancet *i*, 307-310.

Blomme, E. A. G., Dougherty, K. M., Pienta, K. J., Capen, C. C., Rosol, T. J., and McCauley, L. K. (1999). Skeletal Metastasis of Prostate Adenocarcinoma in Rats: Morphometric Analysis and Role of Parathyroid Hormone-Related Protein. The Prostate *39*, 187-197.

Body, J. J., Dumon, J. C., Gineyts, E., Delmas, P. D. (1997). Comparative evaluation of markers of bone resorption in patients with breast cancer-induced osteolysis before and after bisphosphonate therapy. B J Cancer *75(3)*, 408-412.

Bone, H. G., Bolognese, M. A., Yuen, C. K., Kendler, D. L., Wang, H., Liu, Y., and San Martin, J. (2008). Effects of denosumab on bone mineral density and bone turnover in postmenopausal women. J Clin Endocrinol Metab *93*, 2149-2157.

Bonewald, L. F. (2007). Osteocytes as dynamic multifunctional cells. Ann N Y Acad Sci *1116*, 281-290.

Bouxsein, M. L., Myers, K. S., Shultz, K. L., Donahue, L. R., Rosen, C. J., and Beamer, W. G. (2005). Ovariectomy-induced bone loss varies among inbred strains of mice. J Bone Miner Res *20*, 1085-1092.

Boyle, W. J., Simonet, W. S., and Lacey, D. L. (2003). Osteoclast differentiation and activation. Nature *423*, 337-342.

Brown, J. E., and Coleman, R. E. (2002). The present and future role of bisphosphonates in the management of patients with breast cancer. Breast Cancer Res *4*, 24-29.

Brufsky, A. M. (2008). Cancer treatment-induced bone loss: pathophysiology and clinical perspectives. Oncologist *13*, 187-195.

Buijs, J. T, Henriques, N. V., Overveld, P. G. M., van der Horst, G., Que, I., Schwaninger, R., et al. (2007). Bone morphogenetic protein 7 in the development and treatment of bone metastases from breast cancer. Cancer Res *67(18)*, 8742-8751.

Burton, P. B. J., Moniz, C., Knight, D. E. (1990). Parathyroid hormone related peptide can function as an autocrine growth factor in human renal cell carcinoma. Biochem Biophys Res Commun *3*, 1134-1138.

Camacho, P., Kleerekoper, M. (2006) Biochemical Markers of Bone Turnover. In Favus, M. J. (ed) Primer on the metabolic bone diseases and disorders of mineral metabolism, Lippincott-Raven, Philadelphia, pp 127-132.

Cameron, D., Fallon, M., and Diel, I. (2006). Ibandronate: its role in metastatic breast cancer. Oncologist *11 Suppl 1*, 27-33.

Canon, J. R., Roudier, M., Bryant, R., Morony, S., Stolina, M., Kostenuik, P. J., Dougall, W. C. (2008). Inhibition of RANKL blocks skeletal tumor progression and improves survival in a mouse model of breast cancer bone metastasis. Clin Exp Metastasis *25*, 119-129.

Carlinfante, G., Vassiliou, D., Svensson, O., Wendel, M., Heinegard, D., Andersson, G. (2003). Differential expression of osteopontin and bone sialoprotein in bone metastasis of breast and prostate carcinoma. Clin Exp Metastasis *20*, 437-444.

Cenci, S., Weitzmann, M. N., Roggia, C., Namba, N., Novack, D., Woodring, J., and Pacifici, R. (2000). Estrogen deficiency induces bone loss by enhancing T-cell production of TNF-alpha. J Clin Invest *106*, 1229-1237.

Céspredes, M. V., Casanova, I., Parreño, M., Mangues, R. (2006). Mouse models in oncogenesis and cancer therapy. Clin Transl Oncol *8*, 318-329.

Chang, C. H., Jan, M. L., Fan, K. H., Wang, H. E., Tsai, T. H., Chen, C. F., Fu, Y. K., and Lee, T. W. (2006). Longitudinal evaluation of tumor metastasis by an FDG-microPet/microCT dual-imaging modality in a lung carcinoma-bearing mouse model. Anticancer Res *26*, 159-166.

Chao, T. Y., Ho, C. L., Lee, S. H., Chen, M. M., Janckila, A., and Yam, L. T. (2004). Tartrate-resistant acid phosphatase 5b as a serum marker of bone metastasis in breast cancer patients. J Biomed Sci *11*, 511-516.

Chao, T. Y., Yu, J. C., Ku, C. H., Chen, M. M., Lee, S. H., Janckila, A. J., and Yam, L. T. (2005). Tartrate-resistant acid phosphatase 5b is a useful serum marker for extensive bone metastasis in breast cancer patients. Clin Cancer Res *11*, 544-550.

Chou, T. C., O'Connor, O. A., Tong, W. P., Guan, Y., Zhang, Z. G., Stachel, S. J., Lee, C., and Danishefsky, S. J. (2001). The synthesis, discovery, and development of a highly promising class of microtubule stabilization agents: curative effects of desoxyepothilones B and F against human tumor xenografts in nude mice. Proc Natl Acad Sci U S A *98*, 8113-8118.

Chung, Y. C., Ku, C. H., Chao, T. Y., Yu, J. C., Chen, M. M., and Lee, S. H. (2006). Tartrate-resistant acid phosphatase 5b activity is a useful bone marker for monitoring bone metastases in breast cancer patients after treatment. Cancer Epidemiol Biomarkers Prev *15*, 424-428.

Clarke, B. (2008). Normal bone anatomy and physiology. Clin J Am Soc Nephrol *3 Suppl 3*, S131-139.

Coleman, R. (2007). On the horizon: can bisphosphonates prevent bone metastases? Breast *16 Suppl 3*, S21-27.

Coleman, R. E. (1997). Skeletal complications of malignancy. Cancer *80*, 1588-1594.

Coleman, R. E. (2001). Metastatic bone disease: clinical features, pathophysiology and treatment strategies. Cancer Treat Rev *27*, 165-176.

Coleman, R. E. (2004). Bisphosphonates: clinical experience. Oncologist *9 Suppl 4*, 14-27.

Coleman, R. E. (2008). Risks and benefits of bisphosphonates. Br J Cancer *98*, 1736-1740.

Colleoni, M., O'Neill, A., Goldhirsch, A., Gelber, R. D., Bonetti, M., Thurlimann, B., Price, K. N., Castiglione-Gertsch, M., Coates, A. S., Lindtner, J., *et al.* (2000). Identifying breast cancer patients at high risk for bone metastases. J Clin Oncol *18*, 3925-3935.

Cook, G. J., and Fogelman, I. (2001). The role of positron emission tomography in skeletal disease. Semin Nucl Med *31*, 50-61.

Cooper C. (2003). Epidemiology of osteoporosis. In Favus M.J. (ed) Primer on the metabolic bone diseases and disorders of mineral metabolism, Lippincott-Raven, Philadelphia, pp 307-313.

Dai, J., Hall, C. L., Escara-Wilke, J., Mizokami, A., Keller, J. M., and Keller, E. T. (2008). Prostate cancer induces bone metastasis through Wnt-induced bone morphogenetic protein-dependant and independent mechanisms. Cancer Res *68*, 5785-5794.

Davis, H. W., VandenBerg, E., Reid, M. D., Roy-Chaudhury, P., and Edwards, J. D. (2005). Paclitaxel impairs endothelial cell adhesion but not cytokine-induced cellular adhesion molecule expression. Ann Vasc Surg *19*, 398-406.

Delaisse, J. M., Andersen, T. L., Engsig, M. T., Henriksen, K., Troen, T., and Blavier, L. (2003). Matrix metalloproteinases (MMP) and cathepsin K contribute differently to osteoclastic activities. Microsc Res Tech *61*, 504-513.

Delmas, P. D. (1997). Hormone replacement therapy in the prevention and treatment of osteoporosis. Osteoporos Int *7 Suppl 1*, S3-7.

Delmas, P. D., Eastell, R., Garnero, P., Seibel, M. J., Stepan, J. (2000). The use of biochemical markers of bone turnover in osteoporosis. Osteoporos Int *6*, 2-17.

Delmas P.D. (2003). Clinical use of selective estrogen receptor modulators and other estrogen analogs. In Favus M.J. (ed) Primer on the metabolic bone diseases and disorders of mineral metabolism, Lippincott-Raven, Philadelphia, pp 331-336.

Dewan, M. Z., Ahmed, S., Iwasaki, Y., Ohba, K., Toi, M., Yamamoto, N. (2006). Stromal cell-derived factor-1 and CXCR4 receptor interaction in tumor growth and metastasis of breast cancer. Biomed Pharmacother *60*, 273-276.

Dougall, W. C., and Chaisson, M. (2006). The RANK/RANKL/OPG triad in cancer-induced bone diseases. Cancer Metastasis Rev *25*, 541-549.

Dumontet, C., and Sikic, B. I. (1999). Mechanisms of action of and resistance to antitubulin agents: microtubule dynamics, drug transport, and cell death. J Clin Oncol *17*, 1061-1070.

Durr, H. R., Maier, M., Pfahler, M., Baur, A., and Refior, H. J. (1999). Surgical treatment of osseous metastases in patients with renal cell carcinoma. Clin Orthop Relat Res, 283-290.

Dvorak, H. F. (2002). Vascular permeability factor/vascular endothelial growth factor: a critical cytokine in tumor angiogenesis and a potential target for diagnosis and therapy. J Clin Oncol *20*, 4368-4380.

Eastell R. (2003). Pathogenesis of postmenopausal osteoporosis. In Favus M.J. (ed) Primer on the metabolic bone diseases and disorders of mineral metabolism, Lippincott-Raven, Philadelphia, pp 314-316.

Eubank, W. B., Mankoff, D. A. (2005). Evolving role of positron emission tomography in breast cancer imaging. Semin Nucl Med *35(2)*, 84-99.

Even-Sapir, E., Metser, U., Mishani, E., Lievshitz, G., Lerman, H., Leibovitch, I. (2006). The detection of bone metastases in patients with high-risk prostate cancer: 99mTc-MDP Planar bone scintigraphy, single- and multi-field-of-view SPECT, 18F-fluoride PET, and 18F-fluoride PET/CT. J Nucl Med *47*, 287-297.

Festing, S. (2007). On the necessity for animal experimentation. BioEssays *30*, 94-95.

Fidler, I. J., and Kripke, M. L. (1977). Metastasis results from preexisting variant cells within a malignant tumor. Science *197*, 893-895.

Figlin, R. A. (1999). Renal cell carcinoma: management of advanced disease. J Urol *161*, 381-386; discussion 386-387.

Galasko, C. S. (1981). Bone metastases studied in experimental animals. Clin Orthop Relat Res, 269-285.

Gallagher, A., Chambers, T. J., Tobias, J. H. (1993). The estrogen antagonist ICI 182, 780 reduces cancellous bone volume in female rats. Endo *133 (6)*, 2787-2791.

Gauthier, J. Y., Chauret, N., Cromlish, W., Desmarais, S., Duong le, T., Falgueyret, J. P., Kimmel, D. B., Lamontagne, S., Leger, S., LeRiche, T.*, et al.* (2008). The discovery

of odanacatib (MK-0822), a selective inhibitor of cathepsin K. Bioorg Med Chem Lett *18*, 923-928.

Graff, J., Smith, D. C., Neerukonda, L. et al., (2008). Phase II study of sagopilone (ZK-EPO) plus prednisone as first-line chemotherapy in patients with metastatic androgen-independent prostate cancer (AIPC). Poster presented at the 44th ASCO Annual Meeting, May 30-June 3, Chicago, Illinois, USA.

Frangioni, J. V. (2008). New Technologies for Human Cancer Imaging. J Clin Oncol 26, 4012-4021.

Giannakakou, P., Sackett, D. L., Kang, Y. K., Zhan, Z., Buters, J. T., Fojo, T., and Poruchynsky, M. S. (1997). Paclitaxel-resistant human ovarian cancer cells have mutant beta-tubulins that exhibit impaired paclitaxel-driven polymerization. J Biol Chem *272*, 17118-17125.

Girasole, G., Passeri, G., Jilka, R. L., and Manolagas, S. C. (1994). Interleukin-11: a new cytokine critical for osteoclast development. J Clin Invest *93*, 1516-1524.

Gorospe, M., Egan, J. M., Zbar, B., Lerman, M., Geil, L., Kuzmin, I., Holbrook, N. J. (1999). Mol Cell Biol *19(2)*, 1289-1300.

Green, J. R. (2005). Zoledronic acid: pharmacologic profile of a potent a potent bisphosphonate. Journal of Organometallic Chemistry *690*, 2439-2448.

Gueritte, F. (2001). General and recent aspects of the chemistry and structure-activity relationships of taxoids. Curr Pharm Des *7*, 1229-1249.

Guise, T. A. (1997). Parathyroid hormone-related protein and bone metastases. Cancer *80*, 1572-1580.

Guise, T. A. (2000). Molecular mechanisms of osteolytic bone metastases. Cancer *88*, 2892-2898.

Guise, T. A., Kozlow, W. M., Heras-Herzig, A., Padalecki, S. S., Yin, J. J., and Chirgwin, J. M. (2005). Molecular mechanisms of breast cancer metastases to bone. Clin Breast Cancer *5 Suppl*, S46-53.

Guise, T. A., Yin, J. J., Taylor, S. D., Kumagai, Y., Dallas, M., Boyce, B. F., Yoneda, T., and Mundy, G. R. (1996). Evidence for a causal role of parathyroid hormone-related protein in the pathogenesis of human breast cancer-mediated osteolysis. J Clin Invest *98*, 1544-1549.

Guise, T. A., Yin, J. J., Thomas, R. J., Dallas, M., Cui, Y., and Gillespie, M. T. (2002). Parathyroid hormone-related protein (PTHrP)-(1-139) isoform is efficiently secreted in vitro and enhances breast cancer metastasis to bone in vivo. Bone *30*, 670-676.

Hagelschuer, I., Hauff, P., Strube, A., Käkönen, S.M., von Degenfeld, G. (2009). Luminescent Imaging Technology as an opportunity to Reduce, Refine and Replace Animal Experiments. Light at the end of the tunnel? ALTEX (Alternatives to Animal Experimentation), submitted

Hall, T. J., Jeker, H., and Schaueblin, M. (1995). Taxol inhibits osteoclastic bone resorption. Calcif Tissue Int *57*, 463-465.

Halleen, J. M., Räisänen, S., Salos, J. J., Reddy, S. V., Roodman G. D., Hentunen, T. A., Lehenkari, P. P., Kaija, H., Vihko, P., Väänänen, H. K. (1999). Intracellular fragmentation of bone resorption products by reactive oxygen species generated by osteoclastic tartrate-resistant acid phosphatase. J Biol Chem *274(33)*, 22907-22910.

Halleen, J. M., Alatalo, S. L., Suominen, H., Cheng, S., Janckila, A. J., and Vaananen, H. K. (2000). Tartrate-resistant acid phosphatase 5b: a novel serum marker of bone resorption. J Bone Miner Res *15*, 1337-1345.

Halleen, J. M., Tiitinen, S. L., Ylipahkala, H., Fagerlund, K. M., Väänänen, H. K. (2006). Tartrate-resistant acid phosphatase 5b (TRACP 5b) as a marker of bone resorption. Clin Lab *52(9-10)*, 499-509.

Hari, M., Loganzo, F., Annable, T., Tan, X., Musto, S., Morilla, D. B., Nettles, J. H., Snyder, J. P., and Greenberger, L. M. (2006). Paclitaxel-resistant cells have a mutation in the paclitaxel-binding region of beta-tubulin (Asp26Glu) and less stable microtubules. Mol Cancer Ther *5*, 270-278.

Helms, M. W., Brandt, B. H., and Contag, C. H. (2006). Options for visualizing metastatic disease in the living body. Contrib Microbiol *13*, 209-231.

Herrmann, M., Seibel, M. (2008). The amino- and carboxyterminal cross-linked telopeptides of collagen type I, NTX-I and CTX-I: A comparative review. Clinica Chimica Acat *393*, 57-75.

Hoffmann J., Fichtner I., Käkönen S. M., Klar U. (2006). ZK-EPO, a third-generation epothilone, inhibits breast cancer metastasis. Poster presented at the 97th AACR Annual Meeting, Washington, USA.

Hoffmann, J., Fichtner, I., Lemm, M., Lienau, P., Hess-Stumpp, H., Rotgeri, A., Hofmann, B., and Klar, U. (2009). Sagopilone crosses the blood-brain barrier in vivo to inhibit brain tumor growth and metastases. Neuro Oncol *11*, 158-166.

Hoffmann, J., Vitale, I., Buchmann, B., Galluzzi, L., Schwede, W., Senovilla, L., Skuballa, W., Vivet, S., Lichtner, R. B., Vicencio, J. M.*, et al.* (2008). Improved cellular pharmacokinetics and pharmacodynamics underlie the wide anticancer activity of sagopilone. Cancer Res *68*, 5301-5308.

Hortobagyi, G. N. (2002). Novel approaches to the management of bone metastases in patients with breast cancer. Semin Oncol *29*, 134-144.

Horwitz, S. B. (1992). Mechanism of action of taxol. Trends Pharmacol Sci *13*, 134-136.

Horwitz, S. B., Cohen, D., Rao, S., Ringel, I., Shen, H. J., and Yang, C. P. (1993). Taxol: mechanisms of action and resistance. J Natl Cancer Inst Monogr, 55-61.

Hurley, M. M., Lee, S. K., Raisz, L. G., Bernecker, P., and Lorenzo, J. (1998). Basic fibroblast growth factor induces osteoclast formation in murine bone marrow cultures. Bone *22*, 309-316.

Iguchi, H., Yokota, M., Fukutomi, M., Uchimura, K., Yonemasu, H., Hachitanda, Y., Nakao, Y., Tanaka, Y., Sumii, T., Funakoshi, A. (2002). A possible role of VEGF in osteolytic bone metastasis of hepatocellular carcinoma. J Exp Clin Cancer Res *21*, 309-313.

Iwai, A., Fujii, Y., Kawakami, S., Takazawa, R., Kageyama, Y., Yoshida, M. A., and Kihara, K. (2004). Down-regulation of vascular endothelial growth factor in renal cell carcinoma cells by glucocorticoids. Mol Cell Endocrinol *226*, 11-17.

Iwasaki, T., Yamashita, K., Tsujimura, T., Kashiwamura, S., Tsutsui, H., Kaisho, T., Sugihara, A., Yamada, N., Mukai, M., Yoneda, T.*, et al.* (2002). Interleukin-18 inhibits osteolytic bone metastasis by human lung cancer cells possibly through suppression of osteoclastic bone-resorption in nude mice. J Immunother *25 Suppl 1*, S52-60.

Jensen, A. B., Olmeo, N., Wynne, C. et al., (2008). Effect of cathepsin k inhibition on suppression of bone resorption in women with breast cancer and established bone metastases in a 4-week, double-blind, randomized controlled trial. J Clin Oncol *26(20)*, 1023.

Jimi, E., Nakamura, I., Amano, H., Taguchi, Y., Tsurukai, T., Tamura, M., Takahashi, N., and Suda, T. (1996). Osteoclast function is activated by osteoblastic cells through a mechanism involving cell-to-cell contact. Endocrinology *137*, 2187-2190.

Jung, J. I., Kim, H. H., Park, S. H., Song, S. W., Chung, M. H., Kim, H. S., Kim, K. J., Ahn, M. I., Seo, S. B., and Hahn, S. T. (2004). Thoracic manifestations of breast cancer and its therapy. Radiographics *24*, 1269-1285.

Kaijzel, E. L., van der Pluijm, G., and Lowik, C. W. (2007). Whole-body optical imaging in animal models to assess cancer development and progression. Clin Cancer Res *13*, 3490-3497.

Käkönen, S. M., and Mundy, G. R. (2003). Mechanisms of osteolytic bone metastases in breast carcinoma. Cancer *97*, 834-839.

Kamath, A. V., Chang, M., Lee, F. Y., Zhang, Y., and Marathe, P. H. (2005). Preclinical pharmacokinetics and oral bioavailability of BMS-310705, a novel epothilone B analog. Cancer Chemother Pharmacol *56*, 145-153.

Kamb, A. (2005). What´s wrong with our cancer models? Nat Rev Drug Discov *4*, 161-165.

Kang, Y., Siegel, P. M., Shu, W., Drobnjak, M., Käkönen, S. M., Cordón-Cardo, C., Guise, T. A., Massagué, J. (2003). A multigenic program mediating breast cancer metastasis to bone. Cancer Cell *3*, 537-549.

Kanis J.A. (2003). Assessment of fracture risk. Who should be screened?. In Favus M.J. (ed) Primer on the metabolic bone diseases and disorders of mineral metabolism, Lippincott-Raven, Philadelphia, pp 316-323.

Killion, J. J., Radinsky, R., Fidler, I. J. (1999). Orthotopic models are necessary tp redict therapy of transplantable tumors in mice. Cancer and Metastasis Reviews *17*, 279-284.

Kim, H. L., Han, K. R., Zisman, A., Figlin, R. A., and Belldegrun, A. S. (2004). Cachexia-like symptoms predict a worse prognosis in localized t1 renal cell carcinoma. J Urol *171*, 1810-1813.

Kim, R., Osaki, A., and Toge, T. (2003). Feasibility and therapeutic efficacy of weekly 1-h low-dose paclitaxel infusion for relapsed breast cancer. Oncol Rep *10*, 145-150.

Kingsley, L. A., Fournier, P. G., Chirgwin, J. M., and Guise, T. A. (2007). Molecular biology of bone metastasis. Mol Cancer Ther *6*, 2609-2617.

Klar, U., Buchmann, B., Schwede, W., Skuballa, W., Hoffmann, J., and Lichtner, R. B. (2006). Total synthesis and antitumor activity of ZK-EPO: the first fully synthetic epothilone in clinical development. Angew Chem Int Ed Engl *45*, 7942-7948.

Klar, U., Hoffmann, J., and Giurescu, M. (2008). Sagopilone (ZK-EPO): from a natural product to a fully synthetic clinical development candidate. Expert Opin Investig Drugs *17*, 1735-1748.

Kominsky, S. L., Doucet, M., Brady, K., and Weber, K. L. (2007). TGF-beta promotes the establishment of renal cell carcinoma bone metastasis. J Bone Miner Res *22*, 37-44.

Kominsky, S. L., Doucet, M., Thorpe, M., Weber, K. L. (2008). MMP-13 is overexpressed in renal cell carcinoma bone metastasis and is induced by TGF-β1. Clin Exp Metastasis *25*, 865-870.

Kominsky, S. L., Abdelmagid, S. M., Doucet, M., Brady, K., Weber, K. L. (2008). Macrophage inflammatory protein-1δ: A novel osteoclast stimulating factor secreted by renal cell carcinoma bone metastasis. Cancer Res *68(5)*, 1261-1266.

Kozlow, W., and Guise, T. A. (2005). Breast cancer metastasis to bone: mechanisms of osteolysis and implications for therapy. J Mammary Gland Biol Neoplasia *10*, 169-180.

Le Gall, C., Bonnelye, E., and Clezardin, P. (2008). Cathepsin K inhibitors as treatment of bone metastasis. Curr Opin Support Palliat Care *2*, 218-222.

Lehenkari, P. P., Kellinsalmi, M., Näpanakngas, J. P., Ylitalo, K. V., Mönkkönen, J., Rogers, M. J., Ashayev, A., Väänänen, H. K., Hassinen, I. E. (2002). Further insight into mechanism of action of clodronate: inhibition of mitochondrial ADP/ATP translocase by a nonhydrolyzable, adenine-containing metabolite. Mol Pharmacol *61*, 1255-1262.

Leibovich, B. C., and Blute, M. L. (2006). Surgical management of renal cell carcinoma. Semin Oncol *33*, 552-562.

Lelekakis, M., Moseley, J. M., Martin, T. J., Hards, D., Williams, E., Ho, P., Lowen, D., Jeannie, J., Miller, F. R., Slavin, J., and Anderson, R. L. (1999). A novel orthotopic model of breast cancer metastasis to bone. Clin Exp Metastasis *17*, 163-170.

Lichtner, R. B., Rotgeri, A., Bunte, T., Buchmann, B., Hoffmann, J., Schwede, W., Skuballa, W., and Klar, U. (2001). Subcellular distribution of epothilones in human tumor cells. Proc Natl Acad Sci U S A *98*, 11743-11748.

Lindblad-Toh, K. (2004). Three´s company. Nature *428*, 475-476.

Ling, V., Chambers, A. F., Harris, J. F., and Hill, R. P. (1985). Quantitative genetic analysis of tumor progression. Cancer Metastasis Rev *4*, 173-192.

Lipton, A. (2006). Future treatment of bone metastases. Clin Cancer Res *12*, 6305s-6308s.

Lipton, A., Steger, G. G., Figueroa, J., Alvarado, C., Solal-Celigny, P., Body, J. J., de Boer, R., Berardi, R., Gascon, P., Tonkin, K. S., *et al.* (2007). Randomized active-controlled phase II study of denosumab efficacy and safety in patients with breast cancer-related bone metastases. J Clin Oncol *25*, 4431-4437.

Major, P., Lortholary, A., Hon, J., Abdi, E., Mills, G., Menssen, H. D., Yunus, F., Bell, R., Body, J., Quebe-Fehling, E., and Seaman, J. (2001). Zoledronic acid is superior to pamidronate in the treatment of hypercalcemia of malignancy: a pooled analysis of two randomized, controlled clinical trials. J Clin Oncol *19*, 558-567.

Mani, S., Macapinlac, M., Jr., Goel, S., Verdier-Pinard, D., Fojo, T., Rothenberg, M., and Colevas, D. (2004). The clinical development of new mitotic inhibitors that stabilize the microtubule. Anticancer Drugs *15*, 553-558.

Manolagas, S. C. (1995). Role of cytokines in bone resorption. Bone *17*, 63S-67S.

Massfelder, T., Lang, H., Schordan, E., Lindner V., Rothhut, S., Welsch, S., Simon-Assmann, P., Barthelmebs, M., Jacqmin, D., Helwig, J.-J. (2004). Parathyroid hormone-related protein is an essential growth factor for human clear cell renal carcinoma and a target fort he von Hippel-Lindau tumor suppressor gene. Cancer Res *64*, 180-188.

Massagué, J. Cheifetz, S., Laiho, M., Ralph, D. A., Weis, F. M., Zentella, A. (1992). Transforming growth factor β. Cancer Surv *12*, 81-103.

Mbalaviele, G., Dunstan, C. R., Sasaki, A., Williams, P. J., Mundy, G. R., and Yoneda, T. (1996). E-cadherin expression in human breast cancer cells suppresses the development of osteolytic bone metastases in an experimental metastasis model. Cancer Res *56*, 4063-4070.

McCaffrey, A., Kay, M. A., and Contag, C. H. (2003). Advancing molecular therapies through in vivo bioluminescent imaging. Mol Imaging *2*, 75-86.

Melton, L. (2001). Cellular pump changes prospect of disease resistance. Lancet *357*, 1186.

Milowsky, M. I., and Nanus, D. M. (2003). Chemotherapeutic strategies for renal cell carcinoma. Urol Clin North Am *30*, 601-609.

Mincey, B. A. (2003). Osteoporosis in women with breast cancer. Curr Oncol Rep *5*, 53-57.

Mitchison, T. J. (1988). Microtubule dynamics and kinetochore function in mitosis. Annu Rev Cell Biol *4*, 527-549.

Mittra, E., and Quon, A. (2009). Positron emission tomography/computed tomography: the current technology and applications. Radiol Clin North Am *47*, 147-160.

Miyamoto, T., and Suda, T. (2003). Differentiation and function of osteoclasts. Keio J Med *52*, 1-7.

Mönkkönen, H., Auriola, S., Lehenkari, P., Kellinsalmi, M., Hassinen, I. E., Vepsäläinen, J., Mönkkönen, J. (2006). A new endogenous ATP analog (ApppI) inhibits the mitochondrial adenine nucleotide translocase (ANT) and is responsible for the apoptosis induced by nitrogen-containing bisphosphonates. Br J Pharmacol *147*, 437-445.

Morris, P. G., and Fornier, M. N. (2008). Microtubule active agents: beyond the taxane frontier. Clin Cancer Res *14*, 7167-7172.

Motzer, R. J., and Russo, P. (2000). Systemic therapy for renal cell carcinoma. J Urol *163*, 408-417.

Motzer, R. J., Russo, P., Nanus, D. M., and Berg, W. J. (1997). Renal cell carcinoma. Curr Probl Cancer *21*, 185-232.

Müller, A., Homey, B., Soto, H., Ge, N., Catron, D., Buchanan, M. E., et al. (2001). Involvement of chemokine receptors in breast cancer metastasis. Nature *410*, 50-56.

Mundy G.R (1999). Bone remodeling. In Bone remodeling and its disorders. Martin Dunitz Ltd, London, pp 1-11.

Mundy, G. R., Guise, T. A. (2000). Pathophysiology of bone metastasis. In Rubens R. D. and Mundy G. R. (ed) Cancer and the skeleton. Martin Dunitz Ltd, London, pp 43-64.

Mundy, G. R. (2002). Metastasis to bone: causes, consequences and therapeutic opportunities. Nat Rev Cancer *2*, 584-593.

Mydlo, J. H., Michaeli, J., Cordon-Cardo, C., Goldenberg, A. S., Heston, W. D., and Fair, W. R. (1989). Expression of transforming growth factor alpha and epidermal growth factor receptor messenger RNA in neoplastic and nonneoplastic human kidney tissue. Cancer Res *49*, 3407-3411.

Nguyen, T. T., Wright, J. D., Powell, M. A., Gibb, R. K., Rader, J. S., Allsworth, J. E., and Mutch, D. G. (2008). Prognostic factors associated with response in platinum retreatment of platinum-resistant ovarian cancer. Int J Gynecol Cancer *18*, 1194-1199.

Nogales, E., Wolf, S. G., Khan, I. A., Luduena, R. F., and Downing, K. H. (1995). Structure of tubulin at 6.5 A and location of the taxol-binding site. Nature *375*, 424-427.

Norman M.E. (2003). Juvenile osteoporosis. In Favus M.J. (ed) Primer on the metabolic bone diseases and disorders of mineral metabolism, Lippincott-Raven, Philadelphia, pp 382-388.

Ottewell, P. D., Deux, B., Mönkkönen, H., Cross, S., Coleman, R. E., Clézardin, P., Holen, I. (2008). Differential effect of doxorubicin and zoledronic acid on intraosseous versus extraosseous breast tumor growth in vivo. Clin Cancer Res *14(14)*, 4658-4666.

Pacifici, R. (1996). Estrogen, cytokines, and pathogenesis of postmenopausal osteoporosis. J Bone Miner Res *11*, 1043-1051.

Paget, S. (1989). The distribution of secondary growths in cancer of the breast. 1889. Cancer Metastasis Rev *8*, 98-101.

Pan, J., Mestas, J., Burdick, M. D., Phillips, R. J., Thomas, G. V., Reckamp, K., Belperio, J. A., Strieter, R. M. (2006). Stromal derived factor-1 (SDF-1/CXCL12) and CXCR4 in renal cell carcinoma metastasis. Mol Cancer *5*.

Paulus, M. J., Gleason, S. S., Kennel, S. J., Hunsicker, P. R., and Johnson, D. K. (2000). High resolution X-ray computed tomography: an emerging tool for small animal cancer research. Neoplasia *2*, 62-70.

Peng, Z., Tuukkanen, J., Zhang, H., Jamsa, T., and Vaananen, H. K. (1994). The mechanical strength of bone in different rat models of experimental osteoporosis. Bone *15*, 523-532.

Petren-Mallmin, M., Andreasson, I., Ljunggren, O., Ahlstrom, H., Bergh, J., Antoni, G., Langstrom, B., and Bergstrom, M. (1998). Skeletal metastases from breast cancer: uptake of 18F-fluoride measured with positron emission tomography in correlation with CT. Skeletal Radiol *27*, 72-76.

Peyruchaud, O., Winding, B., Pécheur, I., Serre, C.-M., Delmas, P., Clézardin, P. (2001). Early detection of bone metatsases in a murine model using fluorescent human breast cancer cells: application to the use of the bisphosphonate zoledronic acid in the treatment of osteolytic lesions. J Bone Miner Res *16(11)*, 2027-2034.

Pfeilschifter, J., and Diel, I. J. (2000). Osteoporosis due to cancer treatment: pathogenesis and management. J Clin Oncol *18*, 1570-1593.

Pickering, L. M., Pyle, L., Larkin, J. M. G. (2009). Sunitinib is superior to interferon α with respect to quality of life for patients with renal cell carcinoma. Nature *6(1)*, 6-7.

Powles, T., Mc Closkey, E., Kurkilahti, M., et al., (2004). Oral clodronate for adjuvant treatment of operable breast cancer: results of a randomized, double-blind, placebo-controlled multicenter trial. Poster 528 presented at the 40th Annual Meeting of the American Society of Clinical Oncology, June 5-8, New Orleans, USA.

Räikkönen, J., Crockett, J. C., Rogers, M. J., Mönkkönen, H., Auriola, S., Mönkkönen, J. (2009). Zoledronic acid induced formation of a pro-apoptotic ATP analogue and isopentenyl pyrophosphate in osteoclasts in vivo and in MCF-7 cells in vitro. Br J Pharmacol *157*, 427-435.

Raisz, L. G. (2005). Pathogenesis of osteoporosis: concepts, conflicts, and prospects. J Clin Invest *115*, 3318-3325.

Rini, B. I., Small, E. J. (2005). Biology and clinical development of vascular endothelial growth factor-targeted therapy in renal cell carcinoma. J Clin Oncol *23*, 1028-1043.

Rissanen, J. P., Suominen, M. I., Peng, Z., and Halleen, J. M. (2008). Secreted tartrate-resistant acid phosphatase 5b is a Marker of osteoclast number in human osteoclast cultures and the rat ovariectomy model. Calcif Tissue Int *82*, 108-115.

Ritman, E. L. (2004). Micro-computed tomography-current status and developments. Annu Rev Biomed Eng *6*, 185-208.

Rizzoli, R., Burlet, N., Cahall, D., Delmas, P. D., Eriksen, E. F., Felsenberg, D., Grbic, J., Jontell, M., Landesberg, R., Laslop, A.*, et al.* (2008). Osteonecrosis of the jaw and bisphosphonate treatment for osteoporosis. Bone *42*, 841-847.

Robey P.G., Boskey A.L. (2006). Extracellular matrix and biomineralization of bone. In Favus M.J. (ed) Primer on the metabolic bone diseases and disorders of mineral metabolism, Lippincott-Raven, Philadelphia, pp 12-19.

Rogers, M. J., Watts, D. J., and Russell, R. G. (1997). Overview of bisphosphonates. Cancer *80*, 1652-1660.

Rosol, T. J. (2000). Pathogenesis of bone metastases: role of tumor-related proteins. J Bone Miner Res *15*, 844-850.

Rosol, T. J., Tannehill-Gregg, S. H., LeRoy, B. E., Mandl, S., and Contag, C. H. (2003). Animal models of bone metastasis. Cancer *97*, 748-757.

Ross F.P. (2006). Osteoclast biology and bone resorption. In Favus M.J. (ed) Primer on the metabolic bone diseases and disorders of mineral metabolism, Lippincott-Raven, Philadelphia, pp 30-35.

Rubin, H. (2003). Cancer cachexia: its correlations and causes. Proc Natl Acad Sci U S A *100*, 5384-5389.

Rustin, G., Reed, N., Jayson, G., et al., (2007). Phase II trial of the novel epothilone ZK-EPO in patients with platinum-resistant ovarian cancer. Poster 17 presented at the 43rd ASCO Annual Meeting, June 1-5, Chicago, Illinois, USA.

Saad, F., Adachi, J. D., Brown, J. P., Canning, L. A., Gelmon, K. A., Josse, R. G., and Pritchard, K. I. (2008). Cancer treatment-induced bone loss in breast and prostate cancer. J Clin Oncol *26*, 5465-5476.

Sadikot, R. T., and Blackwell, T. S. (2005). Bioluminescence imaging. Proc Am Thorac Soc *2*, 537-540, 511-532.

Sakuragi, T., Oshita, F., Nagashima, S., Kasai, T., Kurata, T., Fukuda, M., Yamamoto, N., Ohe, Y., Tamura, T., Eguchi, K.*, et al.* (1996). Retrospective analysis of the treatment of patients with small cell lung cancer showing poor performance status. Jpn J Clin Oncol *26*, 128-133.

Salo, J., Lehenkari, P., Mulari, M., Metsikkö, K., Väänänen, H. K. (1997). Removal of osteoclast bone resorption products by transcytosis. Science *276*, 270-273.

Sato, A., Klaunberg, B., and Tolwani, R. (2004). In vivo bioluminescence imaging. Comp Med *54*, 631-634.

Schirrmeister, H. (2007). Detection of bone metastases in breast cancer by positron emission tomography. Radiol Clin North Am *45*, 669-676, vi.

Schmid P., Kiewe P., Kuehnhardt D., et al., (2005). A phase I study of the novel, third generation epothilone ZK-EPO in patients with advanced solid tumors. J Clin Oncol *24*, 2051.

Semenza, G. L. (2002). Signal transduction to the hypoxia-inducible factor 1. Biochemical Pharmacology *64*, 993-998.

Silver, I. A., Murrills, R. J., and Etherington, D. J. (1988). Microelectrode studies on the acid microenvironment beneath adherent macrophages and osteoclasts. Exp Cell Res *175*, 266-276.

Sims, N. A., and Gooi, J. H. (2008). Bone remodeling: Multiple cellular interactions required for coupling of bone formation and resorption. Semin Cell Dev Biol *19*, 444-451.

Stackpole, C. W., Alterman, A. L., and Valle, E. F. (1991). B16 melanoma variants selected by one or more cycles of spontaneous metastasis to the same organ fail to exhibit organ specificity. Clin Exp Metastasis *9*, 319-332.

Strube, A., Stepina, E., Klar, U., Hauff, P., Hoffmann, J., Käkönen, S.-M. (2008). Sagopilone (ZK-EPO) inhibits bone destruction and tumor burden more efficiently than paclitaxel in a mouse model of breast cancer bone metastasis. (Poster presented at the IBMS Davos Workshops: Bone Biology & Therapeutics, March 9-14, Davos, Switzerland). Bone *42 (Suppl 1)*,108.

Strube, A., Hoffmann, J., Stepina, E., Hauff, P., Klar, U., Käkönen, S.M. (2009). Sagopilone (ZK-EPO) inhibits breast cancer bone metastasis and bone destruction due to simultaneous inhibition of both tumor growth and bone resorption. Clin Cancer Res *15(11)*, 3751-3759.

Taichman, R. S. (2005). Blood and bone: two tissues whose fates are intertwined to create the hematopoietic stem-cell niche. Blood *105*, 2631-2639.

Takahashi, A., Sasaki, H., Kim, S. J., Tobisu, K., Kakizoe, T., Tsukamoto, T., Kumamoto, Y., Sugimura, T., and Terada, M. (1994). Markedly increased amounts of messenger RNAs for vascular endothelial growth factor and placenta growth factor in renal cell carcinoma associated with angiogenesis. Cancer Res *54*, 4233-4237.

Takahashi, N., MacDonald, B. R., Hon, J., Winkler, M. E., Derynck, R., Mundy, G. R., and Roodman, G. D. (1986). Recombinant human transforming growth factor-alpha stimulates the formation of osteoclast-like cells in long-term human marrow cultures. J Clin Invest *78*, 894-898.

Taschereau, M. P., Chow, P. L., and Chatziioannou, A. F. (2006). Monte carlo simulations of dose from microCT imaging procedures in a realistic mouse phantom. Med Phys *33*, 216-224.

Teicher, B. A. (2006). Tumor models for efficacy determination. Mol Cancer Ther *5(10)*, 2435-2543.

Tonino, R. P., Meunier, P. J., Emkey, R., Rodriguez-Portales, J. A., Menkes, C. J., Wasnich, R. D., Bone, H. G., Santora, A. C., Wu, M., Desai, R., and Ross, P. D. (2000). Skeletal benefits of alendronate: 7-year treatment of postmenopausal osteoporotic women. Phase III Osteoporosis Treatment Study Group. J Clin Endocrinol Metab *85*, 3109-3115.

Turner, R. T., Maran, A., Lotinum, S., Hefferan, T., Evans, G. L., Zhang, M., Sibonga, J. D. (2001). Animal models for osteoporosis. Rev Endocr Metab Disord *2(1)*, 117-127.

Utsunomiya, D., Shiraishi, S., Imuta, M., Tomiquchi, S., Kawanaka, K., Morishita, S., Awai, K., Yamashita, Y. (2006). Added value of SPECT/CT fusion in assessing bone metastasis: comparison with scintigraphy alone and nonfused scintigraphy and CT. Radiology *238*: 264-271.

Vaananen, H. K., and Laitala-Leinonen, T. (2008). Osteoclast lineage and function. Arch Biochem Biophys *473*, 132-138.

Vääräniemi, J., Halleen, J. M., Kaarlonen, K., Ylipahkala, H., Alatalo, S. L., Andersson, G., Kaija, H., Vihko, P., Väänänen, H. K. (2004). Intracellular machineriy for matrix degradation in bone-resorbing osteoclasts. J Bone Miner Res *19*, 1432-1440.

van Spronsen, D. J., de Weijer, K. J., Mulders, P.F., and De Mulder, P. H. (2005). Novel treatment strategies in clear-cell metastatic renal cell carcinoma. Anticancer Drugs *16*, 709-717.

von Stechow, D., Balto, K., Stashenko, P., and Muller, R. (2003). Three-dimensional quantitation of periradicular bone destruction by micro-computed tomography. J Endod *29*, 252-256.

Vuky, J., Isacson, C., Fotoohi, M., dela Cruz, J., Otero, H., Picozzi, V., Malpass, T., Aboulafia, D., and Jacobs, A. (2006). Phase II trial of imatinib (Gleevec) in patients with metastatic renal cell carcinoma. Invest New Drugs *24*, 85-88.

Watts N.B. (2003). Bisphosphonates for treatment of osteoporosis. In Favus M.J. (ed) Primer on the metabolic bone diseases and disorders of mineral metabolism, Lippincott-Raven, Philadelphia, pp 336-341.

Weber, K., Doucet, M., and Kominsky, S. (2007). Renal cell carcinoma bone metastasis--elucidating the molecular targets. Cancer Metastasis Rev *26*, 691-704.

Weber, K. L., Pathak, S., Multani, A. S., and Price, J. E. (2002). Characterization of a renal cell carcinoma cell line derived from a human bone metastasis and establishment of an experimental nude mouse model. J Urol *168*, 774-779.

Weissleder, R., and Pittet, M. J. (2008). Imaging in the era of molecular oncology. Nature *452*, 580-589.

Wronski, T. J., Lowry, P. L., Walsh, C. C., Ignaszewski, L. A. (1985). Skeletal alterations in ovariectomized rats. Calcif Tissue Int *37*, 324-328.

Yang, M., Jiang, P., Sun, F. X., Hasegawa, S., Baranov, E., Chishima, T., Shimada, H., Moossa, A. R., and Hoffman, R. M. (1999). A fluorescent orthotopic bone metastasis model of human prostate cancer. Cancer Res *59*, 781-786.

Yang, Q., McHugh, K. P., Patntirapong, S., Gu, X., Wunderlich, L., and Hauschka, P. V., (2008). VEGF enhancement of osteoclast survival and bone resorption involves VEGF receptor-2 signaling and beta3-integrin. Matrix Biol *27*, 589-599.

Yin, J. J., Pollock, C. B., and Kelly, K. (2005). Mechanisms of cancer metastasis to the bone. Cell Res *15*, 57-62.

Yin, J. J., Selander, K., Chirgwin, J. M., Dallas, M., Grubbs, B. G., Wieser, R., Massague, J., Mundy, G. R., and Guise, T. A. (1999). TGF-beta signaling blockade inhibits PTHrP secretion by breast cancer cells and bone metastases development. J Clin Invest *103*, 197-206.

Yoneda, T. (1997). Arterial microvascularization and breast cancer colonization in bone. Histol Histopathol *12*, 1145-1149.

Yoneda, T. (2000). Cellular and molecular basis of preferential metastasis of breast cancer to bone. J Orthop Sci *5*, 75-81.

Yoneda, T., Michigami, T., Yi, B., Williams, P. J., Niewolna, M., and Hiraga, T. (2000). Actions of bisphosphonate on bone metastasis in animal models of breast carcinoma. Cancer *88*, 2979-2988.

Zekri, J., Ahmed, N., Coleman, R. E., and Hancock, B. W. (2001). The skeletal metastatic complications of renal cell carcinoma. Int J Oncol *19*, 379-382.

7 LIST OF ORIGINAL PUBLICATIONS

Papers

I Strube, A., Hoffmann, J., Stepina, E., Hauff, P., Klar, U., Käkönen, S.-M. (2009). Sagopilone inhibits breast cancer bone metastasis and bone destruction due to simultaneous inhibition of both tumor growth and bone resorption. Clin Cancer Res *15(11)*, 3751-3759.

II Hagelschuer, I., Hauff, P., Strube, A., Käkönen, S.-M., von Degenfeld, G. (2009). Luminescent imaging technology as an opportunity to reduce, refine and replace animal experiments. Light at the end of the tunnel? ALTEX (Alternatives to Animal Experimentation), submitted

Posters

I Strube, A., Stepina, E., Hartmann, B., Neumann, I., Hauff, P., Käkönen, S.-M. (2008). Development and characterization of a new renal cell carcinoma (RCC) bone metastasis mouse model. Cancer Treatment Reviews *34 (Suppl 1)*,17
Poster presented at the VII International Meeting on Cancer Induced Bone Disease, June 29 - July 2, Edinburgh, United Kingdom

II Strube, A., Stepina, E., Klar, U., Hauff, P., Hoffmann, J., Käkönen, S.-M. (2008). Sagopilone (ZK-EPO) inhibits bone destruction and tumor burden more efficiently than paclitaxel in a mouse model of breast cancer bone metastasis. Bone *42 (Suppl 1)*,108
Poster presented at the IBMS Davos Workshops: Bone Biology & Therapeutics, March 9-14, Davos, Switzerland

III Müller, S. A., Strube, A., Stepina, E., Klar, U., Käkönen, S.-M., Hoffmann, J., Hauff, P. (2008). Assessment of sagopilone treatment effects in primary tumor and tumor metastasis models using new in vivo and in vitro technologies
Poster presented at the World Molecular Imaging Congress (WMIC), September 10-13, Nice, France

IV Stepina, E., Strube, A., Käkönen, S.-M., Hauff, P. (2008). Assessment of treatment effects by bioluminescent imaging (BLI) and micro-CT in a mouse model of bone metastasis
Poster presented at the European Congress of Radiology, March 7-11, Vienna, Austria

V Stepina, E., Strube, A., Hartmann, B., Käkönen, S.-M., Hauff, P. (2007). Detection of bone metastases in a breast cancer bone metastasis mouse model using combination of micro-computed tomography, X-ray and Bioluminescent Imaging
Poster presented at “Molekulare Bildgebung”, July 5-7, Kiel, Germany

8 CURRICULUM VITAE

Der Lebenslauf ist in der Online-Version

aus Gründen des Datenschutzes nicht enthalten

Ehrenwörtliche Erklärung

Hiermit versichere ich, dass ich die vorliegende Arbeit selbstständig durchgeführt und verfasst habe. Dabei wurden keine anderen als die angegebenen Quellen und Hilfsmittel verwendet.

Berlin, 11.06.2009

Anne-Kathrin Strube